Roles of aquaporin-4 in brain fluid dynamics

by
Georg Andreas Gundersen

Thesis for the degree of Philosophiae Doctor (PhD)

Letten Centre
Institute of Basic Medical Sciences
Faculty of Medicine
&
Centre for Molecular Medicine Norway
University of Oslo

2013

Series of dissertations submitted to the
Faculty of Medicine, University of Oslo
No. 1583

ISBN 978-82-8264-090-9

Cover: Inger Sandved Anfinsen.
Printed in Norway: AIT Oslo AS.

Produced in co-operation with Akademika publishing.
The thesis is produced by Akademika publishing merely in connection with the thesis defence. Kindly direct all inquiries regarding the thesis to the copyright holder or the unit which grants the doctorate.

Contents

Acknowledgements

I had never been able to write this thesis without help from a lot of good people. In particular I thank my enthusiastic and inspiring main supervisor Erlend Nagelhus for his ability to keep faith in projects despite periods of slow progress. You always keep your head up and find creative, yet legal, solutions at times in which others would have given in to the dark anti-matter of financial despair.

My co-supervisors Anna Thoren and John Michael Burkhardt have served as valuable discussion partners and provided high quality feedback in the writing process.

I owe a lot to my fellow student and friend Rune Enger for his companionship, hard work and bad jokes. We started our scientific career together and your support has been important to me.

Professor Ole Petter Ottersen has provided invaluable support in planning projects, providing supervision, and overseeing the writing processes.

Also my colleagues Finn Mogens Haug, Martine Eilert-Olsen, Nadia Nabil Haj-Yasein, Gry Fluge Vindedal, Eystein Hoddevik, Johannes Helm, Gunnar Lothe, Bjørg Riber, Karen Marie Gujord and Jorunn Knutsen deserve my gratitude.

I would also like to thank our collaborator Maiken Nedergaard and her group in Rochester.

I would like to express my appreciation towards the Medical Student Research Program and in particular Maje Siebke and Jarle Breivik for opening the door to the scientific community.

I want to thank my wonderful girlfriend Benedikte Wendt Ræder for her support, Dr. Lise Wendt for providing a reasonably priced bivouac to a young scientist, my brothers Harald and Kristian for nurturing a competitive attitude to the challenges of life and finally my parents for giving me an open mind.

This research was funded by Civitan Norge, Center for Molecular Medicine Norway (NCMM), Institute of Basic Medical Sciences (IMB), and the Medical Student Research Program, University of Oslo. The present work was carried out at the Letten Centre, Centre for Molecular Biology and Neuroscience (CMBN), Institute of Basic Medical Sciences, University of Oslo.

Sjusjøen, February 20th, 2013
Georg Andreas Gundersen

Abbreviations

AQP4	Aquaporin-4
Aqp4	Aquaporin-4 gene in mouse
APP	Amyloid precursor protein
ATP	Adenosine triphosphate
α-SMA	α-smooth muscle actin
BBB	Blood-brain barrier
CBV	Cerebral blood volume
CNS	Central nervous system
CSF	Cerebrospinal fluid
DAPC	Dystrophin-associated protein complex
EAAT1	Excitatory amino acid transporter 1
EC	Endothelial cell
ECS	Extracellular space
GABA	Gamma-aminobutyric acid
GAT-1	GABA transporter 1
GLUT1	Glucose transporter 1
GS	Glutamine synthetase
ISF	Interstitial fluid
ICF	Intracellular fluid
ICP	Intracranial pressure
JACOP	Junction-associated coiled-coil protein
KCC	K^+/Cl^- cotransporter
Kir4.1	Inwardly rectifying potassium channel 4.1
LRP1	Low-density lipoprotein receptor related protein 1
MCT-1	Monocarboxylate transporter 1
NaDC-1	Na^+/dicarboxylate transporter 1
NKCC1	$Na^+/K^+/2Cl^-$ cotransporter
NMO	Neuromyelitis optica
OAP	Orthogonal array of particles
PDGF-β	Platelet derived growth factor-β
SGLT1	Na^+/glucose linked transporter 1
TGF-β	Transforming growth factor-β
TEER	Transendothelial electrical resistance
VRS	Virchow-Robin space

List of Figures

List of Tables

Papers included

Paper I

Molecular scaffolds underpinning macroglial polarization: an analysis of retinal Müller cells and brain astrocytes in mouse.

Rune Enger, **Georg Andreas Gundersen**, Nadia Nabil Haj-Yasein, Martine Eilert-Olsen, Anna Elisabeth Thoren, Gry Fluge Vindedal, Finn-Mogens S. Haug, Petur Henry Petersen, Maiken Nedergaard and Erlend A. Nagelhus
Glia. 2012 Dec;60(12):2018-26. doi: 10.1002/glia.22416. Epub 2012 Sep 17

Enger and Gundersen contributed equally to this study.

Paper II

Evidence that pericytes regulate aquaporin-4 polarization in mouse cortical astrocytes.

Georg Andreas Gundersen, Gry Fluge Vindedal, Øivind Skare, Erlend A. Nagelhus
Submitted manuscript. 2013.

Paper III

Glial-conditional deletion of aquaporin-4 (Aqp4) reduces blood-brain water uptake and confers barrier function on perivascular astrocyte endfeet.

Nadia Nabil Haj-Yasein, Gry Fluge Vindedal, Martine Eilert-Olsen, **Georg Andreas Gundersen**, Øivind Skare, Petter Laake, Arne Klungland, Anna E. Thoren, John M. Burkhardt, Ole Petter Ottersen and Erlend A. Nagelhus
Proceedings of the National Academy of Sciences U S A. 2011 Oct 25;108(43):17815-20. doi: 10.1073/pnas.1110655108. Epub 2011 Oct 11.

Paper IV

A paravascular pathway facilitates CSF flow through the brain parenchyma and the clearance of interstitial solutes, including amyloid β.

Jeffrey J. Iliff, Minghuan Wang, Yonghong Liao, Benjamin A. Plogg, Weiguo Peng, **Georg Andreas Gundersen**, Helene Benveniste, G. Edward Vates, Rashid Deane, Steven A. Goldman, Erlend A. Nagelhus, Maiken Nedergaard
Science Translational Medicine. 2012 Aug 15;4(147):147ra111. doi: 10.1126/scitranslmed.3003748.

1. Introduction

1.1 Background

The human brain is complex. Its complexity is beyond the threshold required for self-contemplation, and thus, its marvels have intrigued scientists for millennia. In the words of the great Russian-American geneticist Theodosius Dobzhansky:[1]

"In giving rise to man, the evolutionary process has, apparently for the first and only time in the history of the Cosmos, become conscious of itself." [1]

Brain tissue is vulnerable. High intracranial pressure (ICP) is a feared common endpoint of many conditions that cause extensive brain tissue damage, and it is characterized by expansive processes such as tumours or accumulation of fluid inside the cranium. The fluid in question can be blood, cerebrospinal fluid or interstitial fluid. Whatever the cause, high ICP produces symptoms ranging from fairly unpleasant headaches to sudden death. At some point in ancient surgical history, it was established that a practical way to treat high pressure is to lower it.

Archeological findings reveal that the first attempts on curing headaches by trepanation, the act of drilling a hole in the skull, took place in the Middle East at the time of the Neolithic Period, 9500 years BC [2]. Modern medicine has subsequently progressed for almost twelve thousand years, but craniectomy, removal of a part of the skull, is still regarded as an important treatment in severe cases of high ICP. Today, if the cause of high ICP can not be rapidly reversed, treatment options include osmotic diuresis with mannitol, glucocorticoids, hyperventilation, barbiturates, drainage of cerebrospinal fluid, and as a last resort, a craniectomy. Neuroscientists have long had a notion that there are likely other treatment options to be found, more sophisticated and gentle than merely drilling a hole in the skull to relieve pressure. To discover such potential new therapies, one must first know the mechanisms involved in development of high ICP in more detail.

Brain fluid dynamics as a research field attracts a broad range of scientific disciplines such as neurosurgery, neurology, intensive medicine, traumatology and basic neuroscience. This large volume of research activity underlines the crucial role of fluid transport in the pathophysiology of major brain diseases.

The brain is dependent on a stable metabolic state for optimal function. Minute deviations from the metabolic equilibrium affect the extracellular environment of neurons. As their cell

[1] Theodosius Grygorovych Dobzhansky (1900-1975) was a prominent geneticist and evolutionary biologist, and a central figure in the field of evolutionary biology for his work in shaping the unifying modern evolutionary synthesis.

Series of dissertations submitted to the
Faculty of Medicine, University of Oslo
No. 1583

ISBN 978-82-8264-090-9

Cover: Inger Sandved Anfinsen.
Printed in Norway: AIT Oslo AS.

Produced in co-operation with Akademika publishing.
The thesis is produced by Akademika publishing merely in connection with the thesis defence. Kindly direct all inquiries regarding the thesis to the copyright holder or the unit which grants the doctorate.

1.3 Central nervous system (CNS) fluid dynamics

1.3.1 Macroscopic level

Water accounts for 80% of the brain mass [5]. Proper circulation of water is essential for normal brain function. Brain water is distributed among four major fluid compartments: blood, CSF, interstitial fluid (ISF), and intracellular fluid (ICF). Water moves among these compartments to maintain homeostasis, though the compartments are not all interconnected (Figure 1.1, below). It is generally accepted that this movement is driven by osmotic and hydrostatic gradients [6].

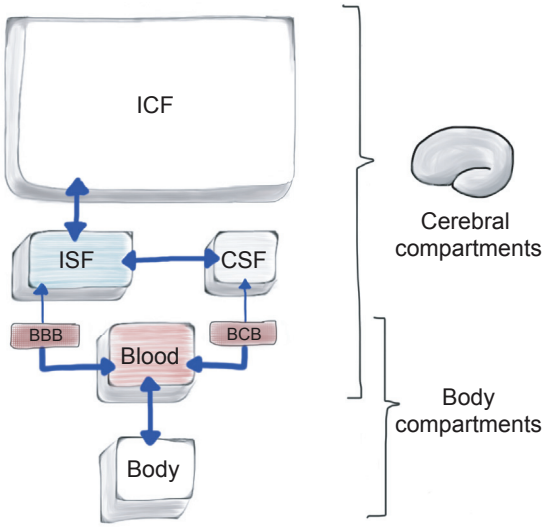

Figure 1.1: Overview of fluid compartments in the central nervous system (CNS). Water (blue arrows) moves freely between adjacent compartments following osmotic and hydrostatic gradients, except when barriers are present. Blood is separated from CSF by the blood-CSF barrier (BCB) and from ISF by the blood-brain barrier (BBB). These are selective barriers that limit the transport of water and solutes between compartments. G. A. Gundersen.

The fluid is not equally distributed among the compartments, as seen when comparing volume fractions as share of total brain volume (Figure 1.2 on the following page). The interfaces between different fluid compartments have variable permeability to water and osmotically active solutes, and thus act as selective barriers [7]. Water crosses these barriers through different mechanisms, which will be discussed in more detail in section 1.4.2. In the following section we will give a brief introduction to the four fluid compartments.

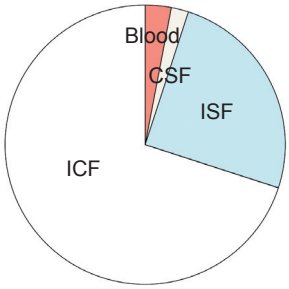

Figure 1.2: Schematic illustrating the volume fractions of the main fluid compartments of the brain as share of total brain volume. Blood vessels (red), 3% [8], cerebrospinal fluid (CSF) (grey), 2% [9], interstitial fluid (ISF) (blue), 20-25% [8, 10], and intracellular fluid (ICF) (white), 70%. G. A. Gundersen.

1.3.1.1 Blood

Blood vessels are estimated to constitute 3% of total brain volume [8]. Blood enters the cranial cavity through the major internal carotid arteries and the vertebral arteries. The arteries interconnect at the base of the brain and then branch out on the surface of the brain, sending penetrating arteries and smaller arterioles perpendicularly into the brain parenchyma [11]. In the parenchyma, hair-thin capillaries supply the brain cells and exchange nutrients for metabolic waste products. Venules and veins drain the blood to wide venous sinuses emptying into the jugular veins and returning blood to the systemic circulation [11]. The total cerebral blood volume (CBV) is distributed in the arterial, capillary and venous segments of the CNS vasculature (Figure 1.3) [12].

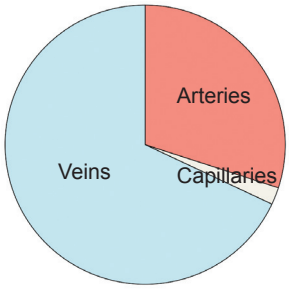

Figure 1.3: Schematic illustrating the volume fractions of the different blood vessel subtypes as share of total cerebral blood volume (CBV). Arteries (red), 30% [12, 13], capillaries (grey) 2% [14], and veins (blue), 68% [12]. G. A. Gundersen.

Water does not move freely from blood to CSF or from blood to interstitial space [7]. The blood-

CSF barrier and the BBB (see 1.4 on page 9) are anatomical and physiological barriers which control the passage of molecules between compartments in a highly regulated fashion [15]. An important function of these barriers is to protect the brain parenchyma from major fluctuations in blood constituents.

1.3.1.2 CSF - the "lymphatic system" of the brain

All metabolically active tissue needs to dispose of waste products. Waste products and surplus water that do not enter the venous blood circulation for transportation accumulate in the interstitial fluid. This surplus fluid is what constitutes the lymph in the majority of the body. The lymphatic system is a network of vessels and part of the circulatory system [16]. It acts as a sewer, its main purpose being drainage of surplus interstitial fluid containing metabolic waste products from peripheral tissue to the central parts of the body [17,18]. Ultimately the lymphatic fluid empties into the great caval veins close to the heart [17]. The only part of the body without lymphatic vessels is the cranial cavity, in which the brain resides. This is puzzling. The brain is an organ of high metabolic rate and energy consumption, receiving 15% of the cardiac output of blood, with a commensurate output of waste and metabolic byproducts. Lacking lymphatic vessels, another mechanism must be in place to perform the lymphatic function, and the widely accepted theory is that the system in question is the cerebrospinal fluid [19].

CSF contains glucose, proteins, electrolytes and other solutes in concentrations specific for the CSF, but no cells. It is primarily produced by the choroid plexus in the ventricles in central areas of the brain, at a rate of about half a liter per day [20]. A CT-study in humans estimated the average volume fraction of the ventricles to be 2% of total brain volume [9]. CSF exits the ventricle systems through three holes in the ceiling of the fourth ventricle and enters subarachnoid space. Here it is distributed outside the pial surface of the brain and spinal cord. It is subsequently drained out of the subarachnoid space through small one-way valves called arachnoid granulations to the sinus venosus and the venous system [21], and also into peripheral lymphatic system through the cribriform plate .

1.3.1.3 Interstitial fluid

When substances diffuse in the brain, they move mainly through the ECS, which separates one cell membrane from the other. The volume fraction (α) of the ECS is the volume occupied by the ECS as share of total brain volume, expressed as:

$$\alpha = V_{ECS}/V_{Tissue}$$

Studies in rats have shown that ECS volume fraction is significantly reduced from postnatal day 2 (40%) to postnatal day 21 (20%) [10]. The volume fraction is generally accepted to be between 15 and 30% in the adult brain, typically being 20% and falling to 5% during global ischemia [8]. It is harder to determine the true size of the ECS between individual cells, and the volume varies across regions [8]. A study using nanocrystals estimated the true average width of ECS in the in vivo rat brain to be between 38 and 64 nm [22]. The ISF is the fluid component of the ECS, enabling nervous tissue cells to engage in a constant exchange of water, electrolytes and metabolites. ISF composition is believed to be similar to the CSF, but in contrast to CSF, direct assay of the ISF is not achievable because of the lack of compartments of sufficient size

to sample from. The ISF is important for several reasons. It enables neurons to perform stable electrical signalling by acting as a reservoir for extracellular ions. It also acts as a conduit for substances moving from cells to the blood. Microscopy studies indicate that the average distance from a neuron to the nearest adjacent blood vessel is about 20 μm [23]. Source of production of ISF is not entirely understood, but the fluid is derived both from blood and CSF from the ventricles [15].

Computer models have been used to simulate the movement trajectories of substances moving randomly in an idealised ECS, between the convex surfaces of individual cells. The models have shown that the ECS allows spreading of substances by diffusion [8]. The same authors suggest at least five factors affecting the diffusion of molecules in the ECS; the geometry of ECS delays diffusion compared to a free medium, dead-space microdomains delay molecules by enabling them to explore a dead end, diffusing molecules are physically obstructed by extracellular matrix molecules, binding sites for the diffusing molecule on adjacent cell membranes or extracellular matrix proteins slow down diffusion, and fixed negative charges, e.g. on extracellular matrix proteins can affect the diffusion of charged molecules [8]. To be able to predict the distribution of a substance, one has to know the diffusion coefficient in neuronal tissue and the relative importance of this diffusion versus other clearance mechanisms for the particular substance. When considering nervous tissues, the term tortuosity (λ) is often used to characterize the observed diffusion hindrance. Tortuosity is defined as the square root of the following ratio: the diffusion coefficient in a free medium (D) divided by the observed diffusion coefficient in the tissue (D*) [8], expressed as:

$$\lambda = \sqrt{D/D*}$$

The concept of tortuosity is useful when considering diffusion of both solutes and water in the ECS. Bulk flow of ISF through the ECS has been hypothesized, but it is unclear how important this mode of water distribution is relative to diffusion. Clearance of ISF has been proposed to occur via three major routes, either across the BBB to the blood stream, across the ependymal cells to the ventricles or across the pial surface to the subarachnoid space [6]. As all blood vessels and the pial surface are almost completely covered by a sheet of glial cell processes [24], all the three exit routes require water transport across interfaces covered by glia (astrocytic endfeet, ependymal cells) that express AQP4 [6].

1.3.1.4 Intracellular fluid

The ICF of the CNS is located within each individual nervous tissue cell in a closed compartment, with no communication to the ECS except through cell membranes. The cell precisely regulates the content of the ICF by active and passive transportation of molecules across the cell membrane, exchanging substances with the ISF. The ICF composition differs both across CNS cell types and within any individual cell. In a typical eukaryotic cell, about 70% of the cell volume is cytosol, while the rest is made up by different organelles [25]. The cytosol consists mostly of water, dissolved ions like potassium, sodium and chloride, small molecules, and large water-soluble molecules like proteins (Table 1.1 on the next page).

Ion	Cytosol concentration (mM)	ISF concentration (mM)
Potassium	139	4
Sodium	12	145
Chloride	4	116
Bicarbonate	12	29
Amino acids in proteins	138	9
Magnesium	0.8	1.5
Calcium	<0.0002	1.8

Table 1.1: Ion concentrations differ between intracellular and interstitial fluid. Gradients are maintained by active transporter molecules. Source: Molecular Cell Biology, Lodish et al (2000) [26].

The different ICF and ISF ion concentrations create ion gradients between the interior and exterior of the cell. The ion gradients are continuously maintained by active and passive ion transport mechanisms as well as by co-transport of ions and other solutes. The Na^+/K^+-ATPase is an active transporter that maintains a negative cell membrane potential by pumping sodium out of and potassium into the cell. Potassium then leaks out following its concentration gradient through potassium-specific ion channels. This leakage of potassium creates a electric potential difference across the cell membrane, being slightly more positive on the outside of the cell. The gradients serve several purposes, such as maintaining an electric membrane potential required for neuronal signalling. The gradient of sodium ions enables transport of specific solutes such as glutamate across the cell membrane against glutamate's concentration gradients by co-transport with sodium ions following their electrochemical gradient. Water, being a relatively small and polar molecule, crosses the cell membrane both by diffusion through the lipid bilayer, by following other molecules through their designated transporter proteins, and by transport through aquaporins (see 1.4.2 on page 21) [27].

1.3.2 Synaptic level

When zooming in from the four macro-level fluid compartments to the micro-level of an individual synapse, we can observe fluid shifts in more detail. Thirty years ago it was observed that the extracellular volume is subject to rapid changes, the driver being synaptic activation [28]. When a synapse is active, the ECS and the intracellular compartments of the synapse's constituent cells undergo reversible volume changes [29]. Using membrane impermeant cations, extracellular space volume reductions in the range of 5 to 30% were observed after high frequency activation of excitatory pathways [8]. The volume changes are assumed to be caused by water redistribution due to ion fluxes between compartments [8, 29]. While the mechanism of these dynamic changes remains to be explained in detail, it is now assumed that they reflect water cotransport coupled to rapid uptake of ions and transmitters in perisynaptic glial cells [30, 31].

Water cotransport has been documented for a number of ions and transmitters, including K^+, bicarbonate, and glutamate [30]. The exact contribution to this water shift by the different ion-channels and -transporters is not known. Several independent studies the last forty years have shown that perisynaptic glial cells swell as function of extracellular K^+ concentration [31]. This K^+-induced swelling response in cortical cells correlates linearly with a K^+-induced intracellular accumulation of chloride-ions, suggesting K^+-dependent chloride influx as the mechanism underlying the observed swelling [31]. Interestingly, pharmacological inhibition or genetic deletion

of the $Na^+/K^+/2Cl^-$ cotransporter (NKCC1) eliminates the K^+-induced swelling response in cultured astrocytes [32, 33].

The Na^+-dependent glutamate transporter-1 (EAAT1) is located in perisynaptic glial membranes and are important for clearing the ECS of glutamate after synaptic activity. Glutamate is toxic to neurons, and thus rapid clearance of glutamate from the ECS after synaptic release is neuroprotective. EAAT1 is a cotransporter, driving glutamate into the glial cell against its electrochemical gradient by cotransportation with H^+ and Na^+, the latter following its electrochemical gradient, in exchange for K^+. This way glutamate is transported into glial cells, adding to the swelling response by favouring movement of water into the cell [30]. One study showed that addition of glutamate to astrocytes in culture increased glial swelling in a concentration-dependent fashion. The authors added different concentrations of glutamate (5μM to 50mM) to the culture and observed average swelling increases ranging from 5 to 18%, respectively [34]. The roles of the water channel AQP4 in regulation of perisynaptic ECS-volume will be described in more detail in section 1.6.2 on page 26.

1.4 The blood-brain barrier and water flux

1.4.1 Anatomy of the BBB

To understand water transport between compartments on the level of capillary blood vessels we must understand the cellular layers that water penetrates. In 1885, the German physician, hematologist, and scientist Paul Ehrlich injected a dye intravenously and discovered that all organs were colored except the brain and the spinal cord [35]. Three decades later Edwin Goldmann, one of Ehrlich's students, observed that brain tissue was colored if the same dye was injected directly into the CSF, but in this case the rest of the body was not [36]. The conclusion was that a barrier must exist, separating the two metabolic compartments blood and brain. This concept came to be known as the blood-brain barrier (BBB).

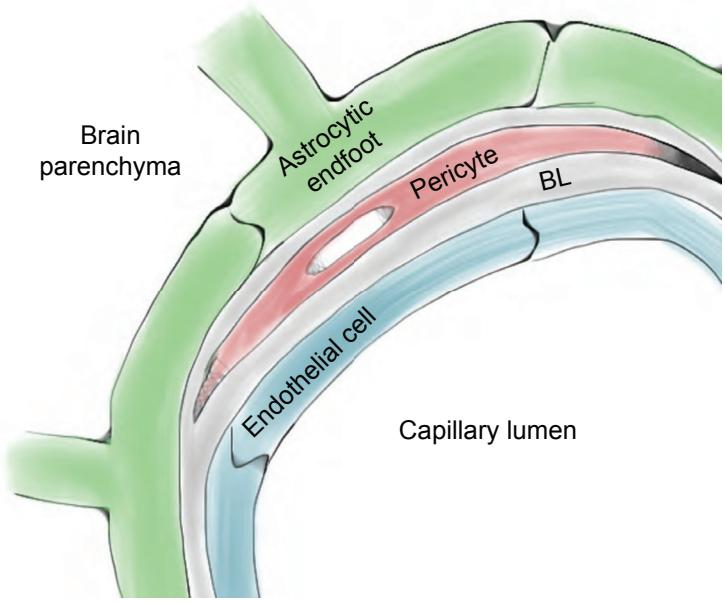

Figure 1.4: Overview of anatomical layers of the BBB. Lining the capillary lumen is the endothelial cell (blue), covered by its basal lamina (grey). The astrocytic endfoot (green) separates the basal lamina from brain neurons. Pericytes (red) are interposed between the endothelium and the astrocytic processes. Tight junctions between endothelial cells prevent paracellular transport. Water, glucose, amino acids and electrolytes have transporter proteins in the cell membranes. Gases and small, polar molecules diffuse across the phospholipid bilayers of the cell membranes. G. A. Gundersen.

The BBB is a conceptual and functional barrier, not a localized physical one. The anatomical substrate of the BBB in mammals is made up of four main components. Moving from blood to

brain, the four components of the BBB are the endothelial cells, the basal lamina, the pericytes and the astrocytes (Figure 1.4 on the preceding page). Some authors do not consider astrocytes as part of the BBB, presumably because they are by definition a CNS cell type, and because the BBB is a functional barrier in which the astrocyte is generally considered a minor contributor. In this case the endothelial cells, pericytes, and basal lamina together with adjacent astrocytes, neurons, and possibly other glial cells, are often collectively referred to as the "neurovascular unit". To clarify, we choose to treat astrocytes as part of the BBB, given that they have been shown to regulate barrier function. Pericytes are not always present between the basal lamina and the astrocyte (see 1.4.1.3 on the next page).

These four BBB components do not contribute equally to the barrier function, and have changed evolutionary over time. Studies on extant vertebrates showed that 4-500 million years ago, the BBB barrier function of all vertebrates was primarily in the glial cells [37]. Today, in elasmobranches, a subclass of cartilaginous fish including sharks, rays and skates, the barrier function is still primarily in the glial endfeet [38, 39].

As will be clear in the following sections, barrier function in modern mammals lies primarily in the endothelial component of the BBB. The development of an endothelial barrier seems to have arisen several times independently in the course of evolution, indicating that an endothelial barrier provides strong selective advantage [37]. On that note, several serious diseases are accompanied by disruption of the BBB, such as brain tumours, multiple sclerosis and stroke [40].

1.4.1.1 Endothelial cells

Endothelial cells line the inner surface of the blood vessel wall (Figure 1.8 on page 20). Tight junctions, also known as zonula occludens, between endothelial cells were first described in 1967 and are the most important factors for the BBB's selective barrier function in mammals [41]. The tight junctions bind the endothelial cells closely together and are unique to the endothelial cell type in the CNS [40]. They provide a potent barrier for virtually all microscopic organisms and large, hydrophilic molecules, and also restrict ions and smaller molecules. The details of the junction components have been the subject of great scientific interest. Our current understanding of the molecular structure of tight junctions is largely based on studies in cultured endothelia and epithelia and BBB endothelium [40].

Among the molecules known to contribute to the tight junctions are the transmembrane proteins occludin and the claudins. Occludin is capable of linking zonula occludens protein 1 (ZO-1), and its main function seems to be regulation of the tight junction [40].

Tight junctions significantly restrict even the movement of small ions such as sodium and chloride across the BBB, so that the transendothelial electrical resistance (TEER) can be increased 50-fold compared to endothelium elsewhere in the body [42]. Claudins 3, 5 and possibly 12 appear to contribute to the increased TEER [40].

In brain endothelial cells, the junctional adhesion molecules JAM-A, JAM-B and JAM-C are maintaining tight junctions [43]. These transmembrane proteins are connected to the interior of the cell by a complex mesh of proteins that form large protein complexes called cytoplasmic plaques [43]. These plaques contain adaptor proteins with many protein-protein interaction domains. This basically means that the proteins are able to interconnect at several sites, facilitating formation of stable multi-protein structures. A recently-discovered protein, junction-associated coiled-coil protein (JACOP) seems to be involved in connecting the junctional complex to the actin cytoskeleton [43].

The endothelial cells also have reduced vesicular transcellular transport compared to endothelium elsewhere in the body, adding further to the barrier function [43].

1.4.1.2 Basal lamina

Separating brain capillaries, astrocytes, and pericytes is the basal lamina (Figure 1.8 on page 20). The perivascular basal lamina is a very complex extracellular structure which originates partly from astrocytes and partly from vascular cells. The basal lamina is a layer of extracellular matrix proteins comprised of a number of collagens, laminin, fibronectins, tenascin and proteoglycans, this list not being exhaustive [44]. The basal lamina provides mechanical support for cell attachment, serves as a substrate for cell migration, separates adjacent tissue, and acts as a barrier to the passage of macromolecules. Cell adhesion to the basal lamina involves the integrins [45]. Integrins are transmembrane receptors that bridge the cytoskeleton of a cell to the extracellular matrix.

1.4.1.3 Pericytes

In 1873 Charles Rouget described for the first time a population of branched cells on the capillary wall of the hyalloid of the frog and regarded them as contractile elements distinct from migratory leukocytes [46]. Vimtrup, when studying capillaries in larvae tails, noted that contraction of capillaries begins in these cells, calling them Rouget cells [47]. Zimmermann has been credited to be the first to use the term pericyte, originating from "peri" - around and "cyto" - cell [48]. Pericytes are contractile cells surrounding the endothelial cell circumference with finger-like projections, controlling the blood permeability of the capillary bed. They are polymorphic cells with an oval cell body and long cytoplasmic projections oriented along the axis of the blood vessels, perpendicularly branching off secondary and tertiary processes that grip the vessel around its circumference [47]. Zimmermann described three subtypes of pericytes depending on the adjacent vessel type, but suggested the existence of a continuum of a multitude of forms of differentiation [49].

The study of pericytes presents some difficulties because pericytes are not easy to extract from their location. There is also no pericyte-specific marker that enable us to perform certain single-labelling immunohistochemical identification. This problem is partly explained by the fact that pericytes are multipotent cells, able to differentiate into different subtypes and expressing various amounts of potential pericyte-marker proteins. Double staining of contractile cell markers such as the surface protein α-smooth muscle actin (α-SMA) in combination with an endothelial cell surface marker is often used to separate pericytes and endothelial cells immunohistochemically [47]. However, α-SMA is also expressed by smooth muscle cells and not by all pericytes. Another frequently used marker is the chondroitin sulfate proteoglycan NG2 which is also a neural progenitor cell marker. Other surface markers in use are PDGF-β, VCAM-1 and ICAM-1, pericytic aminopeptidase N, γ-glutamyl transpeptidase, and alkaline phosphatase, the xLacZ4 transgenic reporter, and the regulator of G-protein signaling-5 (RGS-5) [47]. Many of these markers are expressed in neighbouring cells, creating difficulties when trying to isolate the pericytes.

Pericytes are interspersed along the abluminal side of the endothelial cells in pre-capillary arterioles, capillaries, and post-capillary venules, between the EC and the astrocytic endfoot [48]. They are covered by basal lamina on all sides (Figure 1.8 on page 20). Pericyte density along the vessel tree varies between tissues. In the brain, pericyte-to-endothelia ratio has been estimated

to 1:3, compared to 1:100 in striated muscle [50]. Other studies showed that pericyte coverage around retinal capillaries is even higher than in brain capillaries [51, 52].

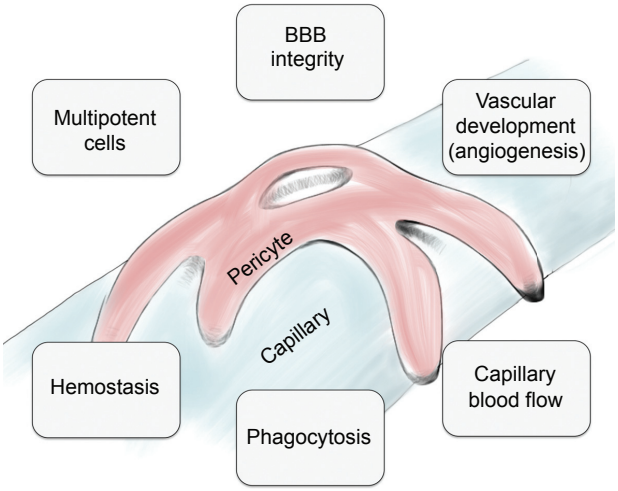

Figure 1.5: Simplified schematic illustrating pericyte functions. Pericyte with processes (red) surrounds a capillary (blue). G. A. Gundersen.

Studies over the past twenty years have begun to disclose important roles of pericytes in regulation of neurovascular functions needed for proper CNS homeostasis, including BBB formation, vascular maintenance and architecture, as well as capillary caliber and blood flow [53], regulation of BBB function, neovascularization and angiogenesis, phagocytosis, and regulation of cerebral blood flow on the capillary level by contracting and thereby narrowing the capillary lumen (Figure 1.5) [47, 48]. Pericytes are believed to play a role as the initiator of thrombin clot formation in primary homeostasis, given its subendothelial localization [47]. Pericytes communicate with endothelial cells through a series of signalling mechanisms, some of the most extensively studied being the platelet derived growth factor-β (PDGF-β), transforming growth factor-β (TGF-β), and Notch signalling, the latter being a group of four distinct heterodimeric receptors known to be involved in embryonic vascular development. Notch-receptors initiate several steps leading to downstream transcriptional changes [53]. This cross-talk via signalling cascades enables recruitment of CNS pericytes, maintains pericyte survival, and induces pericyte differentiation and adhesion [53].

Considering the importance for BBB formation, recent studies in mice deficient in PDGFr-β demonstrated that BBB formation occurs early in embryogenesis, at approximately the same time as pericyte recruitment and before generation of astrocytes [54]. In addition to pericytes being necessary for development of BBB integrity, the authors found pericyte coverage of capillaries to be important for tight junction development between ECs and for transendothelial vesicle transport [54]. Abnormal pericyte function has been observed in CNS diseases such as diabetic retinopathy, neonatal intraventricular haemorrhage and in neurodegenerative processes [53].

However, the detailed mechanisms underlying pericyte dysfunction in specific neurodegenerative disorders such as Alzheimer's disease is less understood.

Another recent study performed on pericyte-deficient mice showed that pericyte-deficiency increased permeability of the BBB to water and other different-sized tracer molecules [55]. The increased permeability was caused by increased transcytosis. The pericyte seemed to influence the BBB in at least two ways. First, it altered endothelial gene expression. Second, it induced polarization of astrocytic endfeet around CNS blood vessels [55]. Three markers for the polarized astrocytic endfoot; the water channel AQP4, α-syntrophin and laminin-α2 chain, all showed reduced vascular staining in absence of pericytes. In addition, AQP4 was redistributed to other regions of the astrocyte [55]. This suggests that pericytes could be necessary for proper localization of AQP4.

1.4.1.4 Astrocytes

In 1895 Lenhossek first used the term "astrocyte" in his textbook on the CNS [56]. He presented it as a replacement for the term "glial cells" in higher vertebrates as an effort to get away from the term "glia" (Greek, "glue"), indicating a passive function of this cell type [57]. The astrocyte is an abundant cell type in the CNS, outnumbering neurons at least in higher species [58]. Some report that neurons outnumber astrocytes by 3 to 1 in mouse and rat cerebral cortex, but in human cerebral cortex, astrocytes outnumber neurons by 1.4 to 1 [59]. The density of astrocytes varies by a factor of 1000, from low levels in the nucleus accumbens to very high in the subventricular zone [57].

1.4.1.4.1 Astrocyte classification and morphology

Astrocytes are star-shaped glial cells located in the CNS. Astrocytes, also known as astroglia, are one of three types of macroglial cells, the others being oligodendrocytes and ependymoglial cells. Classification of astrocytes presents some challenges compared to other CNS cell types such as neurons and microglia, in that it is a heterogeneous group of cells with no unique marker or hallmark characteristic. Classification of astrocytes can be based on morphology, lineage or antigenic phenotype. In the beginning of the 19th century, astrocytes were subclassified into protoplasmic and fibrous astrocytes [57]. In time, more subtypes were discovered and given special names, such as the Müller cell in the retina and the Bergmann glia in the cerebellum. In 2006, Emsley and Macklis defined 9 classes of astrocytes based on three different labelling methods - GFAP-GFP-expressing transgenic mice, and GFAP and S100β immunostaining, both glial markers, although not present in all astrocytes [60]. The 9 subtypes suggested were tanycytes, "radial" cells, Bergmann glia, protoplasmic astrocytes, fibrous astrocytes, velate glia, marginal glia, perivascular glia, and ependymal glia, and the authors clearly stated that several populations can exist within one brain area [60]. In general, primate astrocytes are found to be more complex than rodent astrocytes, they are larger, have more processes, and one specific astrocyte subtype, the interlaminal astrocyte with its long, corkscrewed processes, is unique to primates and not found in the rodent brain [57]. This introduction will not go in detail on specific morphological subtypes. The main subtypes investigated in the experimental body of this thesis are the perivascular astrocytes in the cerebral cortex and the Müller cells of the retina.

1.4.1.4.2 Astrocyte function

In contrast to neurons, astrocytes are not electrically excitable and do not fire action potentials. For many years, astrocytes were considered mere gap-fillers in the brain, with no other functions than their name glia (Greek, "glue") suggests. Today, astrocytes are known to have multiple important functions and prominent roles in brain physiology. The subject of astrocyte function is closely related to astrocyte heterogeneity, which will be discussed below. In the following a selection of important astrocyte functions will be introduced, and more will be discussed in the paragraph on regional heterogeneity.

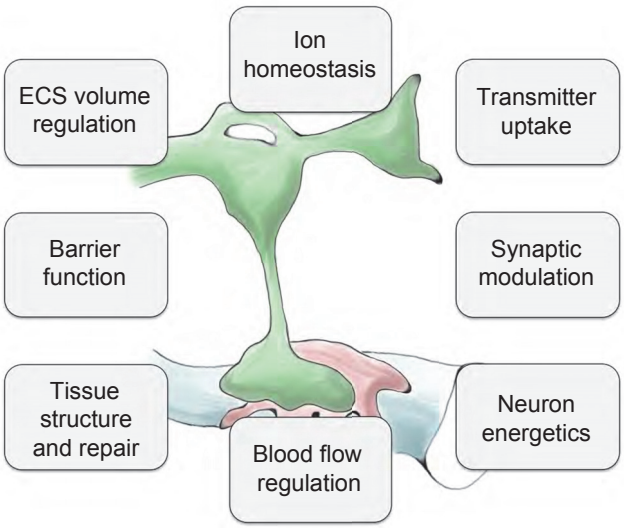

Figure 1.6: Simplified schematic illustrating key astrocyte functions. Illustration shows astrocyte (green) with an endfoot process covering pericyte (red) and capillary (blue). G. A. Gundersen.

Extracellular potassium regulation is one of the crucial functions of astrocytes. Astrocytes contribute to maintaining an optimal and stable extracellular environment for neurons in general, and their synaptic regions in particular. Extracellular potassium homeostasis is maintained by different mechanisms, such as spatial redistribution of K^+ through gap-junction-coupled astrocytes ("spatial buffering"), active uptake by the Na^+/K^+-ATPase, and K^+ uptake through specific transporters and channels. By spatial buffering, K^+ ions enter and leave the astrocytes at regions of high and low extracellular K^+ values, respectively, with no net uptake [61]. Spatial buffering of K^+, as first described by Orkand in 1966, involves influx and efflux of K^+ through astrocytic K^+-channels such as Kir4.1 [62]. The quantitative importance of this mode of K^+-removal is not known, and mathematical modelling indicates that the absolute amount of K^+ actually being cleared away by this mechanism is negligible [31]. The Na^+/K^+-ATPase is an active transport mechanism, continuously transporting K^+ into the cell in exchange for Na^+. Passive transport can occur through the $Na^+/K^+/2Cl^-$ cotransporter 1 (NKCC1) or by

electroneutral KCl uptake through separate K^+ and Cl^- channels [61].

Glutamate uptake and subsequent conversion to glutamine is a well known function of astrocytes. Glutamate is taken up from the perisynaptic ECS, converted to glutamine intracellularly and released to the ECS as part of a process known as the glutamate-glutamine cycle [63]. Following synaptic transmission, glutamate is taken up into the astrocytes via glutamate transporters EAAT1 and EAAT2, moving against its concentration gradient by coupled transport to Na^+ and K^+ [64]. Inside the cell, glutamate is converted by glutamine synthetase (GS) to glutamine and transported out of the astrocyte and back into the ECS for uptake by neurons. In the neurons, glutamine serves as a substrate for glutamate production and thus completing the cycle [63]. In addition to replenishing stores of glutamate, this activity rapidly clears the perisynaptic ECS of glutamate, preventing the neurotoxic effects seen at high concentrations of glutamate. Astrocytes also release neurotransmitters such as glutamate [65], and perform uptake of GABA [66] and ATP [67], although the importance of the latter activity is unknown. Specific transporters for other neurotransmitters such as GABA, glycine, adenosine, monoamines and serotonin has also been characterized [64].

Sensation and modulation of synaptic activity by astrocytes has been an evolving field in recent decades. The close structural and physiological interactions with neurons suggests that glial cells could be an active partner in synaptic transmission. The term "tripartite" synapse was introduced to emphasize the point that the third element of the synapse, the glial cell, is an essential component in determining synaptic function, along with the pre- and postsynaptic neurons [68]. Not all synapses in the CNS are covered by astrocytes. In the hippocampus, it has been reported that 57% of all synapses are associated with astrocytic processes [69], whereas in visual cortex, one study reported 29% endfoot coverage of synapses [70]. The communication between neurons and astrocytes at the synapse appears to be two-way. Neurons signal to astrocytes by release of neurotransmitters, while astrocytes signal in various ways, including release of chemical transmitters [64]. Glial cells express many of the same transmitter receptors as neurons, notably AMPA, NMDA, metabotropic glutamatergic receptors, GABAergic, adrenergic, P2X and P2Y purinergic, serotonergic and muscarinic receptors, and a multitude of peptidergic receptors [64, 71]. Astrocytes are interconnected by gap junctions, creating a network in which they can communicate by intercellular pathways [72]. Following synaptic transmission, the signal from a "sensory" astrocyte can spread through this glial network by intracellular calcium elevations [71]. Intracellular calcium elevations can propagate over long distances in the astrocytic syncytium and are thought to be important communication mechanisms [73]. Calcium signalling will be further discussed below. Astrocytes have also been shown to modulate neuronal activity directly, e.g. by relase of glutamate or ATP, by potentiating inhibitory synaptic transmission [74] and by TNF-α-dependent control of the strength of excitatory synapses [75, 76]. Astrocytes can also modulate synapses indirectly, notably by neurotransmitter uptake or glial release of cofactors, such as the NMDA receptor modulator D-serine [77].

Astrocytes are involved in neuroenergetics. believed to provide neurons with lactate as an alternate energy source to glucose [78]. A study first determined the presence of lactate transporters MCT1 and MCT2 in the adult mouse brain. The authors then showed how the lactate dehydrogenases LDH1 and LDH5 are distributed among neurons and astrocytes in a fashion that suggests a population of astrocytes as the lactate "source" while neurons being a lactate "sink" [78]. The authors move on to provide biochemical evidence that lactate is interchangeable to glucose as a substrate in oxidative metabolism in cortical neurons [78]. Recent studies have suggested a role of astrocyte regulation in controlling neural tissue supply of energy sources through regulation of blood flow. This idea emerged after observations showing that astrocytes stimulated by glu-

tamate released a group of vasodilator substances called epoxyeicosatrienoic adics (EETs) [79]. Later studies have provided data supporting this possible control of blood supply as yet another function of astrocytes [80].

In case of neuronal death, due to for example ischemia after stroke, trauma or infection, the astrocytes proliferate at the site of destruction to form a glial "scar" by a process known as gliosis [81]. Astrocytes also secrete growth factors for neurons and axons and provide structural support as part of the cytoarchitecture in the developing CNS [64].

1.4.1.4.3 Astrocyte heterogeneity

The fact that astrocytes are able to perform such diverse functions as outlined above suggests that they are not all alike. Indeed, for over thirty years it has been known that astrocytes are heterogeneous, meaning that astrocytes differ across different areas of the CNS according to which particular functions they are supposed to perform [82]. As noted above, nine different morphological variants has been described [57], but heterogeneity is more than structural differences. Astrocytes differ in a multitude of functional properties, both across and within brain regions [83]. Astrocyte heterogeneity has been observed in glial development, gene expression, physiologic functions and in response to injury and disease [83]. The following paragraphs will elaborate on astrocyte characteristics expressing heterogeneity. Some of the functions introduced in the previous section will be reconsidered here from a perspective of heterogeneity.

Membrane conductance of astrocytes consists of passive currents, e.g. by uptake of potassium from the perisynaptic ECS following synaptic activity and conductance of that electric unbalance along the cell [57]. This membrane conductance is thought to be mediated by the most abundant potassium channel of CNS astrocytes, Kir4.1, and the TREK potassium channels [84]. Kir4.1 expression levels vary across brain regions, being high in the ventral horn of the ventricles compared to very low Kir4.1 levels in the apex of the dorsal horn [57]. Patch-clamp recordings confirmed significantly smaller K^+ uptake currents in the dorsal horn compared to the ventral horn, suggesting that the uneven Kir4.1 expression levels have functional implications for K^+ clearance rates in these regions [57]. The membrane conductance heterogeneity is observed not only across brain regions, but across developmental stages within one region [84].

Heterogeneity of astrocyte expression has also been shown for other membrane proteins, such as Ca^{2+}-channels and glutamate receptors [57]. Glutamate receptors are considered a general characteristic of astrocytes. In the rat supraoptic nuclei, one has observed a large population of astrocytes that are morphologically similar to radial-type glia, but lacks glutamate receptors [85]. They do, however, express GABA-channels. Interestingly, an adjacent population of astrocytes with round cell bodies and few processes proved to have functional glutamate receptors [85]. To emphasize a general point, this heterogeneity of transmitter receptor expression in astrocytes can be observed for receptors for GABA, glycine, beta-adrenergic agonists, and metabotropic receptors for purinergic agents [57].

An important feature of astrocytes is reuptake of neurotransmitters following synaptic activity in neurons. This clearance of transmitters from the ECS into the astrocyte is mediated by transporters. Also neurotransmitter transporters are subject to regional heterogeneity. A study of the astrocytic GLT-1, a glutamate transporter molecule for clearance of glutamate from the ECS after synaptic release and for prevention of glutamate-related excitotoxicity. The authors made transgenic mice with coexpression of DsRed under control of the GLAST promoter and GFP under the control of the GLT-1 promoter. They found 10-fold higher GLT-1 levels in brain

astrocytes compared to astrocytes in the spinal cord [86].

Astrocytes are connected to each other by gap junctions. Efforts have been made to study the amount of gap-junction connectivity between astrocytes in different regions of the brain and at different developmental time points. Significant differences have been observed [57]. Notably, in grey matter the astrocytes form large networks, syncytia, with many interconnections for any individual cell, whereas in white matter in the corpus callosum, coupling between astrocytes are low and single astrocytes with no gap-junction connections can be observed [87]. Cortical astrocytes form three-dimensional networks in general, whereas Bergmann-glia in the cerebellar cortex are organized in a layer network [57]. When comparing mice of different ages, more gap-junction connectivity, assessed by biocytin-injections, has been observed in younger mice when compared to older adults [88].

Astrocytes have two modes of calcium signaling; spontaneous calcium oscillations in individual cells and a coordinated form as an intercellular calcium wave. Intercellular calcium waves propagate in different ways across different populations of astrocytes. In the cortical three-dimensional networks, the signal is generally transferred by the multitude of gap junctions, whereas in the corpus callosum where gap-junction coupling is low or absent, the signal is conveyed by ATP-release [89]. Studies on mouse brain slices and human astrocytes in culture showed that Ca^{2+}-waves travel faster in human cells [57], it is not known if this is due to morphological differences between species.

Differences in volume-regulatory responses between populations of astrocytes have been observed both after ischemic and hypo-osmotic stress in slices [57].

One interesting subtype of the astrocyte family is located in the retina of the eye. The retina is a highly specialized extension of the CNS, of the same embryological origin. It contains similar cell types as the neocortex of the brain, and its astrocyte subtype is called the Müller cell. The Müller cell structure is tailor-made for fitting the cell layers specific to retina, i. e. it favours the uninterrupted travel of light acting as an optical fiber [90], but in essence it performs similar main functions as the astrocytes found in the cortex of the brain [91].

Taken together, it is clear that astrocytes are a diverse group of cells exhibiting a wide range of subspecialized functions and ample differentiation across many attributes.

1.4.1.4.4 Astrocyte polarity

The concept of functional and morphological subspecialization is well known on the level of macroglial cell types as regional heterogeneity, as described above [91]. The same principle of subspecialization is observed on the level of individual cells. Different cell membrane domains with different functions contain different molecules, e.g. receptors and transporter proteins. This targeted expression of proteins to specific domains of the cell membrane is referred to as polarization or polarity.

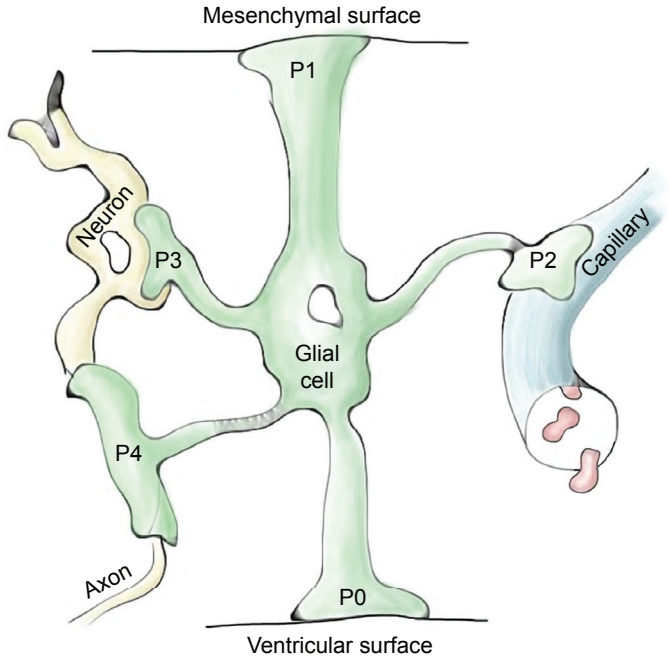

Figure 1.7: Schematic illustrating glial cell polarity. The glial cell (green) has numerous processes facing different compartments in the cells microenvironment. In gliogenesis, radial glia, like Müller cells, first develop two "stem" processes facing a ventricle or the subretinal space (P0) and a mesenchymal surface covering a fluid compartment (P1) like pia, the vitreous body or a blood vessel. Then additional processes develop, such as the perivascular endfeet facing the vascular tree (P2), processes facing neurons (P3), their axons (P4) and dendrites. Not all glial cells contain all process types. G. A. Gundersen.

Cell polarization in the CNS was first described in 1865 by Deiters, who identified axons and dendrites and assigned different functions to them [91]. Polarization enables different membrane domains to perform different functions. Astrocytes are traditionally regarded as polarized cells, but this term indicates a "two-domainal" membrane distribution of molecules. Although this might be descriptive for individual molecules, the astrocyte membrane as a whole is more complex. Astrocytes have several different well-defined membrane domains, hence a multi-domainal perspective might be more appropriate [91].

To understand glial cell polarity, it is useful to review the developmental stages. Mature astrocytes have a cell body with a nucleus and numerous cellular processes (Figure 1.7). These long processes extend to important structures in the cell's surroundings where the astrocytes perform their functions. In the young developing CNS, the bipolar shape of radial glial cells is predetermined by the two surfaces of the neural epithelium which the cells are in contact with

by their two opposite stem processes. Some subgroups of radial astrocytes such as tanycytes and Müller cells preserve this fundamental basal-apical polarity, although the mature cells also develop additional processes to nearby structures [91]. As the CNS develops, the growing microenvironment of an astrocyte increases the number of possible contacts, and thus increases in complexity from the embryological starting point of just two nearby epithelial surfaces. Given this situation, it has been proposed that the definition of astrocyte cell polarity should not be based on the two-sided embryological "stem"-process, but on the numerous "side"-processes that emerges during development [91].

The distal end of an astrocytic process is called the astrocytic endfoot. The endfeet are in contact with all structures surrounding astrocytes such as neurons, neuronal synapses, capillaries and the pial surface, and in case of the Müller cell, the subretinal space [91]. Polarity has been observed and partially characterized in processes facing microvilli, the outer retina, and peripheral astrocytic processes [91]. However, in this thesis we will focus on the subgroup of endfeet facing capillaries, namely the perivascular astrocytic endfeet. These specialized structures exhibit strong polarization of membrane proteins and appear to be important entities at the BBB. In this thesis we are particularly interested in these processes as they appear to serve important functions for flow of water, transport of electrolytes and as regulators of local cerebral blood flow. Notably, the water channel AQP4, the K^+-channel Kir4.1 and anchoring proteins of the dystrophin family are polarized to these astrocytic processes, while existing in relatively lower levels in other astrocytic membrane domains. We will in the following sections focus on the perivascular astrocytic endfoot and its membrane proteins.

1.4.1.5 The perivascular astrocytic endfoot

The astrocytic endfeet cover more than 99% of the capillary endothelial cells along the capillary [24]. The area of endothelial wall that supplies the brain is large; in each cubic centimeter of brain there is about 100 cm^2 of endothelial membrane [92]. Accordingly, the concentration of endfoot membrane per brain volume can be assumed to be almost as high.

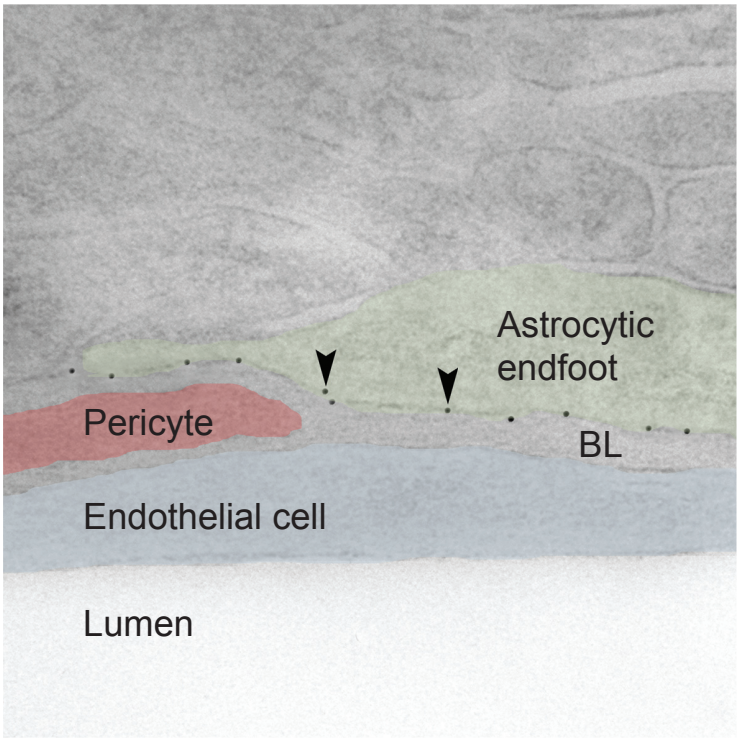

Figure 1.8: EM-micrograph from the cerebral cortex shows the astrocytic endfoot (green) covering the endothelial cell (blue) and the pericyte (red), separated only by their basal laminas (BL). Gold particles (arrows), 15nm in diameter, represent AQP4 water channels in the endfoot membrane facing the capillary. G. A. Gundersen.

The perivascular endfoot is only separated by a distance of 35-40 nm from the endothelial cell of the capillary wall by the basal lamina (Figure 1.8). Perivascular endfeet appear in several stages of astrogliogenesis, first by the development of the primary glial process abutting pre-existing mesenchymal surfaces such as pia or a vessel wall [91]. Other perivascular processes facing "younger" capillaries are developed "en passant" as the angioarchitecture matures and the capillary system develops. The perivascular endfeet express high levels of specific transporter proteins, ion-channels, and water channels, suggesting that this is an active zone of molecule

exchange.

All the astrocytic and Müller cell processes facing a basal membrane share a typical structure and similar anchoring protein complexes. They contain an unusually high amount of intramembranous orthogonal arrays of particles (OAPs), which main component is the water channel AQP4 [91]. Studies of the endfoot membrane using immunogold labelling and mice knockout models revealed that AQP4 is colocalized with the K^+-channel Kir4.1 [93], and both channels are associated with the dystrophin-associated protein complex (DAPC). Much is known about the relationships and interdependency between AQP4 and members of the DAPC, this will be discussed in more detail in later sections.

The endfoot membranes are practically covering all CNS capillaries and thus the majority of BBB area, and therefore they are assumed to be important for both brain nutrient exchange and water flux [94]. They might also be involved in local regulation of cerebral blood flow by crosstalk with pericytes [4]. The perivascular endfeet can be important in at least two other functional aspects. Uptake of glucose and lactate from peripheral blood is crucial for CNS energy metabolism. The relative distribution of the CNS glucose transporter GluT1 or the lactate transporter MCT1 in perivascular endfeet compared to other astrocyte cell domains is not known . Today, there is no evidence of a endfoot restriction of MCT1, and GluT1 is observed in perisynaptic neuropil processes [95, 96]. Having introduced the anatomical substrates of the BBB, we will no look at ways to transport water across these layers.

1.4.2 Water transport across the BBB

As outlined above, water is constantly moving between the different fluid compartments (Figure 1.1 on page 3). Here we will take a closer look at water transport across the BBB. Water crosses the layers of the BBB by several different mechanisms.

Water can diffuse directly through the lipid bilayer membranes of the BBB cell layers. As outlined above, it is generally accepted that water diffusion is driven by osmotic and hydrostatic gradients and limited by the intrinsic water permeability of the membranes. This traditional view is being challenged, as recent studies have shown that water can be transported against its osmotic gradient by co-transport with other molecules (see below) [30]. The intrinsic water permeability of CNS membranes that do not contain water channels is unknown. In general, water permeability of biological membranes differ, and some, like the apical membrane epithelial cells of the thin ascending loop of Henle, are virtually impermeable [97].

Water can follow hydrostatic and osmotic gradients through bidirectional water channels across the BBB. This is dependent on the presence of water channels in the membranes. AQP4 water channels are concentrated in perivascular astrocytic endfeet [98], but also present in endothelial cells [99]. However, endothelial cells in brain, in contrast to other organs, lack AQP1 [27]. It is important to note that not all the anatomical layers of the BBB contains AQP4 water channels [27]; they are primarily localized in the astrocytic endfoot membranes facing blood vessels.

Water can be co-transported along with other molecules such as electrolytes, amino acids, glucose, or lactate through their designated transporter proteins. This transport of water occurs through both uniports or cotransporters [100]. This is believed to be an important mode of water transport, particularly in the non-endfoot region of the astrocyte, which faces neuropil and synapses [30]. Although supposed to be less important in the AQP4-rich astrocytic endfeet

abutting the BBB, these mechanisms merit a more thorough discussion, because it offers us a broader perspective on astrocyte water dynamics.

Compared to the perivascular endfoot membrane, AQP4 is relatively scarce in the perisynaptic parts of the astrocyte membrane [98]. The latter contains transporter molecules which maintain homeostasis in the synapse. During neuronal activity, the synaptic cleft is flooded with transmitters, potassium and other substances from the pre- and postsynaptic neurons. A priori, the osmotic gradients created should favor water flux into the synaptic cleft during neuronal activity. Surprisingly, a study performed three decades ago revealed that the ECS actually shrinks in volume during neuronal activity [28]. The shrinking of ECS is a robust finding, estimates vary from 4-30%, depending on the mode of stimulation, preparation type, and area under investigation [28, 101–103].

For the ECS volume in the synaptic cleft to be reduced during neuronal activity, water has to flow out of the ECS. Hence, water must be transported *against* its osmotic gradient. This can not be achieved by passive, bidirectional water channels. Specific transporter proteins moving substances out of the synapse following neuronal activity carry a fixed amount of water molecules per transported molecule [30]. This way, water can move against its osmotic gradients.

Considering the astrocyte as a whole, several transporters have been shown to be capable of this "uphill" water transport; the K^+/Cl^- cotransporter, KCC [104, 105], the $Na^+/K^+/2Cl^-$ cotransporter, NKCC1 [106], the glucose cotransporter, SGLT1 [107–113], the glial glutamate transporter, EAAT1 [114], the GABA transporter, GAT-1 [115], the monocarboxylate transporter 1, MCT-1 [116–118] and the dicarboxylate transporter 1, NaDC-1 [119].

Focusing again on the BBB, the question presents itself: which proteins contribute significantly to the water permeability? A variety of water-transporting transport proteins are expressed in one or both of the endothelial membranes and in the astrocytic endfoot. Notably, the glucose transporter 1 (GLUT1), NKCC1 and MCT1 may be involved in water homeostasis [30,120]

Finally, water can follow macromolecules across the interior of cells via receptor-mediated transcytosis, a phenomenon characterised by an invagination of the plasma membrane following receptor stimulation on the cell surface [7]. This is the mode of transport for insulin. Another mechanism is adsorptive transcytosis, in this case low-volume invaginations of the cell membrane occur independent of receptor-stimulation, and water follows along with albumin and other plasma proteins before subsequently being released on the contralateral side of the cell [7].

Moving from blood to brain, the last anatomical component for water to cross is the perivascular astrocytic endfoot. In the endfoot, membrane transporter proteins like AQP4 are anchored to the interior of the cell by anchoring molecules [121]. These are scaffolding proteins associated with the plasma membrane and the cytoskeleton. They constitute a framework which holds membrane transporters within their intended membrane domains and prevent them from moving freely in the phospholipid membrane plane. This is thought to be an important mechanism for maintaining cell polarization.

It should be emphasized that we do not know the relative contributions of the various water transport mechanisms. To cross all layers of the BBB, any individual water molecule can utilize all the above modes of transport.

1.5 Anchoring of aquaporin-4

Polarized expression of transporter molecules in specific domains of the cell membrane is dependent on two things. First, the transporter must get to the designated membrane domain. Second, it must be prevented from leaving. Membrane proteins can by default move freely within the plane of the lipid bilayer membrane. To stay in one place they need anchoring. Anchoring proteins contribute to maintaining the position of transporters in specific membrane domains.

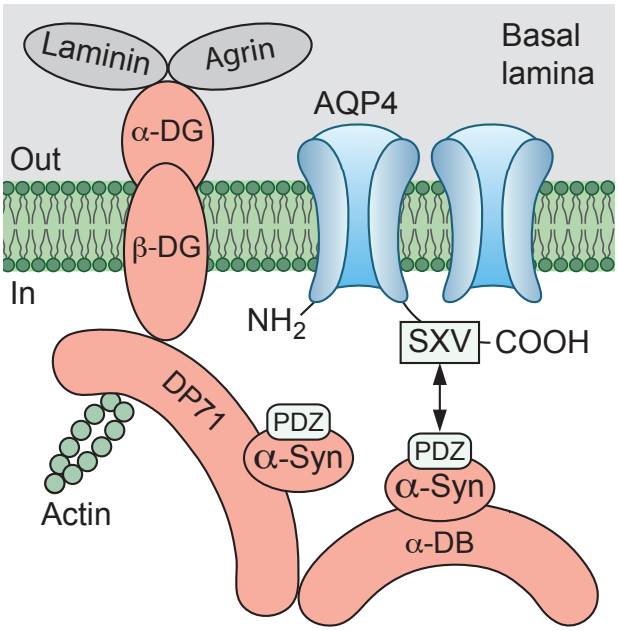

Figure 1.9: Diagram of the dystrophin-associated protein complex (red) in the membrane of an astrocytic endfoot. Note the relationship between the anchoring molecules dystrophin (DP71) and α-syntrophin. AQP4 (blue) is linked to α-syntrophin at its PDZ-domain (red). AQP4 is dependent on α-syntrophin for normal expression and localization. G. A. Gundersen.

Loss of glial polarization is a feature of a number of diseases, including temporal lobe epilepsy, Alzheimer's disease, stroke, trauma and glioblastoma [122–128]. Loss of polarity implies loss of normal function. This section will introduce the anchoring proteins known to be associated with AQP4: dystrophin and the dystrophin-associated protein complex (DAPC), in particular α-syntrophin.

1.5.1 Dystrophin and the DAPC

1.5.1.1 Description

Dystrophin is a key component of the DAPC (Figure 1.9 on the previous page), a multiprotein complex located near the plasma membrane. The DAPC is known to be important for anchoring membrane proteins in skeletal muscle and other tissues, e.g. in the brain. The individual proteins in the DAPC are interdependent on proper polarization and localization. The dystrophin gene is the largest gene known in man, making up 1,5% of the X-chromosome. The dystrophin protein comes in a variety of isoforms that are expressed in various degrees in different cells and tissues. The dystrophin isoform expressed in astrocytes is DP71 [129].

1.5.1.2 Role in pathophysiology

Defects in the DAPC are associated with a group of diseases called muscular dystrophies. Loss of dystrophin causes Duchenne muscular dystrophy, a severe X-linked disorder characterized by muscle degeneration, cognitive deficits [130] and an abnormal electroretinogram [131]. The cognitive impairment seen in these patients are associated with mutations in the gene coding for the brain isoform of dystrophin, DP71 [132]. Loss of dystrophin is correlated with an upregulation of utrophin, a dystrophin-related peptide [133, 134]. This could be a compensation mechanism to preserve dystrophin function.

A milder disease variant than Duchenne is Becker's muscular dystrophy, in which dystrophin is expressed, but in insufficient amounts, producing milder symptoms.

1.5.2 α-Syntrophin

1.5.2.1 Description

The anchoring molecule α-syntrophin is localized in the plasma membrane of the astrocytic endfoot. It is a member of the DAPC and one of five members of the syntrophin family. All syntrophin isoforms express two PDZ domains and a unique C-terminal region which can bind to different proteins and subsequently generate functional protein complexes (Figure 1.9 on the preceding page) [135, 136]. In general, it is important for correct localization of other proteins within the cell membrane. Several studies have mapped out these relationships in more detail. α-Syntrophin is required for proper polarized expression of AQP4 to the perivascular astrocytic endfoot [137]. It is also necessary for proper localisation of the scaffolding proteins dystrophin, γ2-syntrophin and α-dystrobrevin-2, being itself dependent on the latter for proper localization [138, 139].

1.5.2.2 Role in pathophysiology

Studies on α-syntrophin knockout mice have shown a loss of polarization of AQP4 in astrocytic endfeet in brain. In endfeet facing the pial surface the reduction was 50%, and in endfeet facing capillaries the reduction was 90% [99], suggesting different anchoring mechanisms in these two subtypes of endfeet. There is no specific pathological phenotype associated with loss of α-syntrophin.

Having introduced the main anchoring molecules of AQP4, we will now turn to the water channel itself, exploring it in more detail.

1.6 Aquaporin-4

1.6.1 Description

AQP4 is one of thirteen known aquaporins and aquaglyceroporins (Table 1.2 on the next page) [140]. AQPs are present in a variety of tissues and cell types. For many years it was assumed that cell membranes were freely permeable to water. During the 1960s through the 1980s, following up on biophysical studies of the water permeability of erythrocytes and kidney tubules, evidence of different permeabilites between cell types emerged. The differences were consistent with a pore-like mechanism. The first identification of an aquaporin (AQP1) was reported in 1992 [141]. Subsequent research in the field has flourished. Propelled by the assumption that aquaporins are key players in brain water transport, and thus a key player in serious brain conditions such as brain edema, the idea of AQP4 as a therapeutic target emerged.

AQP4 is the predominant water channel in the brain and in the basolateral membrane of principal collecting duct cells in the kidney. It is particularly abundant at brain-fluid interfaces as the BBB and the ependymal-CSF barrier.

1.6.1.1 Molecular and supramolecular structure

AQP4 exists in three functional isoforms, and studies in oocytes have shown that they have different unit water permeability [142]. M23 is the prevalent isoform in the mammalian brain [143]. AQP4 is expressed in the plasma membrane of astrocytes, supportive cells in tissue containing electrically excitable cells such as neurons, olfactory epithelial cells, sensory hair cells of the inner ear, and bipolar cells in the retina. The ~30kDA AQP monomer is made of six membrane-spanning helical domains and two short helical domains. In the middle is a narrow water pore of ~25Å (1Å=0.1nm). Four monomers combine into tetramers in the cell membrane. In the middle of the tetramer is a central pore. AQP4 tetramers further assemble into supramolecular square arrays, also called orthogonal arrays of particles (OAPs) [140, 144]. Freeze-fracture analysis has estimated that square arrays, composed of AQP4, span as much as 50% of the surface area of astrocytic endfeet [98, 145]. Given that astrocytic endfeet cover more than 99% of the capillaries [24], it is fair to assume that AQP4 has a crucial role in brain physiology.

Protein name	Aquaporin-4
Gene	*Aqp4*
Gene location, human	Chr 18: 22.69-22.7 Mb
Isomers	M1, M23, Mz
Size	323 (M1), 301 (M23) and 364 (Mz) amino acids
Subunit	Homotetramer
Tissue expression	CNS, kidney, skeletal muscle
Subcellular location	Membrane, multi-pass membrane protein
Function	Water conduction through plasma membranes

Table 1.2: Aquaporin-4 (www.genecards.org)

AQP4 plays a prominent role in a variety of pathophysiological conditions, and this is where the major breakthroughs in our understanding of the water channel have been made. However, research on the physiology of AQP4 has made slower progress. Until now, investigators have yet to establish a plausible main physiologic function of AQP4 in brain. In the following we will look at what is known of AQP4's role in physiology and then turn to roles of AQP4 in the pathophysiology of different conditions.

1.6.2 Physiologic function of AQP4 in brain

In cells expressing AQPs in the plasma membrane, the permeability of water increases 5-50 fold compared to cells lacking AQPs [146]. Aquaporin-4 (AQP4) is one of the most abundant molecules in brain and is particularly prevalent in astrocytic membranes at the blood-brain and brain-liquor interfaces. Only recently has evidence accumulated to suggest that AQP4 is involved in such diverse functions as regulation of extracellular space volume, potassium buffering, cerebrospinal fluid circulation, waste clearance, neuroinflammation, osmosensation, cell migration, and Ca2+ signaling. In the absence of a selective AQP4 inhibitor, our knowledge of AQP4 is largely based on experiments on knockout mice.

In *Aqp4* knockout mice there is evidence of reduced seizure threshold, prolonged seizure activity [147] and impaired olfaction [148], hearing [149], and vision [150].

AQP4 could play a role in K^+ clearance from the synaptic cleft following neuronal activity. K^+ is cleared by glial cells by several mechanisms, the main transporter proteins being the NKCC1, Kir4.1 and the Na^+K^+ ATPase [31]. It was previously hypothesized that AQP4 could facilitate potassium-buffering during neuronal activity, given its co-localization with the potassium channel Kir4.1 [93]. Neurons release K^+ when generating an action potential. It has been suggested that astrocytes remove K^+ from the extracellular space and distribute it to distant sites through "siphoning" mechanisms [93]. Water follows the osmotic gradient created by this clearance, leading to a shrinkage of the extracellular space. This in turn maintains the gradient for K^+ by maintaining a high extracellular concentration compared to the interior of the astrocyte. Although data supporting this hypothesis exists, it remains controversial [147, 151–156]

That AQPs could be involved in cell migration and motility was proposed after AQP1-null mice showed impaired tumor angiogenesis [157]. Later it was shown that astrocytes in brain expressing AQP4 had increased migration towards a chemotactic stimulus [158]. The mechanism underlying this increased motility is unknown. One hypothesis is that an osmotic gradient is created at the leading edge of a astrocytic process pulling water in from the extracellular space

to the migrating leading edge. This, however, has yet to be proven, and other mechanisms have been proposed.

Studies in oocytes expressing both AQP4 and the vasopressin receptor $V1_aR$ have shown that vasopressin-induced activation of $V1_aR$ was followed by a substantial reduction in cell water permeability. This indicates that AQP4-mediated water permeability might be partly regulated by vasopressin. The reduced permeability seemed to be effected by $V1_aR$-dependent internalization of AQP4 [159].

AQP4 has been shown to regulate ECS volume during neuronal activity, presumably by facilitating water flux in response to changes in extracellular concentrations of ions and transmitters [160].

Despite its abundance at the BBB, it is generally believed that the most important physiologic role of AQP4 is yet to be determined, and there is a need for new studies to pursue this.

1.6.3 Role in pathophysiology

1.6.3.1 AQP4 in brain edema

Brain edema is a feared complication of brain disease, seen in conditions like ischemic stroke, brain tumor, bacterial meningitis, or head trauma. It is characterized by water accumulation in the brain. Based data from the World Health Organization from 2004, stroke is currently the second leading cause of death in the Western world, ranking after heart disease and before cancer. The pathophysiology of stroke is complicated, but one of the lethal complications is brain herniation due to brain edema and high ICP. Reducing the development of brain edema would greatly reduce the mortality in ischemic stroke and improve the prognosis for patients afflicted.

There are two main types of brain edema: cytotoxic and vasogenic. In cytotoxic brain edema there is a leakage of intracellular osmolytes into the extracellular space. This can be due to excess hypo-osmotic stress or ischemic stroke [161]. The osmotic gradient that develops pulls water from the circulation into the brain. This in turn leads to high ICP and risk of brain herniation, a potentially lethal condition. Mice lacking AQP4 show reduced mortality and reduced water accumulation compared with wild-type mice in models of cytotoxic edema. The current concept is that lack of AQP4 protects the brain by decreasing water permeability over the BBB [162].

In vasogenic edema water enters the brain due to a leakage in the BBB. The excess water exits via the AQP4-rich astrocytic endfeet in the glia limitans towards the subarachnoid space and to a lesser degree over the BBB in capillaries. Vasogenic edema is seen in obstructive hydrocephalus, brain tumors, brain abscesses, or in experimental models of intraparenchymal water infusion. In models of vasogenic edema, mice lacking AQP4 show worse outcomes and increased mortality compared to wild-type mice. In contrast to the situation in cytotoxic edema, in vasogenic edema the lack of AQP4 worsens the condition by decreasing the water permeability over the brain-fluid interfaces, functionally obstructing the outflow of surplus water [163, 164].

Aqp4 knockouts seem to have the same effect in the spinal cord as in the brain in cytotoxic [165] and vasogenic [166] edema, respectively.

1.6.3.2 AQP4 in neuroinflammatory disease

Astrocyte expression of AQP4 has been shown to be altered in inflammatory diseases of the brain. Studies have shown increased AQP4 expression in human multiple sclerosis [167, 168], whereas in neuromyelitis optica (NMO) it was reduced [168]. Another study showed that the polarized expression pattern was lost along with the organisation of AQP4 in OAPs in autoimmune encephalomyelitis [169].

NMO is an autoimmune inflammatory disease in which antibodies are produced against AQP4 in the host cells [170]. NMO-like lesions have been reproduced by passive infusion of AQP4-antibodies in animal studies [171]. The optic nerve and the spinal cord are most commonly affected. The lesions differ from those seen in multiple sclerosis, as do prognosis and optimal treatment. NMO can also affect the brain. The main symptoms come from loss of function of the spinal cord or the visual system. Patients have varying degrees of visual disturbances, blindness, weakness or paralysis in the extremities, loss of sensation and/or bladder, and bowel dysfunction. Main treatment is high-dose intravenous corticosteroids, and when resistant to medical therapy, plasmapheresis.

1.6.3.3 Alzheimer's disease and fluid transport

Alzheimer's disease is a serious neurodegenerative disease leading to gradual cognitive impairment and dementia. Cause and progression of the disease are not well understood. Studies have shown that neurodegenerative processes are associated with atrophy of astroglia, and at later stages of disease, later stages, astrocytes become activated and contribute to the neuroinflammatory component of neurodegeneration [172]. Alzheimer's disease is associated with increased levels of amyloid-β in the CNS. Amyloid-β is created by cleavage of the amyloid precursor protein (APP) [173]. Amyloid-β exists in two forms, as a solute and as aggregates called neurofibrillary tangles. The fibrils form plaques in the CNS parenchyma. There are several theories that try to explain what the main pathological process in Alzheimer's disease really is. The amyloid hypothesis states that deposition of amyloid-β leads to the accumulation of neurofibrillary tangles, neuronal loss, and ultimately dementia [174].

Turnover of amyloid-β in the CNS is high, approximately 8% per hour [175]. Even modest increases in production or decreases in clearance will lead to accumulation and deposition of amyloid-β in the brain. Effective clearance is dependent on adequate transport systems.

There are two main mechanisms for removal of amyloid-β from the brain: efflux of the soluble form into the peripheral circulation and enzymatic cleavage of both the soluble and the fibrillar form [176]. The main known receptors for amyloid-β transport from brain to blood and vice versa are the low-density lipoprotein receptor related protein-1 (LRP1) [177]. LRP1 facilitates transport of amyloid-β across the BBB from brain to blood. In the blood plasma, a soluble form of LRP1, sLRP1, acts as a "sink" and binds 70-90% of plasma amyloid-β peptides. In Alzheimer's disease patients the level of sLRP1 is reduced and the free fraction of amyloid-β in plasma increased [177].

The treatment options for Alzheimer's disease spans wide, from symptomatic treatment to molecular transportation aids as described above. This is an attractive field of research from both a medical, pharmaceutical and public health perspective. Given that the amyloid hypothesis is correct, there is much value to be gained in a thorough understanding of the clearance of amyloid-β.

Immunotherapy has been developed in which anti-amyloid-β is administrated. The antibodies bind amyloid-β in blood plasma and brain and facilitates its transportation across the BBB and away from the CNS, thus mimicking the action of sLRP1 [177].

Regardless of whether amyloid-β is cleared from the brain parenchyma as a solute bound to native proteins, or bound to drugs, removal from the brain is ultimately dependent on fluid transport. Hence, if it is dependent on fluid transport, it is dependent on water transport across brain fluid compartments. This opens up the possibility that AQP4 could be involved in clearance of amyloid-β and thus of importance in Alzheimer's disease. Interestingly, a study performed on the tg-ArcSwe mouse model of Alzheimer's disease shows that astrocytes lose their polarized expression pattern of AQP4 [125]. In endfeet in close proximity of the perivascular plaques, the AQP4 is redistributed both by a reducted expression in the perivascular endfeet and an increased expression in the astrocytic processes in synaptic regions [125].

1.6.4 AQP4 as a potential target for therapy

We have seen how AQP4 plays a central part in worsening or improving the outcome of disease, depending on the pathophysiological mechanism in play. After observing these disease-modulating effects, the scientific community has become excited about whether drugs could be produced to enhance the beneficial effects of AQP4 in disease [178, 179]. Perhaps the most obvious scenario in which to apply a drug is to use an AQP4-inhibitor during the acute phase of ischemic stroke, to limit development of brain edema. Importantly, if a safe AQP4 inhibitor is to be developed, we need both a profound theoretical knowledge of the molecular mechanisms in action, a drug design that yields efficient drug distribution in the target tissue and a thorough analysis of possible side-effects.

It should be emphasized that this approach to treatment is based on manipulation of water fluxes, hence it will also be important to assess and quantify the water transporting capabilities of other proteins to expand the range of potential therapeutic targets.

1.7 Unresolved issues

Molecular organization in the astrocytic endfoot is a relatively young field of study in neuroscience. There are high hopes that this line of research in the long term can lead to new therapies for serious diseases.

Brain water transport is important in pathophysiology of disease, but the mechanisms are poorly understood on the molecular level. In spite of years of intense effort, a drug that inhibits AQP4 *in vivo* has still not been developed. Nevertheless, promising results have emerged and drugs have been shown to inhibit AQP4 water transport *in vitro* [180]. In the meantime, there are a myriad related problems remaining to be solved. A subject of ongoing debate is the physiological function of AQP4. This key function is still not believed to be clear. What is the likely role of a molecule this abundant, located in such a strategically important position in the neuron's supply chain of nutrients? One study supports the hypothesis that AQP4 is involved in gas exchange via its central pore [181]. Data from our group supports the hypothesis that AQP4 balance electrolyte concentration changes by regulating the volume of perisynaptic extracellular space [160].

At the molecular level there are important unanswered questions regarding AQP4. How is it anchored? We do know that both dystrophin and α-syntrophin are involved [135, 182], but a direct interaction between AQP4 and DAPC molecules has not yet been demonstrated. Thus, it is likely that hitherto unknown anchoring molecules participate. One of these unknown anchoring molecules could be the drug target or genetic target of choice in medical treatment of disease. The astrocytic endfoot is certainly rich in AQP4, but could there also be subdomainal differences in AQP4 abundance? These are intriguing questions to pursue.

On a macroscopic level is the question of how AQP4 affects brain fluid dynamics. It might be that the true purpose of AQP4 water transport action is hidden from the observers when studied up close on a molecular level. A broader "bird's eye" view of the fluid transport in the CNS as a whole might be a more appropriate perspective. Water flux is a major exit route for substances in the brain. It would be interesting to address whether AQP4 is so important for water transport that loss of it leads to accumulation of unwanted substances. And if this is the case the next question would be whether the substances are accumulated in amounts necessary for disease development, parallel to the build-up of amyloid-β in Alzheimer's disease.

There are multiple interesting threads to follow. We embarked on the issues we found most compelling and had the appropriate methods to explore.

1.8 Aims of studies

The overriding aim of this work was to better understand water transport in the brain and, in particular, the precise distribution and roles of AQP4. We wanted to study the subject of anchoring mechanisms of AQP4, using our tools for precise identification and localization of membrane proteins on the subcellular level. This section will present the aims of our individual studies by giving a short clarifying explanation and then the plain scientific hypotheses.

1.8.1 Paper I

1.8.1.1 Aims

AQP4 is unevenly distributed in the cell membrane of astrocytes, a group of supporting cells in the brain. This is known as polarization. The aim of this study was to get a better understanding of the mechanisms underlying this AQP4 polarization in brain and retina. We also wanted to clarify the importance of specific anchoring molecules for correct AQP4 polarization in macroglial membrane domains.

1.8.1.2 Hypotheses

H1: Dystrophin expression in perivascular endfeet is equal in brain and retina.

H2: α-Syntrophin expression in perivascular endfeet is equal in brain and retina.

H3: AQP4 polarization in brain and retina is equally dependent on dystrophin.

H4: AQP4 polarization in brain and retina is equally dependent on α-syntrophin.

1.8.2 Paper II

1.8.2.1 Aims

AQP4 polarization in the endfoot is defective in animals that lack pericytes. In paper I we showed that AQP4 is enriched in perivascular astrocytic endfeet facing capillaries. However, we noticed that AQP4 seemed to be even more clustered in membrane regions facing pericytes. Are pericytes influencing the polarization of the endfoot? The aim of this study was to assess whether or not the expression of AQP4 differed between endfoot subdomains. We also wanted to test whether the pericyte affects polarization of AQP4 anchoring molecules, such as α-syntrophin.

1.8.2.2 Hypotheses

H1: AQP4 is equally distributed in the astrocytic endfoot membrane subdomains facing endothelial cells and pericytes in WT mice.

H2: α-Syntrophin is equally distributed in the astrocytic endfoot membrane domains facing endothelial cells and pericytes in WT mice.

H3: α-Syntrophin expression in the astrocytic endfoot membrane is not different in the WT and *Aqp4* knockout genotypes.

H4: If H3 are false, α-syntrophin expression is not different in astrocytic endfoot subdomains facing endothelial cells and pericytes in *Aqp4* knockout mice.

1.8.3 Paper III

1.8.3.1 Aims

We wanted to characterize AQP4 expression at the BBB and to resolve whether glial endfeet and their AQP4 water channels actually regulate water transport between blood and brain. By trying to establish a new glial-conditional $Aqp4^{-/-}$ mouse line and use this and a global $Aqp4^{-/-}$ mouse line we also aimed to resolve the controversy concerning whether AQP4 is expressed in endothelial cells.

1.8.3.2 Hypotheses

H1: Part of the perivascular pool of AQP4 is located in endothelial cells.

H2: Deletion of perivascular pool of AQP4 has no effect on water accumulation in brain during hypo-osmotic stress.

H3: Deletion of perivascular pool of AQP4 has no effect on brain reabsorption of water in the early postnatal period.

H4: Deletion of perivascular pool of AQP4 leads to increased permeability of the BBB to large macromolecules.

1.8.4 Paper IV

1.8.4.1 Aims

This study was partly inspired by the results of paper III, in which we showed that water accumulates in mice lacking AQP4. Given the unfortunate situation of excess interstitial water seen in pathological conditions such as brain edema, the question arose, how does water and other superfluous waste products leave brain tissue? Does AQP4 play a role in this?

1.8.4.2 Hypotheses

H1: CSF does not enter the brain from the ventricular compartment.

H2: CSF does not enter the brain from the subarachnoid compartment.

H3: CSF does not follow paravascular pathways along large arterioles to penetrate into deeper into the brain parenchyma.

H4: CSF does not migrate from the paravascular space to the interstitial space of brain parenchyma.

H5: Interstitial fluid in brain parenchyma is not transported to the cortical surface via a paravascular pathway along venules and veins.

H6: Increasing parenchymal resistance to fluid flux by the global knockout of the *Aqp4* gene does not alter CSF flux through the interstitium.

H7: If there is a transparenchymal CSF flux, it does not aid in the clearance of fluid and solutes from the brain interstitium.

H8: If there is a transparenchymal CSF flux, it does not aid in the clearance of amyloid β from the brain interstitium.

2. Materials and methods

This chapter will describe the methods used by the author when contributing to the studies in the thesis. The other methods used in the studies is described in detail in the respective papers.

2.1 Methods to study astrocytic endfoot proteins

We used two different imaging modalities of immunocytochemistry. The immunofluorescence method and confocal microscopy are used to study protein distribution on a cellular and regional level. Proteins can be localized to specific cell-types and within a limited area of interest, e.g. the cerebral cortex. To study subcellular distribution we use preembedding immunohistochemistry and postembedding immunogold cytochemistry combined with electron microscopy.

2.1.1 Immunofluorescence microscopy

2.1.1.1 Description

Immunofluorescence microscopy provides the ability to detect the location and relative abundance on a cellular level of any protein for which you there is an antibody. While conventional light microscopy is useful for describing micro anatomical structures, immunofluorescence can show the distribution of specific proteins within those structures. We used indirect immunofluorescence, meaning that two antibodies are involved. A primary antibody is linked to the target-protein. Subsequently, a secondary antibody covalently attached to a fluorescent dye binds to the primary antibody. Exposed to light, the fluorescent dye emits light and is visualized and photographed in the confocal microscope. We can study several proteins in the same experiment by using multiple different primary and secondary antibodies. The immunoreactivity in immunofluorescence microscopy is superior to postembedding immunogold cytochemistry.

2.1.1.2 Limitations of immunofluorescence microscopy

Antibodies are notoriously unspecific. Although they are designed to target specific epitopes in the protein of interest, sometimes the fixation process crosslinks proteins of interest to neighboring molecules, creating false positive or false negative results due to unspecific binding. We addressed this potential problem by including knockout-mice lacking the protein of interest as negative controls in the experiments.

A common problem with fluorescence techniques is photobleaching, which is the photochemical destruction of a fluorophore. The light needed to stimulate the fluorophore is also destructive to it at high intensities or prolonged periods of illumination. The time available to study the section is limited by this process. This issue is, however, not a major concern in our studies. Most sections are thoroughly analyzed and photographed in less time than what is needed for fluorophore dysfunction.

2.1.2 Electron microscopy

The study of proteins on the subcellular level requires a method for visualization and imaging that conventional microscopy or immunofluorescence microscopy can not provide. Modern electron microscopy combined with high-resolution cameras and imaging software can provide this resolution [183, 184]. The method can localize target-proteins down to an error margin of 17 nm [183]. Nevertheless, membrane proteins are to small to show directly, so for proper visualization they must be linked to something big enough and with sufficient electron density to be visible in the electron microscope.

2.1.2.1 Semi-quantitative postembedding immunogold cytochemistry

The principal experimental procedure used by the author in this work is postembedding immunogold cytochemistry. Brain tissue is fixated, embedded in resin polymers for structural integrity and cut in thin slices appropriate for electron microscopy. A primary antibody is linked to the target-protein. Subsequently, a secondary antibody connected to a gold particle binds to the primary antibody. The gold particle is electron-dense and can easily be visualized in the electron microscope and photographed. Every gold particle represents a molecule of the target protein. Images are analyzed digitally followed by a statistical analysis to get a numerical value of the density of target-protein in different parts of the cell membrane. This section will cover the details of the procedure, from tissue preparation to the final analysis of data.

2.1.2.1.1 Tissue preparation

Animals were anesthetized by an intraperitoneal injection of a mixture of chloral hydrate, magnesium sulphate, and pentobarbital (142, 70, and 32 mg/kg, respectively). Absence of interdigital reflexes was assured before commencing perfusion. Retinas and brains were fixed by transcardiac perfusion of fixative (~10 ml/min) [185]. The first 0.2% dextran (MW 70,000) in phosphate buffer (15 sec) was used to flush the blood out of the vasculature. The mice were then fixed with a so-called pH-shift protocol [186]. This is a method that enables relatively good morphology without using glutaraldehyde, which is a major advantage as formaldehyde fixation preserves immunoreactivity to a much higher degree than glutaraldehyde [186]. It involves the use bicarbonate-buffered 4% formaldehyde, pH 6.0, followed by 4% formaldehyde, pH 10.5 (0.2% picric acid was added to both solutions). The low pH in the first solution prevents polymerization of the formaldehyde, and thus enables better penetration and distribution of the fixative. When the pH is increased by the second solution, the polymerization process starts and the tissue fixates quickly [186]. Neck stiffness was acquired within 90 sec after thoracotomy, indicative of successful fixation. If the morphology was unacceptable, the alternative to the pH-shift protocol was fixation by 0.1% glutaraldehyde at pH 7.4. As outlined above, the trade off by using glutaraldehyde is losing immunoreactivity.

For immunogold cytochemistry, small blocks of the eyecup and the parietal cortex were subjected to freeze substitution and infiltration in Lowicryl HM 20 resin (Polysciences Inc., Warrington, PA, Cat 15924), before labeling with primary and secondary antibodies, as described previously [184, 187].

1. Small blocks of the eyecup and parietal cortex were cryoprotected by immersion in increasing concentrations of glycerol in phosphate buffer: 10% (0.5 h), 20% (0.5 h), and 30% (overnight, 4°C).
2. They were then placed on a specimen pin and plunged into propane holding -170°C, cooled by liquid nitrogen in a cryofixation unit.
3. The specimens were then transferred to 1.5% uranyl acetate dissolved in anhydrous methanol (-90°C) in a cryosubstitution unit (AFS; Reichert, Vienna, Austria). After 30 h, the temperature was raised stepwise by 4°C per hour to -45°C.
4. The samples were then washed three times with anhydrous methanol.
5. Sections were infiltrated with Lowicryl HM 20 resin (Polysciences Inc.) at -45°C by adding the following solutions: (a) Lowicryl/methanol in 1:1 ratio for 2 h; (b) Lowicryl/methanol in 2:1 ratio for 2 h; (c) Pure Lowicryl for 2 h; (d) Pure Lowicryl overnight. The Lowicryl was then changed to freshly prepared resin and the capsules (Reichert) with the specimens were moved to Lowicryl-filled gelatin capsules in the G-chamber.
6. The capsules were then transferred to a container filled with ethanol, and then polymerized with UV light. The process starts at -45°C for 24 h, and then the temperature is increased by 5°C per hour to a final temperature of 0°C.

2.1.2.1.2 Incubation

Sections were cut with a ultramicrotome (Reichert). Semi-thin sections of 500 nm were cut with a glass-knife for light microscopic morphologic analysis. This enables the investigator to recognize the area of interest, e.g. the cerebral cortex. Ultrathin sections of 80-100 nm were then cut with a diamond knife, mounted on nickel grids, and processed for immunogold cytochemistry [188]. The sections were incubated sequentially in the following solutions at room temperature:

Day 1:

1. 50 mM glycine in Tris buffer (5 mM) containing 0.1% Triton X-100 and 50 mM NaCl (TBST) for 10 min: to bind free aldehyde groups from fixation.
2. Blocking solution, e.g. 0.2% milk powder in TBST for 10 min: to prevent unspecific binding of IgG.
3. Primary antibody (e.g. anti-AQP4, 1 μg/ml; anti-α-syntrophin, 12 μg/ml) diluted in the solution used in the preceding step, to label the protein of interest. Incubated overnight.

Day 2:

4. Rinsing in TBST in following sequence: 3 short dips, 10 min of incubation, followed by 3 short dips and 10 min of incubation
5. Same solution as in step 2 for 10 min, to prevent unspecific binding of IgG.

6. Gold-conjugated secondary antibody (AQP4, 15 nm particles; Syn259 (the primary antibody for α-syntrophin), 10 nm particles) diluted 1:20 in TBST containing milk powder (0.2%) and polyethylene glycol (0.5 mg/ml) for 2 h to prevent unspecific binding and clumping of gold particles.
7. Gentle rinsing in distilled water: 6 brief dips. The sections were then dried.
8. First contrasting step by immersion in 5% uranyl acetate in 40% ethanol for 90s and then rinsing briefly 3 times in distilled water and dried to visualize membranes.
9. Second contrasting step by immersion in lead nitrate for 90s then rinsing briefly in distilled water and dried to visualize cellular and tissue components.

2.1.2.1.3 Evaluation

The sections were then examined in a FEI Tecnai 12 transmission electron microscope (FEI Company, Hillsboro, OR). Wild-type and AQP4 knockout tissue were included in all experiments for positive and negative controls. In all projects, all tissue used for quantification and analysis originated from one experiment. The investigators were blind to section genotypes at all times.

2.1.2.1.4 Quantification

The number of animals included from each genotype differed between studies. Images were taken from each animal and analyzed. Digital images were acquired with commercially available image analysis software (analySIS; Soft Imaging Systems GmbH, Münster, Germany). We used a version of the program called IMGAP that is custom-made for acquisition of high-resolution digital images [189] and to enable semiautomatic quantification of immunogold-labeled membranes [190, 191].

To analyze density of gold particles along a membrane, images of membrane segments were recorded at a nominal magnification of 34,000-46,000 in 1376 x 1032 (8-bit) images. All membrane segments were collected from Müller cell endfeet in the outer plexiform layer of the retina or astrocytic endfeet in the parietal cortex. Endfoot membranes facing pericytes were analyzed separately, but were merged in the final analysis, as there at the time was no apparent difference in labeling intensity compared to endfeet facing endothelium.

Membrane segments of interest were drawn in the overlay and assigned a type label. Gold particles in close proximity (23 nm; maximal theoretical distance of antibody-gold particle-complexes) of each membrane curve were detected semi-automatically, and the program calculated the distance between the centre of gravity of each particle and its membrane curve. This distance was used to exclude non-membrane-associated particles in the subsequent calculations.

Density was measured in number of particles per unit length of membrane (linear density of particles).

All images, with associated curves, particles, and measurements, were saved to allow later verification and correction. Before unblinding, data quality was assured by evaluating outliers, i.e. extreme values in gold particle linear density. Further analyses were done in analySIS and SPSS (SPSS Inc., Chicago, IL).

For membrane types with low labeling density, short segments will frequently show zero or very low particle density. To control for this phenomenon in the statistical analysis, the total number of gold particles associated with all membrane domains of one type was divided by total membrane length analyzed. We found that this did not alter the statistical analysis significantly; hence the original data was used.

2.1.2.1.5 Statistical model and analysis

The following is a detailed description of the mixed model statistical method used specifically for the quantitative analysis of immunogold experiments. It is fairly complex due to variation on several levels in the data hierarchy. Our data varies both between genotypes, between individuals within genotypes and between blood vessels within an individual animal. Statistical expertise associated with our group aided in the choice of statistical method after a thorough exploratory data analysis. Other statistical methods are described in the respective papers.

We let Y_{ijk} be count measurements for section (animal) i, membrane (ROI) j and image k. The sections were divided into groups of different genotypes. The observed counts were modeled by a Poisson mixed model

$$\begin{aligned} Y_{ijk}|u_i, v_{ij}, w_{ijk} &\sim \text{Poisson}(\lambda_{ijk}) \\ \log(\lambda_{ijk}) &= \log(\text{RSeLen}_{ijk}) + \mu + \beta_j + \gamma_{jg(i)} + u_i + v_{ij}. \end{aligned} \tag{2.1}$$

Here, g_i is the genotype of section i and μ, β_j and γ_{jg} are fixed effects, where μ is the intercept (the expected value when genotype and membrane are equal to their reference values (depending upon the analysis)). Furthermore, β_j represents the difference between membranes, and γ_{jg} represents the difference between genotypes for different membranes. In a second analysis, we let β represent difference between genotypes and γ the difference between membranes for different genotypes. The segment length RSeLen_{ijk} was included in the model (as an offset) to take into account that the expected count λ_{ijk} is proportional to RSeLen_{ijk}. The random effect u_i represents variation between sections, the term v_{ij} represents variation between membranes (inside sections), while w_{ijk} represents the variations inside membranes. The terms u_i, v_{ij} and w_{ijk} have the following distributions

$$u_i \sim \mathcal{N}(0, \sigma_u^2),\ v_{ij} \sim \mathcal{N}(0, \sigma_v^2),\ w_{ijk} \sim \mathcal{N}(0, \sigma_{w,j}^2)$$

We allowed the residual term $\sigma_{w,j}^2$ to vary between membranes. The chosen model structure was based on likelihood ratio tests.

The fixed effects and variances of the random effects were estimated by the R function glmer in the lme4 package.

2.1.2.2 Preembedding electron microscopy cytochemistry

This technique differs from the above in that primary, secondary and enzyme-linked tertiary antibodies are linked to the target proteins before embedding in resin. The enzyme, when activated by a reagent, yields electron-dense products that can be visualized in the electron microscope. After embedding there is no need for post-processing of tissue slices other than contrasting before photographed in the electron microscopy. Images are analyzed digitally to evaluate the presence of target-protein in different tissue areas cellular compartments.

2.1.2.3 Limitations of electron microscopy

The postembedding technique are subject to problems of antibody unspecificity, as described in 2.1.1.2 on page 35. To control for this phenomenon, knockout-mice were included in the experiments as negative controls.

An issue specific for the immunogold procedure is the fact that the gold particle is not in the exact same position as the protein of interest. The theoretical distance from antigen to the gold particle's center of gravity in our experiments are maximally 23.5 nanometers. It is impossible to determine the precise location of the target protein. We met this problem by using the smallest gold particles possible and counted only gold particles within this theoretical maximum distance from the cell membrane.

Antibodies are not able to penetrate the resin used to embed the tissue before cutting and imaging. This means that there are a limited number of epitopes available for the primary antibodies. This is part of the explanation why the immunoreactivity in this method appears inferior to immunofluorescence microscopy. In practice this means that some antibodies can yield a strong signal in immunofluorescence experiments yet still be useless for immunogold experiments.

In the preembedding technique, the additional number of steps in the experimental protocol introduces variability and lessens reproducibility. The method is qualitative, and measure of antigen quantity in a specific tissue area beyond "present" or "non-present" are not satisfactorily accurate.

2.2 Technical description of methods

Detailed descriptions of the other methods, necessary for reproducing our experiments, are to be found in the papers I-IV.

2.3 Animal models

Transgenic animals played a key role in the projects of this thesis. The past decade's commercialization of production of transgenic mouse lines enabled us to investigate phenotypes and perform proper validation of antibodies in ways considered impossible only fifteen years ago. This has substantially improved the quality of antibody-based scientific projects by introducing reliable negative controls.

2.3.1 Mdx^{3cv}

This mouse line has mutation leading to a severe deficiency in all dystrophin isoforms, in contrast to the regular *Mdx* mouse lines that only lack in full-length dystrophin. It has been used extensively in studies on Duchenne muscular dystrophy. The mutation is located to the 5' end of the dystrophin gene [192]. However, it does not completely eliminate translation of the gene transcript [193].

The phenotype shows alterations of breeding performance and both motor and behavioural characteristics. The *Mdx*^{3cv} mice have more unsuccessful matings that other strains and slightly lower breeding performance than regular *Mdx* mice [192]. Muscle pathology has developed by 4 weeks of age, and the skeletal and diaphragm muscle pathology is similar to that observed in regular *Mdx* mice. The animals also develop mild cardiopathy [192]. A behavioural study concluded that the mice have expressed enhanced anxiety-related behaviour and reduced locomotion compared to control mice [194]. Learning deficits in *Mdx*^{3cv} was weaker or similar to regular *Mdx* mice [194].

2.3.2 Constitutive α-syntrophin knockout

This mouse line does not express α-syntrophin. It is a useful model for assessing the relationship between this anchoring molecule and the membrane proteins potentially connected to it [195]. It is particularly interesting to us because of α-syntrophin's close association with AQP4 [135].

The abnormal phenotype of this mouse line is more subtle than for the *Mdx*^{3cv}. Gross anatomy and behaviour are indistinguishable from litter controls. The BBB has not been shown to be abnormal. The animals have a delayed brain water increase and edema development following hypoosmotic stress [99], as well as increased severity of hypothermia-induced seizure severity and delayed potassium-clearance [94]. In a study comparing effect of osmotherapy with hypertonic and isotonic iv infusion of saline following ischemic stroke, the added effect on brain water resorption of hypertonic saline was eliminated in the α-syntrophin knockout line [126].

2.3.3 Constitutive *Aqp4* knockout

Aqp4$^{-/-}$ mice were generated by GenOway by cloning and sequencing of a targeted region of the murine *Aqp4* gene in a 129/Sv genetic background. The strategy was to design a targeted locus allowing us to delete exons 1Ð3 to avoid any expression of putative splice variants. Hence, a flippase recognition target (FRT)-neomycin-FRT-LoxPÐvalidated cassette was inserted downstream of exon 3, and a LoxP site was inserted upstream of exon 1. After homologous recombination in ES cells, ES-cell injection into blastocytes, and generation of chimeras, heterozygous floxed mice were obtained by breeding chimeras with C57BL/6J females. Heterozygous floxed mice were bred with C57BL/6J Cre expressing mice to generate mice heterozygous for the KO allele, *Aqp4*$^{+/-}$. The *Aqp4*$^{+/-}$ mice were then backcrossed with C57BL/6J mice for five generations before intercrossing to yield *Aqp4*$^{-/-}$ and *Aqp4*$^{+/+}$ (WTs). In this mouse line the *Aqp4* gene is deleted in all cells and tissues, and hence the mouse is deficient in AQP4 [196].

Aqp4$^{-/-}$ does not exhibit any abnormal growth, development, survival or neuromuscular function if not stressed. They have prolonged stimulation-evoked seizure duration and slowed potassium kinetics [147], while another study established altered gap-junction connectivity and postulated that the *Aqp4*$^{-/-}$ had increased spatial buffering of potassium [197]. On that note, it was published that no functional interaction exists between AQP4 and Kir4.1 in retinal Müller cells [153]. No major structural abnormalities in the brain is observed [198], this was reported in a study by Verkman et al. following a report stating that *Aqp4*$^{-/-}$ significantly altered BBB integrity [199]. In a subset of 612 mouse, about 10% manifested progressive encephalomegaly originating in triventricular hydrocephalus and elevated ICP [200]. *Aqp4*$^{-/-}$ mice have increased extracellular space without tortuosity change [201], impairment of selected forms of spatial memory and

neurotrophin-dependent synaptic plasticity [202], and reduced expression of α-syntrophin and dystrophin in perivascular endfeet [203]. Another study published findings that imply a role for AQP4 in synaptic plasticity and associative fear memory in the amygdala by regulating GLT-1 expression [204]. The same group found recently that *Aqp4*$^{-/-}$ mice exhibited impaired memory consolidation in the Morris water maze and reduced theta-burst induced LTP [205].

Taken together, the majority of findings on BBB integrity suggests that the BBB is largely intact without major disruption.

2.3.4 *GLT1*-eGFP/*NG2*-DsRed double-transgenic mouse line

This mouse line was developed for two-photon *in vivo* laser microscopy and immunofluorescence microscopy by crossing *GLT1*-eGFP (developed by Rothstein) with *NG2*-DsRed mice (developed by Jackson). Two genetic sequences has been added. The eGFP expression is driven by the *GLT1*-promoter, so that green fluorescence is seen in astrocytes [86]. The DsRed expression is driven by the *NG2*-promoter, hence red fluorescence is seen in contractile cells such as pericytes and smooth muscle cells in the vessel wall (details in paper IV). It is a reporter mouse line, no abnormal phenotype have yet been reported.

3. Summary of results

In this chapter we address our scientific hypotheses (see 1.8 on page 31) for the individual projects and draw brief conclusions.

3.1 Paper I

Immunofluorescence showed that perivascular expression of dystrophin and α-syntrophin was weaker in retina than in three different regions of brain (dentate gyrus, cortex, and cerebellum). Immunogold cytochemistry revealed a strong α-syntrophin signal in perivascular endfeet in cortex, whereas in retina the signal was absent.

In cortex, deletion of dystrophin and α-syntrophin markedly reduced perivascular AQP4 immunofluorescence. Immunogold cytochemistry showed that deletion of dystrophin and α-syntrophin reduced the AQP4 signal over perivascular astrocytic endfoot membranes in cortex by 65% and 88%, respectively.

In retina, the AQP4 immunofluorescence did not differ between genotypes. Immunogold cytochemistry showed that the AQP4 signal in perivascular Müller cell membranes was 70% higher than in cortical astrocytes. Deletion of dystrophin reduced the AQP4 signal over perivascular Müller endfoot membranes in retina by 35%, whereas, in contrast to our findings in cortex, deletion of α-syntrophin did not change the AQP4 signal.

We concluded that the macroglial expression of dystrophin and α-syntrophin differed between brain and retina, and that AQP4 seems to have different anchoring mechanisms in these two regions of the CNS.

3.2 Paper II

AQP4 immufluorescence labeling of *GLT1*-eGFP/*NG2*-DsRed double-transgenic mice, which express fluorescent reporters in astrocytes and pericytes, revealed distinct AQP4 signal in astrocytic processes adjacent to pericytes.

Immunogold cytochemistry confirmed AQP4's polarized distribution, with AQP4-signaling gold particles clustered over astrocytic endfoot membranes adjacent to pericytes. Quantitative analysis revealed that the density of gold particles was 40% higher over membrane domains abutting pericytes than over those facing endothelial cells.

We next investigated whether this abundance of AQP4 in specific endfoot membrane domains was paralleled with increased expression of the AQP4 anchoring molecule α-syntrophin. α-Syntrophin immunogold signal was also concentrated in membrane domains adjacent to pericytes.

Deletion of *Aqp4* reduced perivascular α-syntrophin labeling overall, as reported previously.

The differentiated pattern of α-syntrophin signal *within* the endfoot membrane was preserved in the *Aqp4*$^{-/-}$ mice. Thus, in *Aqp4*$^{-/-}$ mice the α-syntrophin immunogold signal was significantly higher over endfoot membrane domains next to pericytes than over those next to endothelial cells.

Our data support the concept that pericytes are important for regulating polarization of AQP4.

3.3 Paper III

The strategy to use the GFAP promoter to drive recombination in glia resulted in a complete loss of glial AQP4 in the mutants, as measured by immunofluorescence, and quantitative immunoblotting. Glial-conditional *Aqp4*$^{-/-}$ mice displayed normal AQP4 expression in kidney and muscle.

Quantitative immunogold cytochemistry of wild-type, glial-conditional *Aqp4*$^{-/-}$, and global *Aqp4*$^{-/-}$ mice revealed that endothelial membranes does not contain AQP4 labeling.

Having resolved the controversy regarding the endothelial expression of AQP4, we went on to study whether the glial pool of AQP4 regulates blood-brain water uptake. We showed that under systemic hypo-osmotic stress, glial-conditional deletion of the perivascular pool of AQP4 led to significantly less water accumulation in the brain.

We also found that baseline brain water content was elevated in glial-conditional and global *Aqp4*$^{-/-}$ mice. This effect was evident already at postnatal day 8, suggesting that AQP4 facilitates water reabsorption in early postnatal life.

There was no difference in BBB permeability of large molecular-weight molecules based on between glial-conditional *Aqp4*$^{-/-}$ and control mice.

We concluded that the blood-brain barrier is more complex than anticipated and that the glial covering of brain microvessels in certain circumstances acts as a functional barrier to water movement. Moreover, our data do not support the hypothesis that AQP4 is expressed in endothelial cells.

3.4 Paper IV

Infusion of fluorescent tracers of different sizes into the lateral ventricle and the cistern magna and subsequent analysis of vibratome sections, showed that CSF enters the brain parenchyma mainly from the subarachnoid space, and not from the ventricular compartments. By electron microscopy we confirmed tracer accumulation in the paravascular space.

Intracisternal injection of radioactive tracers confirmed this CSF recirculation behaviour. Within 45 minutes of injection, 40% of radioactive mannitol was detectable in the brain. Larger-sized radioactive dextran accumulated more slowly.

Two-photon *in vivo* laser scanning microscopy showed that subarachnoid CSF flows into the brain parenchyma from the cortical surface through a paravascular space along the outside of penetrating arteries and arterioles. Tracers of different sizes was equally transported, indicating that their transit from the surface to the deeper parts of the brain occurs via bulk flow of CSF.

To follow the tracers in deeper parts of the brain, we did *ex vivo* analysis of fixed vibratome sections. At early time points, tracers was observed migrating out of para-arterial space into parenchyma. At later time points, tracer was observed alongside veins in a para-venous space. Tracer injected directly into the interstitial space in brain parenchyma was cleared along para-venous pathways, either posterior-medially toward the internal cerebral veins or posterior-lateral-ventrally along the external capsule until its exit from the parenchyma along the caudal rhinal veins. This suggests that both CSF and ISF moving through the brain parenchyma are cleared along the same para-venous drainage pathways.

Loss of AQP4 had no effect on para-arterial bulk flow transport of CSF tracer from the surface to deeper parts of the brain.

Ex vivo imaging showed that deletion of *Aqp4* markedly reduced CSF tracer influx from the paravascular space into the brain parenchyma.

Measurements of radioactive tracers injected directly into the interstitial space showed that deletion of *Aqp4* markedly reduced clearance of tracers, thus demonstrating that astroglial AQP4 supports the bulk ISF flow that drives the clearance of interstitial solutes from the brain parenchyma.

After intrastriatal injection of radioactive amyloid-β, the compound was rapidly cleared from the brain. Deletion of *Aqp4* reduced the rate of amyloid-β clearance by 55%.

Fluorescent amyloid-β moved rapidly along the vasculature when injected in the striatum, accumulating along the microvasculature and large-caliber internal cerebral and caudal rhinal veins.

After intracisternal injection of radioactive amyloid-β, total brain radioactive amyloid-β levels increased in a manner comparable to radioactive dextran, indicating that a portion of amyloid-β within the CSF compartment recirculates. Deletion of *Aqp4* significantly reduced bulk influx of radioactive amyloid-β into brain parenchyma.

We concluded that there seems to be a previously unknown CSF circulation system involved in clearance of water and solutes from the interstitial space of brain parenchyma. AQP4 seems to play an important role in this system.

4. Discussion

In this chapter I will discuss the implications of our findings. First I will reflect on the new insights on astrocyte polarity and AQP4 anchoring mechanisms in endfeet. Next, the role of endfeet in controlling water exchange between blood and brain will be discussed. Then I will zoom out and discuss the new circulation pathway that might serve as a lymphatic-like system in the brain. Finally, I will deal with some translational aspects of our findings and look ahead.

4.1 Astrocyte polarity and AQP4 anchoring mechanisms

Our interest in this subject was kindled by the observation that endfoot polarity of AQP4 is lost in a number of diseases. Deeper knowledge of the anchoring patterns underlying endfoot polarity might be useful for understanding disease pathophysiology. This thesis has increased our understanding of AQP4 anchoring mechanisms. We find that anchoring mechanisms of perivascular AQP4 vary across two regions of the CNS, that is, between the Müller cells in the retina and astrocytes in the cerebral cortex. We provide evidence that dystrophin and α-syntrophin are more important anchoring proteins for AQP4 in brain than in retina, but that the polarity of endfeet, measured by AQP4 expression patterns, is comparable in the two regions. A possible explanation for this is that different DAPC-molecules or scaffolding molecules are responsible for endfoot polarity in retina as compared to those in brain. The idea of different DAPC subsets is supported by our findings that the relative contributions of dystrophin and α-syntrophin seem to differ in brain and retina. However, compensatory mechanisms might be in play to different extents in the two regions. We speculate that loss of dystrophin might be associated with compensatory upregulation of utrophin, a dystrophin homologue in cortex [133, 134], and less so in retina.

Our novel observations of regional differences in anchoring of AQP4 are in line with the concept of macroglial heterogeneity, considering the astrocytes a cell type of great diversity, expressing regional subspecialization both in terms of morphology and membrane protein composition in astrocytic processes [83]. These findings add a new level of complexity to the understanding of anchoring of AQP4.

It seems feasible that other proteins could display the same phenomenon as observed for AQP4, that is, to express different anchoring mechanisms across regions of the CNS. It might be fair to assume that it applies to many other CNS membrane proteins. It is important that future projects take this possibility into account when investigating anchoring molecules in the brain. In practice, this means that extrapolating from results in one brain region to another should be done with caution.

After clarifying the different regional patterns of anchoring proteins and linking this to the polarized expression of AQP4 in glial cells in paper (I), we wanted to look in more detail at the expression pattern within the perivascular endfoot. In paper II we found variable expression of AQP4 not only across brain regions, brain cell types, or cell membrane domains, but also across subdomains *within* the specialized cell membrane domain of the perivascular astrocytic endfoot. These findings challenge the concept of astrocyte polarization as a "two-domainal" distribution of proteins, and thus supports the view of a "multi-domainal" specialization of the astrocyte membrane [91].

We find evidence supporting that pericytes regulate perivascular AQP4 expression. In essence, what we find is that the endfoot AQP4 expression is higher when abutting a pericyte. This suggests that the pericytes and the astrocytes interact. This is interesting in many aspects. The presence of a pericyte often increases the distance from capillary lumen to neurons. One of our hypotheses is that the endfoot membrane increases its water permeability to compensate for the increased distance to capillaries. If so, what are the mechanisms regulating this compensation? We speculate that pericyte secretion of agrin, known to bind β-dystroglycan [206], a member of the DAPC, might contribute to the enhanced polarization of AQP4 in the endfoot membrane facing pericytes. Evidence of pericyte-astrocyte crosstalk and indirect evidence that this partially regulates the BBB has been described earlier [4]. If pericytes affect polarity in astrocytes, other cell types adjacent to astrocytic endfeet, like pial cells, might have the same ability. These are intriguing subjects for future projects. Our findings reinforce the concept of multidomainal polarity, and suggest that the astrocytic endfoot membrane subdomain towards the pericyte is indeed specialized.

4.2 Roles of endfeet in controlling bidirectional water transport between blood and brain: possible barrier function of endfeet

There has been uncertainty regarding the presence of AQP4 in cells adjacent to the astrocytic endfoot, i. e. endothelial cells. Notably, Amiry-Moghaddam et al. reported immunogold electron microscopy data indicating an endothelial pool of AQP4 [99]. By combining gene knockout technology with Western blotting and quantitative immunogold electron microscopy, we were able to show that the AQP4 pool in the neurovascular unit is located exclusively in astrocytic endfeet and not in endothelial cells (paper III). Our assertion is that previous studies documenting an endothelial pool of AQP4 by electron microscopy studies have in fact misinterpreted "spillover" signal of gold particles from the astrocytic endfoot as endothelial AQP4. This is possible because the antigen-antibody-gold particle complex can span the short distance between an astrocytic endfoot membrane and the adjacent endothelial membrane. Thus, if not controlling for this phenomenon, one can misinterpret a gold particle really originating from an endfoot as being of endothelial origin.

Our finding that brain endothelial cells are devoid of AQP4 is important. It is clear that efforts towards pharmaceutical interventions on AQP4 must adjust to this finding. Potential brain edema-reducing AQP4 inhibitors should be designed to permeate the endothelial cell layer to reach the astrocytic pool of AQP4.

After having ruled out an endothelial pool of AQP4, we were left with the glial pool. This enabled us to study whether endfoot AQP4 limits water flux into and out of the brain. We

found that glial-conditional *Aqp4* knockout mice have reduced brain water uptake compared to wild-type controls during hypoosmotic stress. This suggests that the astrocytic endfoot AQP4 is a rate-limiting step in water transport across the BBB. The insights gained from study of glial-conditional *Aqp4* knockouts differ conceptually from the traditional view of the BBB, as they confer barrier function on the astrocytic endfeet, and not only on the endothelial cell as previously believed.

The discovery that glial-conditional *Aqp4* knockout mice had higher brain water content than wild-types, both postnatally and as adults, suggests that endfoot AQP4 is important for resorption of interstitial fluid both early in development and in adulthood. The differences in postnatal brain water content between *Aqp4* knockouts and controls coincided with the developmental stage in which AQP4 expression became detectable in the wild-types, supporting the hypothesis that reduced brain water absorption is AQP4-dependent.

We wanted to follow up on this and study how AQP4 was involved in drainage of interstitial fluid from the CNS. Along which pathways are ISF cleared? After resolving that AQP4 is absent in endothelial cells, it was appropriate to raise the question of whether water released from endfeet is drained along blood vessels instead of inside them. Theoretically, such a pathway could also facilitate influx of water along blood vessels and through the glial endfeet to brain parenchyma.

4.3 AQP4-dependent CSF circulation pathway and waste clearance

The brain is the only organ in the body without a lymphatic system. In paper IV we identified a new brain-wide circulation pathway for CSF in mice, addressing a long-standing question of how excess interstitial fluid is cleared from the brain. This pathway involves rapid para-arterial influx of subarachnoid CSF into the brain interstitium, followed by clearance of ISF along large-caliber draining veins. The continuous movement of fluid appears to be a main contributor to clearance of interstitial solutes, exemplified by our results on mannitol and amyloid-β. Given that this pathway is dependent on transglial water flux and that it seems to serve functions similar to the lymphatic system elsewhere in the body, we suggest that this system be called the "glymphatic" pathway.

As described in the introductory part of this thesis, it has long been known that CSF is cleared from the cranial cavity both by entering venules in subarachnoid villi and by drainage to lymphatic vessels in the cribriform plate. This led to a hypothesis stating that CSF might serve "lymphatic" functions by exchanging solutes and fluid with the brain ISF along the perivascular space, and that the clearance route was largely para-arterial. This hypothesis was supported by previous studies observing tracer accumulating around arteries after injections into the interstitium [207, 208]. After obtaining results favouring a para-venous clearance route rather than a para-arterial, our belief is that these observations of high para-arterial tracer concentrations might be artifacts due to high intraparenchymal pressure after injection. Supporting this, when injecting tracer intraparenchymally in our own experiments, we observed para-arterial accumulation close to the injection site, but in areas at the furthest distance from the injection site, the accumulation was largely para-venous.

By following different-sized tracers, we were able to track the direction of CSF flow. Both TR-d3 and FITC-d2000 molecular tracers injected intracisternally moved along para-arterial

pathways along pial surface arteries and into the Virchow-Robin spaces (VRS) of penetrating arteries without mixing with the subarachnoid CSF compartment. This suggests that the para-arterial space of surface arteries and the VRS is an anatomically distinct subcompartment of the subarachnoid space. This propulsion of CSF along arteries are believed to be driven by arterial pulsations [209, 210]. Small-size tracers followed the CSF fluid from para-arterial space into brain parenchyma, whereas large molecular-weight tracers were restricted. Previous studies have addressed paravascular flow and the distribution of tracers in the perivascular space [211–214]. Our belief is that these studies have underestimated the magnitude of paravascular flow. Methodological differences may be the cause of these discrepancies. In our experiments, we noticed that loss of hydraulic integrity of dural and subarachnoid space significantly reduced the paravascular flow. This disruption could be caused e.g. by establishing external openings for taking samples of fluid, as has been done in some of the previous studies [211, 212]. Another explanation for discrepancy could be the use of different-sized tracers. Whatever the underlying cause, our recent findings refute previous conclusions that para-vascular fluid fluxes are "slow and variable in direction" [211, 212].

Perivascular endfeet cover brain microvasculature almost completely, with only 20 nm clefts between adjacent overlapping endfeet providing direct communication with the ISF [24]. Our observations indicate that perivascular AQP4 facilitates the influx of subarachnoid CSF from para-arterial spaces into the brain interstitium, as well as the subsequent clearance of ISF via convective bulk flow. By characterizing this "glymphatic" pathway in both normal and AQP4-deficient mice, we show that it is largely dependent on AQP4, and that the recirculation of CSF via para-arterial space is of considerable volume. Our observations suggest that in normal mice, >40% of CSF recirculated through brain parenchyma in 45 minutes. Loss of AQP4 reduced estimated recirculation by 70%. We speculate that arterial pulsations are the main driving force of fluid from para-arterial space and VRS through specific transporters in the glial sheet and/or between glial processes. Our findings indicate that AQP4 is one of the transport molecules in question. Out of all the different water transport mechanisms across the BBB, our findings might outline the relative contribution of the AQP4-mediated water flux. We consider 70% a substantial reduction, but notably about 30% of the recirculation volume remains in circulation. This circulaton of water not being eliminated by knockout of *Aqp4* must be accounted for by other mechanisms and might be a rough quantitative estimation of the combined relative contributions of co-transport of water through transporters and diffusion [30]. In light of our knowledge of disrupted astrocyte AQP4 polarization in specific conditions like experimental stroke models, Alzheimer's disease and epilepsy, it would be of interest to address whether the "glymphatic" pathways is affected in these conditions. Another approach to explore the effect of astrocyte polarity disruption on the "glymphatic" system would be to do paravascular flow experiments on α-syntrophin knockout mice and glial-conditional *Aqp4* knockouts.

After fluid from the CSF has entered the ECS and mixed with the ISF, it is cleared together with associated solutes along paravenous pathways. We speculate that the these paravenous spaces and the dural sinuses provide a lowpressure sink that, in combination with arterial pulsations within the subarachnoid space, create an arteriovenous hydrostatic gradient that drives paravascular CSF bulk flow and ISF clearance. When ISF reaches the parenchymal border and the sheet of glial endfeet covering the paravenous space, water and solutes may cross this barrier by different modes of transport. In the case of amyloid-β, different specific transporters have been identified, notably the sLRP1, whereas for water the presence of AQP4 might provide a low-resistance barrier for entering paravenous space. We do find that amyloid-β is cleared from brain interstitial more rapidly than comparable sized dextran, suggesting that solute-specific receptor-mediated transport can increase the clearance rate. The hypothesis that AQP4 is rate-limiting

for efflux of water from the interstitium is supported by observations of enlarged ECS in *Aqp4* knockouts [215]. This might be a compensatory mechanism to counteract higher para-venous water efflux resistance in these mice. The "glymphatic" pathway does not necessarily provide terminal clearance of fluid from the paravenous space and out of the cranium. Previous studies has suggested two routes for this clearance. First, the paravenous spaces enables the cleared solutes to interact with BBB transporters and uptake. Second, for solutes not recycled over the BBB, fluid and solutes drained along caudal rhinal and internal cerebral veins could be cleared to the systemic circulation through arachnoid granulations [216–218].

The "glymphatic" pathway seems to transport not only water, but also small to moderate-sized molecules like amyloid-β, a key factor in the development of Alzheimer's disease. Previous studies have reported that intraparenchymally injected amyloid-β is cleared along paravascular pathways [219]. We report that amyloid-β is cleared along the same paravascular pathway as other solutes and that this pathway is significantly compromised in *Aqp4* knockouts. This is intriguing, because reactive gliosis is one of the pathophysiological changes observed in Alzheimer's disease and the ageing brain [220–222]. We speculate that the altered AQP4 polarization and expression observed in neuropathological conditions may reduce ISF bulk flow and efflux and thus the clearance of solutes contributing to the pathophysiological processes, such as amyloid-β [223]. On a slightly different note, our observations on amyloid-β-clearance support the previously proposed link between AQP4 and Alzheimer's disease [125], but from a slightly different angle. In the cited study, the Alzheimer's disease mouse model showed alterations in AQP4 polarization following plaque formation. In our present study the sequence of events are reversed, in that the initial deficiency of AQP4 leads to a slowed clearance of amyloid-β, the protein known to form plaques in Alzheimer's disease patients. Although the distinction between redistribution of AQP4 and plain loss of AQP4 is important, the main effect of total loss of AQP4 is a reduction of the perivascular endfoot pool, and thus the end result is not unlike loss of AQP4 polarization.

In contrast to diffusion, bulk flow transport of molecules is independent of molecule size [224,225]. Based on this, Cserr et al. postulated that the bigger the brain, the longer would be the diffusion distances needed to clear a solute from a given location in the interstitium, and thus the relative importance of bulk flow would increase as brain size increases [20]. This concept might be important to keep in mind when extrapolating our insights from study of the rodent brain to the human scale. In other words, the relative importance of the "glymphatic" pathway and ECS bulk flow of ISF could be more pronounced in humans than in mice.

This new circulation pathway could be a major breakthrough in the search for AQP4's main function. That being said, it reinforces one of the most puzzling traits of the AQP4-deficient mice: AQP4-deficient mice does not have a lethal or even moderately disabling phenotype. This holds true both for the global and the glial-conditional *Aqp4* knockouts. This is plainly surprising given AQP4's abundance and importance for fluid transport, and even more so in the face of this new circulation pathway. What are the evolutionary selection criteria that favor the abundant expression of AQP4 on brain fluid compartment interfaces?

4.4 Translational aspects

The discovery of the "glymphatic" pathway opens up for intriguing new therapeutic possibilities. By improving the AQP4-dependent bulk flow one could speed up clearance of neurotoxic or neurodegenerative agents, such as amyloid-β. One could also imagine increased "glymphatic" flow rate to increase immunosurveillance of the CNS, enabling faster immune responses when detect-

ing foreign antigens originating in brain parenchyma without compromising immune privilege. Immune cells like lymphocytes and antigen-presenting cells reside in the subarachnoid space, and previous studies have indeed showed a reduced immune response in *Aqp4* knockouts following intraparenchymal LPS (a foreign antigen) injections [226]. On the other hand, slowing the "glymphatic" pathway could increase tissue concentration and exposure time in CNS parenchyma for therapeutic agents such as anti-tumor drugs, immune modulators, and antibiotic agents.

Several groups, independently of each other, are trying to develop AQP4 inhibitors. This could prove of therapeutic significance in the long term, but in the meantime could prove important for revealing functional aspects of AQP4. The inhibitor-enabled study of AQP4 functions will be important for reducing patient risk before potential drug trials in humans can be considered [227].

4.5 Future perspectives

The present work made an effort to increase understanding of the localization and functions of AQP4. We studied fluid transport in the CNS on different levels, spanning from the global CSF circulation patterns to the molecular level of water channels in the membrane of individual cells. This is basic science, but our hope is that these insights from animal experiments will contribute the common scientific effort towards new treatment regimes that will benefit patients. We are now initiating several follow-up studies.

We wonder if astrocyte heterogeneity can be important for clearance of ISF. If water permeability of the perivascular glial "cuff" varies along the vessel tree, such differences could direct ISF flow by creating low-resistance exit routes in areas of high-permeability.

We have already initiated an immunogold project that will resolve whether endfoot AQP4 expression varies along the vasculature. Today there are no generally accepted exclusion or inclusion criteria to reliably differentiate arteries and veins in electron microscopy sections. We intend to work around this problem by identifying the vessel type using two-photon imaging *before* preparing tissue for electron microscopy. Arteries and veins can be identified in the two-photon setup based on blood flow characteristics, vessel morphology, and presence of contractile cells expressing fluorescent markers. Subsequently, we can dissect out the brain area and cut tissue sections for microscopy. Vessels observed in the sections can then be compared to a 3D-reconstruction of the two-photon recordings and identified as either artery or vein.

Our *in vivo* experiments were performed on wild-type and global *Aqp4* knockout mice. The growing body of evidence of *Aqp4* knockouts having abnormal expression of different proteins must be considered when interpreting data. The sum of the many compensatory mechanisms in play working to counteract the loss of AQP4 creates confounding effects, setting investigators up for misinterpretation of data. In upcoming projects, we intend to study the CSF circulation patterns in several other mouse lines. By developing and characterizing the glial-conditional *Aqp4* knockout mice we have introduced a new tool and thus set the stage for interesting follow-up studies. Glial-conditional *Aqp4* knockouts, α-syntrophin knockouts and mdx^{3cv} mice are genotypes of interest in our upcoming projects. It must be emphasized, however, that the glial-conditional *Aqp4* knockout model are not strictly astrocyte-specific, but it can be considered organ-specific, in that the only GFAP-expressing cells that also express AQP4 is located in the CNS. This could prove useful in exposing animals for systemic stressors like hypoosmostic infusions or hypoxic conditions, by eliminating the possibly confounding effects of extra-cerebral

AQP4, such as in kidney and lung tissue. In future research on AQP4 one can refine the design of the experimental setups by using glial-conditional *Aqp4* knockout models and remain confident that AQP4 is absent in the neurovascular unit. This targeted elimination of AQP4 and its anchoring molecules in different cell lines could enable us elaborate on the individual contributions of each protein to the CSF circulation and ISF clearance. To follow up on the role of AQP4 in clearance of amyloid-β, it would be interesting to study expression of AQP4 in tissue obtained from the autopsy of Alzheimer's disease patients.

Our ultimate long term objective is to deepen our understanding of brain fluid dynamics to enable development of better treatment for CNS diseases in humans and increase patient survival and quality of life. Our studies are performed in mice and can never be more than a proxy for the human brain.

A general limitation inherent in our experimental setups is the need to partly compromise biological, *in vivo* conditions to enable standardization of experiments and optimal control over confounders. To illustrate a general point, injection of amyloid-β directly into mouse brain parenchyma is no perfect simulation of the amyloid plaques in the human adult brain accumulating over years and decades. This inevitable discrepancy between "real" and "experimental" conditions is important and requires that we be careful when developing our conclusions so as not to make claims not supported by data. A more specific description of the limitations of our methods are found under materials and methods in Chapter 2 and in the respective papers.

The present work was performed on tissue slices, sections, homogenates and in living mice. The author has mostly done electron microscopy, to this date the only way of obtaining high-magnification, high-resolution images of structures on the subcellular level. Experimental setups for *in vivo* imaging have now fully entered the field of basal neuroscience and are already exceeding the limits for what was previously thought possible. PET scanners, fMRI, CT, and multi-photon laser scanning microscopy make real-time *in vivo* non-invasive imaging a reality, and the resolution these techniques provide is continuously improving. There are high hopes that future breakthroughs in the study of the gliovascular unit will come when combining scientific curiosity and creativity with these powerful tools.

The candidate's experimental contribution

Paper I

Molecular scaffolds underpinning macroglial polarization: an analysis of retinal Müller cells and brain astrocytes in mouse.

My contribution to this project was to quantify the amount of AQP4 and α-syntrophin in the end-feet of astrocytes in the different genotypes using semiquantitative post embedding immunocytochemistry. I did image acquisition, statistical analysis, designed figures and contributed to writing and proof-reading the manuscript.

Paper II

Evidence that pericytes regulate aquaporin-4 polarization in mouse cortical astrocytes.

My contribution to this project was to quantify the amount of AQP4 and α-syntrophin in the end-feet of astrocytes in the different genotypes using semiquantitative post embedding immunocytochemistry. I did image acquisition, performed statistical analysis, designed figures and had the main responsibility for writing and proof-reading the manuscript.

Paper III

Glial-conditional deletion of aquaporin-4 (Aqp4) reduces blood-brain water uptake and confers barrier function on perivascular astrocyte endfeet.

My contribution to this project was to quantify the amount of AQP4 in the end-feet of astrocytes in the different genotypes using semiquantitative post embedding immunogold cytochemistry. I did image acquisition, statistical analysis, designed figures and proof-read the manuscript.

Paper IV

A paravascular pathway facilitates CSF flow through the brain parenchyma and the clearance of interstitial solutes, including amyloid β.

My contribution to this project was to identify VRS on electron microscopy in the different genotypes and qualitatively determine distribution patterns of different sized tracers using DAB immunohistochemistry. I performed experiments, image acquisition and analysis, designed figures and proof-read the manuscript.

Bibliography

[1] Dobzhansky T. Changing man. Science. 1967;155(761):409–15.

[2] Brothwell DR. Digging up bones; the excavation, treatment and study of human skeletal remains. British Museum, London; 1963.

[3] Haydon PG, Carmignoto G. Astrocyte control of synaptic transmission and neurovascular coupling. Physiological reviews. 2006;86(3):1009–1031.

[4] Bonkowski D, Katyshev V, Balabanov RD, Borisov A, Dore-Duffy P. The CNS microvascular pericyte: pericyte-astrocyte crosstalk in the regulation of tissue survival. Fluids and barriers of the CNS. 2011;8(1):8.

[5] Tait MJ, Saadoun S, Bell BA, Papadopoulos MC. Water movements in the brain: role of aquaporins. Trends in Neurosciences. 2008;31(1):37–43.

[6] Papadopoulos MC, Verkman AS. Aquaporin-4 and brain edema. Pediatr Nephrol. 2007;22(6):778–84.

[7] Abbott NJ, Patabendige AA, Dolman DE, Yusof SR, Begley DJ. Structure and function of the blood–brain barrier. Neurobiology of disease. 2010;37(1):13–25.

[8] Syková E, Nicholson C. Diffusion in brain extracellular space. Physiological reviews. 2008;88(4):1277–1340.

[9] Akdogan I, Kiroglu Y, Onur S, Karabulut N. The volume fraction of brain ventricles to total brain volume: a computed tomography stereological study. Folia Morphologica. 2010;69(4):193–192.

[10] Lehmenkühler A, Syková E, Svoboda J, Zilles K, Nicholson C. Extracellular space parameters in the rat neocortex and subcortical white matter during postnatal development determined by diffusion analysis. Neuroscience. 1993;55(2):339–351.

[11] Edvinsson L, MacKenzie ET, McCulloch J, et al. Cerebral blood flow and metabolism. vol. 1185. Raven Press New York:; 1993.

[12] Duong TQ, Kim SG. In vivo MR measurements of regional arterial and venous blood volume fractions in intact rat brain. Magnetic resonance in medicine. 2000;43(3):393–402.

[13] Ito H, Kanno I, Iida H, Hatazawa J, Shimosegawa E, Tamura H, et al. Arterial fraction of cerebral blood volume in humans measured by positron emission tomography. Annals of nuclear medicine. 2001;15(2):111–116.

[14] Jespersen SN, Østergaard L. The roles of cerebral blood flow, capillary transit time heterogeneity, and oxygen tension in brain oxygenation and metabolism. Journal of Cerebral Blood Flow & Metabolism. 2011;32(2):264–277.

[15] Kimelberg HK. Water homeostasis in the brain: basic concepts. Neuroscience. 2004;129(4):851–60.

[16] Rouvière H, Tobias MJ. Anatomy of the human lymphatic system. Edwards Brothers, Incorporated; 1938.

[17] Swartz MA. The physiology of the lymphatic system. Advanced drug delivery reviews. 2001;50(1):3–20.

[18] Moody DM. The blood-brain barrier and blood-cerebral spinal fluid barrier. In: Seminars in cardiothoracic and vascular anesthesia. vol. 10. SAGE Publications; 2006. p. 128–131.

[19] Weller RO, et al. Pathology of cerebrospinal fluid and interstitial fluid of the CNS: significance for Alzheimer disease, prion disorders and multiple sclerosis. Journal of neuropathology and experimental neurology. 1998;57(10):885.

[20] Cserr HF. Physiology of the choroid plexus. Physiological reviews. 1971;51(2):273–311.

[21] Welch K, Pollay M. Perfusion of particles through arachnoid villi of the monkey. American Journal of Physiology–Legacy Content. 1961;201(4):651–654.

[22] Thorne RG, Nicholson C. In vivo diffusion analysis with quantum dots and dextrans predicts the width of brain extracellular space. Proceedings of the National Academy of Sciences. 2006;103(14):5567–5572.

[23] Mabuchi T, Lucero J, Feng A, Koziol JA, del Zoppo GJ. Focal cerebral ischemia preferentially affects neurons distant from their neighboring microvessels. Journal of Cerebral Blood Flow & Metabolism. 2005;25(2):257–266.

[24] Mathiisen TM, Lehre KP, Danbolt NC, Ottersen OP. The perivascular astroglial sheath provides a complete covering of the brain microvessels: an electron microscopic 3D reconstruction. Glia. 2010;58(9):1094–103.

[25] Luby-Phelps K. Cytoarchitecture and physical properties of cytoplasm: volume, viscosity, diffusion, intracellular surface area. International review of cytology. 1999;192:189–221.

[26] Lodish H, Berk A, Zipursky SL, Matsudaira P, Baltimore D, Darnell J. Molecular cell biology. New York. 2000;.

[27] Amiry-Moghaddam M, Ottersen OP. The molecular basis of water transport in the brain. Nat Rev Neurosci. 2003;4(12):991–1001.

[28] Dietzel I, Heinemann U, Hofmeier G. Transient changes in the size of the extracellular space in the sensorimotor cortex of cats in relation to stimulus-induced changes in potassium concentration. Experimental Brain Research. 1980;40(4):432–439.

[29] Svoboda J, Syková E. Extracellular space volume changes in the rat spinal cord produced by nerve stimulation and peripheral injury. Brain research. 1991;560(1):216–224.

[30] MacAulay N, Zeuthen T. Water transport between CNS compartments: contributions of aquaporins and cotransporters. Neuroscience. 2010;168(4):941–956.

[31] MacAulay N, Zeuthen T. Glial K+ Clearance and Cell Swelling: Key Roles for Cotransporters and Pumps. Neurochemical research. 2012;p. 1–11.

[32] Su G, Kintner DB, Flagella M, Shull GE, Sun D. Astrocytes from Na+-K+-Cl-cotransporter-null mice exhibit absence of swelling and decrease in EAA release. American Journal of Physiology-Cell Physiology. 2002;282(5):C1147–C1160.

[33] Su G, Kintner DB, Sun D. Contribution of Na+-K+-Cl- cotransporter to high-[K+] o-induced swelling and EAA release in astrocytes. American Journal of Physiology-Cell Physiology. 2002;282(5):C1136–C1146.

[34] Schneider GH, Baethmann A, Kempski O. Mechanisms of glial swelling induced by glutamate. Canadian journal of physiology and pharmacology. 1992;70(S1):S334–S343.

[35] Ehrlich P. Das Sauerstoff-bedürfnis des Organismus. Eine Farbenanalytische Studie. Habilitationsschrift, Universität Berlin; 1885.

[36] Goldmann E. Vitalfarbung am Zentralnervensystem. Abhandl Konigl preuss Akad Wiss; 1913.

[37] Bundgaard M, Abbott NJ. All vertebrates started out with a glial blood-brain barrier 4–500 million years ago. Glia. 2008;56(7):699–708.

[38] Brightman M, Reese T, Olsson Y, Klatzo I. Morphologic aspects of the blood-brain barrier to peroxidase in elasmobranchs. Prog Neuropathol. 1971;1:146–161.

[39] Bundgaard M, Cserr H. A glial blood-brain barrier in elasmobranchs. Brain Research. 1981;226(1):61–73.

[40] Wolburg H, Lippoldt A. Tight junctions of the blood–brain barrier: development, composition and regulation. Vascular pharmacology. 2002;38(6):323–337.

[41] Reese T, Karnovsky MJ. Fine structural localization of a blood-brain barrier to exogenous peroxidase. The Journal of cell biology. 1967;34(1):207–217.

[42] Butt AM, Jones HC, Abbott NJ. Electrical resistance across the blood-brain barrier in anaesthetized rats: a developmental study. The Journal of physiology. 1990;429(1):47–62.

[43] Abbott NJ, Ronnback L, Hansson E. Astrocyte-endothelial interactions at the blood-brain barrier. Nat Rev Neurosci. 2006;7(1):41–53.

[44] Heimark RL. Cell-cell adhesion molecules of the blood-brain barrier. The Blood-brain Barrier: Cellular and Molecular Biology, ed Pardridge WM (Lippincott-Raven, New York). 1993;p. 88–106.

[45] Hynes RO. Integrins: versatility, modulation, and signaling in cell adhesion. Cell. 1992;69(1):11–25.

[46] Rouget C. Mémoire sur le développement, la structure et les propriétés physiologique des cappilaires sanguins et lymphatiques. Arch Physiol Norm Path. 1873;.

[47] Sá-Pereira I, Brites D, Brito MA. Neurovascular unit: a focus on pericytes. Molecular neurobiology. 2012;45(2):327–347.

[48] Krueger M, Bechmann I. CNS Pericytes: Concepts, Misconceptions, and a Way Out. Glia. 2010;58(1):1–10.

[49] Ribatti D, Nico B, Crivellato E. The role of pericytes in angiogenesis. International Journal of Developmental Biology. 2011;55(3):261.

[50] Dalkara T, Gursoy-Ozdemir Y, Yemisci M. Brain microvascular pericytes in health and disease. Acta neuropathologica. 2011;122(1):1–9.

[51] Frank RN, Dutta S, Mancini MA. Pericyte coverage is greater in the retinal than in the cerebral capillaries of the rat. Investigative ophthalmology & visual science. 1987;28(7):1086–1091.

[52] Frank RN, Turczyn TJ, Das A. Pericyte coverage of retinal and cerebral capillaries. Investigative ophthalmology & visual science. 1990;31(6):999–1007.

[53] Winkler EA, Bell RD, Zlokovic BV. Central nervous system pericytes in health and disease. Nature neuroscience. 2011;14(11):1398–1405.

[54] Daneman R, Zhou L, Kebede AA, Barres BA. Pericytes are required for blood-brain barrier integrity during embryogenesis. Nature. 2010 Sep;.

[55] Armulik A, Genové G, Mäe M, Nisancioglu MH, Wallgard E, Niaudet C, et al. Pericytes regulate the blood-brain barrier. Nature. 2010 Oct;.

[56] Lenhossék M. Der feinere Bau des Nervensystems im Lichte neuester Forschungen. Fischer; 1893.

[57] Matyash V, Kettenmann H. Heterogeneity in astrocyte morphology and physiology. Brain research reviews. 2010;63(1):2–10.

[58] Papadopoulos MC, Verkman AS. Aquaporin water channels in the nervous system. Nature Reviews Neuroscience. 2013;.

[59] Bass NH, Hess HH, Pope A, Thalheimer C. Quantitative cytoarchitectonic distribution of neurons, glia, and DNA in rat cerebral cortex. Journal of Comparative Neurology. 1971;143(4):481–490.

[60] Emsley JG, Macklis JD. Astroglial heterogeneity closely reflects the neuronal-defined anatomy of the adult murine CNS. Neuron glia biology. 2006;2(3):175.

[61] Kofuji P, Newman E. Potassium buffering in the central nervous system. Neuroscience. 2004;129(4):1043–1054.

[62] Orkand R, Nicholls J, Kuffler S. Effect of nerve impulses on the membrane potential of glial cells in the central nervous system of amphibia. Journal of Neurophysiology. 1966;29(4):788–806.

[63] Westergaard N, Sonnewald U, Schousboe A. Metabolic trafficking between neurons and astrocytes: the glutamate/glutamine cycle revisited. Developmental neuroscience. 1995;17(4):203–211.

[64] Kettenmann H, Ransom B, editors. Neuroglia, 2nd edition. Oxford University Press New York:; 2005.

[65] Bezzi P, Carmignoto G, Pasti L, Vesce S, Rossi D, Rizzini BL, et al. Prostaglandins stimulate calcium-dependent glutamate release in astrocytes. Nature. 1998;391(6664):281–285.

[66] Schousboe A, Hertz L, Svenneby G. Uptake and metabolism of GABA in astrocytes cultured from dissociated mouse brain hemispheres. Neurochemical Research. 1977;2(2):217–229.

[67] Coco S, Calegari F, Pravettoni E, Pozzi D, Taverna E, Rosa P, et al. Storage and release of ATP from astrocytes in culture. Journal of Biological Chemistry. 2003;278(2):1354.

[68] Araque A, Parpura V, Sanzgiri RP, Haydon PG. Tripartite synapses: glia, the unacknowledged partner. Trends in neurosciences. 1999;22(5):208–215.

[69] Ventura R, Harris KM. Three-dimensional relationships between hippocampal synapses and astrocytes. The Journal of neuroscience. 1999;19(16):6897–6906.

[70] Spacek J, et al. Three-dimensional analysis of dendritic spines. III. Glial sheath. Anatomy and embryology. 1985;171(2):245.

[71] Verkhratsky A, Orkand RK, Kettenmann H. Glial calcium: homeostasis and signaling function. Physiological reviews. 1998;78(1):99–141.

[72] Bennett M, Goodenough DA. Gap junctions, electrotonic coupling, and intercellular communication. Neurosciences Research Program Bulletin. 1978;16(3):1.

[73] Finkbeiner S. Calcium waves in astrocytes-filling in the gaps. Neuron. 1992;8(6):1101–1108.

[74] Kang J, Jiang L, Goldman SA, Nedergaard M. Astrocyte-mediated potentiation of inhibitory synaptic transmission. Nature neuroscience. 1998;1(8):683–692.

[75] Ransom B, Behar T, Nedergaard M. New roles for astrocytes (stars at last). TRENDS in Neurosciences. 2003;26(10):520–522.

[76] Volterra A, USER CS. Glial modulation of synaptic transmission in the hippocampus. Physiol Rev. 1998;78:99–141.

[77] Barañano DE, Ferris CD, Snyder SH. Atypical neural messengers. Trends in neurosciences. 2001;24(2):99–106.

[78] Pellerin L, Pellegri G, Bittar PG, Charnay Y, Bouras C, Martin JL, et al. Evidence supporting the existence of an activity-dependent astrocyte-neuron lactate shuttle. Developmental neuroscience. 2000;20(4-5):291–299.

[79] Harder DR, Zhang C, Gebremedhin D. Astrocytes function in matching blood flow to metabolic activity. Physiology. 2002;17(1):27–31.

[80] Zonta M, Angulo MC, Gobbo S, Rosengarten B, Hossmann KA, Pozzan T, et al. Neuron-to-astrocyte signaling is central to the dynamic control of brain microcirculation. Nature neuroscience. 2002;6(1):43–50.

[81] Hampton D, Rhodes K, Zhao C, Franklin R, Fawcett J. The responses of oligodendrocyte precursor cells, astrocytes and microglia to a cortical stab injury, in the brain. Neuroscience. 2004;127(4):813–820.

[82] Hansson E. Regional heterogeneity among astrocytes in the central nervous system. Neurochemistry international. 1990;16(3):237–245.

[83] Zhang Y, Barres BA. Astrocyte heterogeneity: an underappreciated topic in neurobiology. Current opinion in neurobiology. 2010;20(5):588–594.

[84] Seifert G, Hüttmann K, Binder DK, Hartmann C, Wyczynski A, Neusch C, et al. Analysis of astroglial K+ channel expression in the developing hippocampus reveals a predominant role of the Kir4. 1 subunit. The Journal of Neuroscience. 2009;29(23):7474–7488.

[85] Israel JM, Schipke CG, Ohlemeyer C, Theodosis DT, Kettenmann H. GABAA receptor-expressing astrocytes in the supraoptic nucleus lack glutamate uptake and receptor currents. Glia. 2003;44(2):102–110.

[86] Regan MR, Huang YH, Kim YS, Dykes-Hoberg MI, Jin L, Watkins AM, et al. Variations in promoter activity reveal a differential expression and physiology of glutamate transporters by glia in the developing and mature CNS. The Journal of neuroscience. 2007;27(25):6607–6619.

[87] Haas B, Schipke CG, Peters O, Söhl G, Willecke K, Kettenmann H. Activity-dependent ATP-waves in the mouse neocortex are independent from astrocytic calcium waves. Cerebral Cortex. 2006;16(2):237–246.

[88] Peters O, Schipke CG, Philipps A, Haas B, Pannasch U, Wang LP, et al. Astrocyte function is modified by Alzheimer's disease-like pathology in aged mice. Journal of Alzheimer's Disease. 2009;18(1):177–189.

[89] Schipke CG, Ohlemeyer C, Matyash M, Nolte C, Kettenmann H, Kirchhoff F. Astrocytes of the mouse neocortex express functional N-methyl-D-aspartate receptors. The FASEB Journal. 2001;15(7):1270–1272.

[90] Franze K, Grosche J, Skatchkov SN, Schinkinger S, Foja C, Schild D, et al. Muller cells are living optical fibers in the vertebrate retina. Science Signalling. 2007;104(20):8287.

[91] Derouiche A, Pannicke T, Haseleu J, Blaess S, Grosche J, Reichenbach A. Beyond Polarity: Functional Membrane Domains in Astrocytes and Müller Cells. Neurochemical Research. 2012;p. 1–11.

[92] Paulson OB, Hertz MM, Bolwig TG, Lassen NA. Filtration and diffusion of water across the blood-brain barrier in man. Microvascular research. 1977;13(1):113–123.

[93] Nagelhus EA, Horio Y, Inanobe A, Fujita A, Haug Fm, Nielsen S, et al. Immunogold evidence suggests that coupling of K+ siphoning and water transport in rat retinal Müller cells is mediated by a coenrichment of Kir4.1 and AQP4 in specific membrane domains. Glia. 1999;26(1):47–54.

[94] Ottersen O, Williamson A, Palomba M, Eid T, Adams ME, Froehner SD, et al. Delayed potassium clearance and increased seizure severity in mice lacking perivascular aquaporin-4. Society for Neuroscience Abstract Viewer and Itinerary Planner. 2003;2003:Abstract No. 53.21.

[95] Hertz L, Dienel GA. Lactate transport and transporters: general principles and functional roles in brain cells. Journal of neuroscience research. 2005;79(1-2):11–18.

[96] Hertz L, Peng L, Dienel GA. Energy metabolism in astrocytes: high rate of oxidative metabolism and spatiotemporal dependence on glycolysis/glycogenolysis. Journal of Cerebral Blood Flow & Metabolism. 2006;27(2):219–249.

[97] Morgan T, Berliner RW. Permeability of the loop of Henle, vasa recta, and collecting duct to water, urea, and sodium. American Journal of Physiology–Legacy Content. 1968;215(1):108–115.

[98] Nielsen S, Nagelhus EA, Amiry-Moghaddam M, Bourque C, Agre P, Ottersen OP. Specialized membrane domains for water transport in glial cells: high-resolution immunogold cytochemistry of aquaporin-4 in rat brain. J Neurosci. 1997;17(1):171–80.

[99] Amiry-Moghaddam M, Xue R, Haug FM, Neely JD, Bhardwaj A, Agre P, et al. Alpha-syntrophin deletion removes the perivascular but not endothelial pool of aquaporin-4 at the blood-brain barrier and delays the development of brain edema in an experimental model of acute hyponatremia. FASEB J. 2004 Mar;18(3):542–4.

[100] Zeuthen T, MacAulay N. Passive water transport in biological pores. International review of cytology. 2002;215:203–230.

[101] Holthoff K, Witte OW. Intrinsic optical signals in rat neocortical slices measured with near-infrared dark-field microscopy reveal changes in extracellular space. The Journal of neuroscience. 1996;16(8):2740–2749.

[102] Syková E, Kubinová Sá, Jendelová P, Chvátal A, et al. The relationship between changes in intrinsic optical signals and cell swelling in rat spinal cord slices. Neuroimage. 2003;18(2):214–230.

[103] Viitanen T, Ruusuvuori E, Kaila K, Voipio J. The K+–Cl- cotransporter KCC2 promotes GABAergic excitation in the mature rat hippocampus. The Journal of physiology. 2010;588(9):1527–1540.

[104] Zeuthen T. Secondary active transport of water across ventricular cell membrane of choroid plexus epithelium of Necturus maculosus. The Journal of physiology. 1991;444(1):153–173.

[105] Zeuthen T. Water permeability of ventricular cell membrane in choroid plexus epithelium from Necturus maculosus. The Journal of Physiology. 1991;444(1):133–151.

[106] Hamann S, Herrera-Perez JJ, Bundgaard M, Alvarez-Leefmans FJ, Zeuthen T. Water permeability of Na+–K+–2Cl- cotransporters in mammalian epithelial cells. The Journal of physiology. 2005;568(1):123–135.

[107] Loo DD, Zeuthen T, Chandy G, Wright EM. Cotransport of water by the Na+/glucose cotransporter. Proceedings of the National Academy of Sciences. 1996;93(23):13367–13370.

[108] Zeuthen T, Meinild AK, Klaerke DA, Loo DD, Wright EM, Belhage B, et al. Water transport by the Na+/glucose cotransporter under isotonic conditions Proceedings of a meeting held in Paris, 27–30 April, 1997, as a tribute to Jacques Bourguet.*. Biology of the Cell. 1997;89(5-6):307–312.

[109] Zeuthen T, Meinild AK, Loo D, Wright E, Klaerke D. Isotonic transport by the Na+-glucose cotransporter SGLT1 from humans and rabbit. The Journal of physiology. 2004;531(3):631–644.

[110] Zeuthen T, Zeuthen E, Klaerke DA. Mobility of ions, sugar, and water in the cytoplasm of Xenopus oocytes expressing Na+-coupled sugar transporters (SGLT1). The Journal of physiology. 2004;542(1):71–87.

[111] Zeuthen T, Belhage B, Zeuthen E. Water transport by Na+-coupled cotransporters of glucose (SGLT1) and of iodide (NIS). The dependence of substrate size studied at high resolution. The Journal of Physiology. 2006;570(3):485–499.

[112] Meinild A, Klaerke D, Loo D, Wright E, Zeuthen T. The human Na+–glucose cotransporter is a molecular water pump. The Journal of physiology. 1998;508(1):15–21.

[113] Zeuthen T, Zeuthen E. The mechanism of water transport in Na+-coupled glucose transporters expressed in Xenopus oocytes. Biophysical journal. 2007;93(4):1413.

[114] MacAulay N, Gether U, Klærke DA, Zeuthen T. Water transport by the human Na+-coupled glutamate cotransporter expressed in Xenopus oocytes. The Journal of physiology. 2001;530(3):367–378.

[115] MacAulay N, Zeuthen T, Gether U. Conformational basis for the Li+-induced leak current in the rat γ-aminobutyric acid (GABA) transporter-1. The Journal of physiology. 2004;544(2):447–458.

[116] Zeuthen T, Hamann S, La Cour M. Cotransport of H+, lactate and H2O by membrane proteins in retinal pigment epithelium of bullfrog. The Journal of physiology. 1996;497(Pt 1):3–17.

[117] Hamann S, la Cour M, Lui GM, Bundgaard M, Zeuthen T. Transport of protons and lactate in cultured human fetal retinal pigment epithelial cells. Pflügers Archiv European Journal of Physiology. 2000;440(1):84–92.

[118] Hamann S, Kiilgaard JF, Cour Ml, Prause JU, Zeuthen T. Cotransport of H+, lactate, and H2O in porcine retinal pigment epithelial cells. Experimental eye research. 2003;76(4):493–504.

[119] Meinild AK, Loo DD, Pajor AM, Zeuthen T, Wright EM. Water transport by the renal Na+-dicarboxylate cotransporter. American Journal of Physiology-Renal Physiology. 2000;278(5):F777–F783.

[120] Zeuthen T, MacAulay N. Cotransport of water by Na+–K+–2Cl- cotransporters expressed in Xenopus oocytes: NKCC1 versus NKCC2. The Journal of Physiology. 2012;590(5):1139–1154.

[121] Amiry-Moghaddam M, Frydenlund DS, Ottersen OP. Anchoring of aquaporin-4 in brain: molecular mechanisms and implications for the physiology and pathophysiology of water transport. Neuroscience. 2004;129(4):999–1010. Amiry-Moghaddam, M Frydenlund, D S Ottersen, O P Review United States Neuroscience Neuroscience. 2004;129(4):999-1010.

[122] Eid T, Lee TSW, Thomas MJ, Amiry-Moghaddam M, Bjornsen LP, Spencer DD, et al. Loss of perivascular aquaporin 4 may underlie deficient water and K+ homeostasis in the human epileptogenic hippocampus. Proceedings of the National Academy of Sciences of the United States of America. 2005;102(4):1193–1198.

[123] Noell S, Wolburg-Buchholz K, Mack AF, Ritz R, Tatagiba M, Beschorner R, et al. Dynamics of expression patterns of AQP4, dystroglycan, agrin and matrix metalloproteinases in human glioblastoma. Cell and Tissue Research. 2012;p. 1–13.

[124] Robel S, Berninger B, Götz M. The stem cell potential of glia: lessons from reactive gliosis. Nature Reviews Neuroscience. 2011;12(2):88–104.

[125] Yang J, Lunde LK, Nuntagij P, Oguchi T, Camassa LMA, Nilsson LNG, et al. Loss of astrocyte polarization in the Tg-ArcSwe mouse model of Alzheimer's disease. Journal of Alzheimer's Disease. 2011;27(4):711–722.

[126] Zeynalov E, Chen CH, Froehner SC, Adams ME, Ottersen OP, Amiry-Moghaddam M, et al. The perivascular pool of aquaporin-4 mediates the effect of osmotherapy in postischemic cerebral edema. Critical Care Medicine. 2008;36(9):2634–2640.

[127] Frydenlund DS, Bhardwaj A, Otsuka T, Mylonakou MN, Yasumura T, Davidson KG, et al. Temporary loss of perivascular aquaporin-4 in neocortex after transient middle cerebral artery occlusion in mice. Proceedings of the National Academy of Sciences. 2006;103(36):13532–13536.

[128] Heuser K, Eid T, Lauritzen F, Thoren AE, Vindedal GF, Taubøll E, et al. Loss of Perivascular Kir4. 1 Potassium Channels in the Sclerotic Hippocampus of Patients With Mesial Temporal Lobe Epilepsy. Journal of Neuropathology & Experimental Neurology. 2012;71(9):814–825.

[129] Aleman V, Osorio B, Chavez O, Rendon A, Mornet D, Martinez D. Subcellular localization of Dp71 dystrophin isoforms in cultured hippocampal neurons and forebrain astrocytes. Histochemistry and Cell Biology. 2001;115(3):243–254.

[130] Billard C, Gillet P, Signoret J, Uicaut E, Bertrand P, Fardeau M, et al. Cognitive functions in duchenne muscular dystrophy: A reappraisal and comparison with spinal muscular atrophy*. Neuromuscular Disorders. 1992;2(5-6):371–378.

[131] Pillers DA, Bulman DE, Weleber RG, Sigesmund DA, Musarella MA, Powell BR, et al. Dystrophin expression in the human retina is required for normal function as defined by electroretinography. Nat Genet. 1993;4(1):82–6.

[132] Daoud F, Angeard N, Demerre B, Martie I, Benyaou R, Leturcq F, et al. Analysis of Dp71 contribution in the severity of mental retardation through comparison of Duchenne and Becker patients differing by mutation consequences on Dp71 expression. Human molecular genetics. 2009;18(20):3779.

[133] Culligan K, Glover L, Dowling P, Ohlendieck K. Brain dystrophin-glycoprotein complex: persistent expression of beta-dystroglycan, impaired oligomerization of Dp71 and up-regulation of utrophins in animal models of muscular dystrophy. BMC cell biology. 2001;2(1):2.

[134] Fort PE, Sene A, Pannicke T, Roux MJ, Forster V, Mornet D, et al. Kir4.1 and AQP4 associate with Dp71- and utrophin-DAPs complexes in specific and defined microdomains of Muller retinal glial cell membrane. Glia. 2008;56(6):597–610.

[135] Neely JD, Amiry-Moghaddam M, Ottersen OP, Froehner SC, Agre P, Adams ME. Syntrophin-dependent expression and localization of Aquaporin-4 water channel protein. Proc Natl Acad Sci U S A. 2001;98(24):14108–13.

[136] Adams ME, Mueller HA, Froehner SC. In vivo requirement of the α-syntrophin PDZ domain for the sarcolemmal localization of nNOS and aquaporin-4. The Journal of cell biology. 2001;155(1):113–122.

[137] Amiry-Moghaddam M, Otsuka T, Hurn PD, Traystman RJ, Haug FM, Froehner SC, et al. An alpha-syntrophin-dependent pool of AQP4 in astroglial end-feet confers bidirectional water flow between blood and brain. Proc Natl Acad Sci U S A. 2003;100(4):2106–11.

[138] Bragg AD, Amiry-Moghaddam M, Ottersen OP, Adams ME, Froehner SC. Assembly of a perivascular astrocyte protein scaffold at the mammalian blood-brain barrier is dependent on alpha-syntrophin. Glia. 2006;53(8):879–890. Times Cited: 21.

[139] Bragg AD, Das SS, Froehner SC. Dystrophin-associated protein scaffolding in brain requires alpha-dystrobrevin. Neuroreport. 2010;21(10):695–9.

[140] Verkman AS. Aquaporins at a glance. Journal of cell science. 2011;124(Pt 13):2107–12.

[141] Preston GM, Carroll TP, Guggino WB, Agre P. Appearance of water channels in Xenopus oocytes expressing red cell CHIP28 protein. Science. 1992;256(5055):385–7.

[142] Fenton RA, Moeller HB, Zelenina M, Snaebjornsson MT, Holen T, MacAulay N. Differential water permeability and regulation of three aquaporin 4 isoforms. Cellular and molecular life sciences. 2010;67(5):829–840.

[143] Neely JD, Christensen BM, Nielsen S, Agre P. Heterotetrameric composition of aquaporin-4 water channels. Biochemistry. 1999;38(34):11156–11163.

[144] Walz T, Fujiyoshi Y, Engel A. The AQP structure and functional implications. Handbook of experimental pharmacology. 2009;190(1):31–56.

[145] Rash JE, Yasumura T. Direct immunogold labeling of connexins and aquaporin-4 in freeze-fracture replicas of liver, brain, and spinal cord: factors limiting quantitative analysis. Cell and tissue research. 1999;296(2):307–321.

[146] Verkman A, Mitra AK. Structure and function of aquaporin water channels. American Journal of Physiology-Renal Physiology. 2000;278(1):F13.

[147] Binder DK, Yao X, Zador Z, Sick TJ, Verkman AS, Manley GT. Increased seizure duration and slowed potassium kinetics in mice lacking aquaporin-4 water channels. Glia. 2006;53(6):631–636.

[148] Lu DC, Zhang H, Zador Z, Verkman A. Impaired olfaction in mice lacking aquaporin-4 water channels. The FASEB Journal. 2008;22(9):3216.

[149] Li J, Verkman A. Impaired hearing in mice lacking aquaporin-4 water channels. Journal of Biological Chemistry. 2001;276(33):31233.

[150] Li J, Patil RV, Verkman A. Mildly abnormal retinal function in transgenic mice without Müller cell aquaporin-4 water channels. Investigative ophthalmology & visual science. 2002;43(2):573.

[151] Amiry-Moghaddam M, Williamson A, Palomba M, Eid T, de Lanerolle NC, Nagelhus EA, et al. Delayed K+ clearance associated with aquaporin-4 mislocalization: Phenotypic defects in brains of alpha-syntrophin-null mice. Proceedings of the National Academy of Sciences of the United States of America. 2003;100(23):13615–13620.

[152] Binder DK, Nagelhus EA, Ottersen OP. Aquaporin-4 and epilepsy. Glia. 2012;.

[153] Ruiz-Ederra J, Zhang H, Verkman AS. Evidence against functional interaction between aquaporin-4 water channels and Kir4.1 potassium channels in retinal Muller cells. J Biol Chem. 2007;282(30):21866–72.

[154] Zhang H, Verkman A. Aquaporin-4 independent Kir4. 1 K< sup>+</sup> channel function in brain glial cells. Molecular and Cellular Neuroscience. 2008;37(1):1–10.

[155] Jin BJ, Zhang H, Binder DK, Verkman A. Aquaporin-4–dependent K+ and water transport modeled in brain extracellular space following neuroexcitation. The Journal of general physiology. 2013;141(1):119–132.

[156] Soe R, MacAulay N, Klaerke DA. Modulation of Kir4. 1 and Kir4. 1–Kir5. 1 channels by small changes in cell volume. Neuroscience letters. 2009;457(2):80–84.

[157] Saadoun S, Papadopoulos MC, Hara-Chikuma M, Verkman A. Impairment of angiogenesis and cell migration by targeted aquaporin-1 gene disruption. Nature. 2005;434(7034):786–792.

[158] Saadoun S, Papadopoulos MC, Watanabe H, Yan D, Manley GT, Verkman AS. Involvement of aquaporin-4 in astroglial cell migration and glial scar formation. J Cell Sci. 2005;118(Pt 24):5691–8.

[159] Moeller H, Fenton R, Zeuthen T, Macaulay N. Vasopressin-dependent short-term regulation of aquaporin 4 expressed in< i> Xenopus</i> oocytes. Neuroscience. 2009;164(4):1674–1684.

[160] Haj-Yasein NN, Jensen V, Østby I, Omholt SW, Voipio J, Kaila K, et al. Aquaporin-4 regulates extracellular space volume dynamics during high-frequency synaptic stimulation: A gene deletion study in mouse hippocampus. Glia. 2012;.

[161] Manley GT, Fujimura M, Ma T, Noshita N, Filiz F, Bollen AW, et al. Aquaporin-4 deletion in mice reduces brain edema after acute water intoxication and ischemic stroke. Nat Med. 2000;6(2):159–63.

[162] Papadopoulos MC, Verkman AS. Aquaporin-4 gene disruption in mice reduces brain swelling and mortality in pneumococcal meningitis. J Biol Chem. 2005;280(14):13906–12.

[163] Papadopoulos MC, Manley GT, Krishna S, Verkman AS. Aquaporin-4 facilitates reabsorption of excess fluid in vasogenic brain edema. FASEB J. 2004;18(11):1291–3.

[164] Bloch O, Papadopoulos MC, Manley GT, Verkman AS. Aquaporin-4 gene deletion in mice increases focal edema associated with staphylococcal brain abscess. J Neurochem. 2005;95(1):254–62.

[165] Saadoun S, Bell BA, Verkman A, Papadopoulos MC. Greatly improved neurological outcome after spinal cord compression injury in AQP4-deficient mice. Brain. 2008;131(4):1087.

[166] Kimura A, Hsu M, Seldin M, Verkman AS, Scharfman HE, Binder DK. Protective role of aquaporin-4 water channels after contusion spinal cord injury. Annals of neurology. 2010;67(6):794–801.

[167] Aoki-Yoshino K, Uchihara T, Duyckaerts C, Nakamura A, Hauw JJ, Wakayama Y. Enhanced expression of aquaporin 4 in human brain with inflammatory diseases. Acta neuropathologica. 2005;110(3):281–288.

[168] Sinclair C, Kirk J, Herron B, Fitzgerald U, McQuaid S. Absence of aquaporin-4 expression in lesions of neuromyelitis optica but increased expression in multiple sclerosis lesions and normal-appearing white matter. Acta neuropathologica. 2007;113(2):187–194.

[169] Wolburg-Buchholz K, Mack AF, Steiner E, Pfeiffer F, Engelhardt B, Wolburg H. Loss of astrocyte polarity marks blood–brain barrier impairment during experimental autoimmune encephalomyelitis. Acta neuropathologica. 2009;118(2):219–233.

[170] Lennon VA, Kryzer TJ, Pittock SJ, Verkman A, Hinson SR. IgG marker of optic-spinal multiple sclerosis binds to the aquaporin-4 water channel. The Journal of experimental medicine. 2005;202(4):473–477.

[171] Jarius S, Wildemann B. AQP4 antibodies in neuromyelitis optica: diagnostic and pathogenetic relevance. Nature Reviews Neurology. 2010;6(7):383–392.

[172] Verkhratsky A, Olabarria M, Noristani HN, Yeh CY, Rodriguez JJ. Astrocytes in Alzheimer's disease. Neurotherapeutics. 2010;7(4):399–412.

[173] Sinha S, Lieberburg I. Cellular mechanisms of beta-amyloid production and secretion. Proceedings of the National Academy of Sciences. 1999;96(20):11049–11053.

[174] Hardy JA, Higgins GA. Alzheimer's disease: the amyloid cascade hypothesis. Science; Science. 1992;.

[175] Bateman RJ, Munsell LY, Morris JC, Swarm R, Yarasheski KE, Holtzman DM. Human amyloid-β synthesis and clearance rates as measured in cerebrospinal fluid in vivo. Nature medicine. 2006;12(7):856–861.

[176] Lee CYD, Landreth GE. The role of microglia in amyloid clearance from the AD brain. Journal of neural transmission. 2010;117(8):949–960.

[177] Deane R, Bell R, Sagare A, Zlokovic B. Clearance of amyloid-β peptide across the blood-brain barrier: implication for therapies in Alzheimer's disease. CNS & neurological disorders drug targets. 2009;8(1):16.

[178] Wang F, Feng X, Li Y, Yang H, Ma T. Aquaporins as potential drug targets. Acta Pharmacologica Sinica. 2006;27(4):395–401.

[179] Frigeri A, Nicchia GP, Svelto M. Aquaporins as targets for drug discovery. Current pharmaceutical design. 2007;13(23):2421–2427.

[180] Huber VJ, Tsujita M, Kwee IL, Nakada T. Inhibition of aquaporin 4 by antiepileptic drugs. Bioorganic & medicinal chemistry. 2009;17(1):418–424.

[181] Wang Y, Tajkhorshid E. Nitric oxide conduction by the brain aquaporin AQP4. Proteins: Structure, Function, and Bioinformatics. 2010;78(3):661–670.

[182] Frigeri A, Nicchia GP, Nico B, Quondamatteo F, Herken R, Roncali L, et al. Aquaporin-4 deficiency in skeletal muscle and brain of dystrophic mdx mice. FASEB J. 2001;15(1):90–98.

[183] Ottersen OP. Quantitative electron microscopic immunocytochemistry of neuroactive amino acids. Anat Embryol (Berl). 1989;180(1):1–15. Ottersen, O P Research Support, Non-U.S. Gov't Review Germany, west Anatomy and embryology Anat Embryol (Berl). 1989;180(1):1-15.

[184] Mathiisen TM, Nagelhus EA, Jouleh B, Torp R, Frydenlund DS, Mylonakou MN, et al. Postembedding Immunogold Cytochemistry of Membrane Molecules and Amino Acid Transmitters in the Central Nervous System. In: Laszlo Zaborszky FGW, Lanciego JL, editors. Neuroanatomical Tract-Tracing 3. Springer US; 2006. p. 72–108.

[185] Palay SL, McGee-Russell S, Gordon Jr S, Grillo MA. Fixation of neural tissues for electron microscopy by perfusion with solutions of osmium tetroxide. The Journal of cell biology. 1962;12(2):385–410.

[186] Berod A, Hartman B, Pujol J. Importance of fixation in immunohistochemistry: use of formaldehyde solutions at variable pH for the localization of tyrosine hydroxylase. Journal of Histochemistry & Cytochemistry. 1981;29(7):844–850.

[187] Hjelle OP, Chaudhry FA, Ottersen OP. Antisera to glutathione: characterization and immunocytochemical application to the rat cerebellum. Eur J Neurosci. 1994;6(5):793–804.

[188] Matsubara A, Laake JH, Davanger S, Usami S, Ottersen OP. Organization of AMPA receptor subunits at a glutamate synapse: a quantitative immunogold analysis of hair cell synapses in the rat organ of Corti. J Neurosci. 1996;16(14):4457–67.

[189] Haug FMS. Widefield digital images in biological transmission electron microscopy (TEM) obtained by automatic image montage. Proceedings: Microscopy and Microanalysis. 1996;p. 618–619.

[190] Laake JH, Slyngstad TA, Haug FM, Ottersen OP. Glutamine from glial cells is essential for the maintenance of the nerve terminal pool of glutamate: immunogold evidence from hippocampal slice cultures. J Neurochem. 1995;65(2):871–81.

[191] Haug FMS. Particle-counting in immunogold labelled ultrathin sections by transmission electron microscopy and image analysis. Analytical Cellular Pathology. 1994;6:297.

[192] Cox GA, Phelps SF, Chapman VM, Chamberlain JS. New mdx mutation disrupts expression of muscle and nonmuscle isoforms of dystrophin. Nat Genet. 1993;4(1):87–93.

[193] Dalloz C, Claudepierre T, Rodius F, Mornet D, Sahel J, Rendon A. Differential distribution of the members of the dystrophin glycoprotein complex in mouse retina: effect of the mdx(3Cv) mutation. Mol Cell Neurosci. 2001;17(5):908–20.

[194] Vaillend C, Ungerer A. Behavioral characterization of< i> mdx3cv</i> mice deficient in C-terminal dystrophins. Neuromuscular Disorders. 1999;9(5):296–304.

[195] Adams ME, Kramarcy N, Krall SP, Rossi SG, Rotundo RL, Sealock R, et al. Absence of α-syntrophin leads to structurally aberrant neuromuscular synapses deficient in utrophin. The Journal of cell biology. 2000;150(6):1385.

[196] Thrane AS, Rappold PM, Fujita T, Torres A, Bekar LK, Takano T, et al. Critical role of aquaporin-4 (AQP4) in astrocytic Ca2+ signaling events elicited by cerebral edema. Proceedings of the National Academy of Sciences. 2011;108(2):846–851.

[197] Strohschein S, Hüttmann K, Gabriel S, Binder DK, Heinemann U, Steinhäuser C. Impact of aquaporin-4 channels on K+ buffering and gap junction coupling in the hippocampus. Glia. 2011;59(6):973–980.

[198] Saadoun S, Tait M, Reza A, Davies DC, Bell B, Verkman A, et al. AQP4 gene deletion in mice does not alter blood–brain barrier integrity or brain morphology. Neuroscience. 2009;161(3):764–772.

[199] Zhou J, Kong H, Hua X, Xiao M, Ding J, Hu G. Altered blood-brain barrier integrity in adult aquaporin-4 knockout mice. Neuroreport. 2008;19(1):1–5.

[200] Feng X, Papadopoulos MC, Liu J, Li L, Zhang D, Zhang H, et al. Sporadic obstructive hydrocephalus in Aqp4 null mice. Journal of neuroscience research. 2009;87(5):1150–1155.

[201] Yao X, Hrabětová S, Nicholson C, Manley GT. Aquaporin-4-deficient mice have increased extracellular space without tortuosity change. The Journal of Neuroscience. 2008;28(21):5460–5464.

[202] Skucas VA, Mathews IB, Yang J, Cheng Q, Treister A, Duffy AM, et al. Impairment of select forms of spatial memory and neurotrophin-dependent synaptic plasticity by deletion of glial aquaporin-4. The Journal of Neuroscience. 2011;31(17):6392–6397.

[203] Eilert-Olsen M, Haj-Yasein NN, Vindedal GF, Enger R, Gundersen GA, Hoddevik EH, et al. Deletion of aquaporin-4 changes the perivascular glial protein scaffold without disrupting the brain endothelial barrier. Glia. 2012;.

[204] Li YK, Wang F, Wang W, Luo Y, Wu PF, Xiao JL, et al. Aquaporin-4 deficiency impairs synaptic plasticity and associative fear memory in the lateral amygdala: involvement of downregulation of glutamate transporter-1 expression. Neuropsychopharmacology. 2012;.

[205] Fan Y, Liu M, Wu X, Wang F, Ding J, Chen J, et al. Aquaporin-4 promotes memory consolidation in Morris water maze. Brain Structure and Function. 2013;218(1):39–50.

[206] Wolburg H, Wolburg-Buchholz K, Fallier-Becker P, Noell S, Mack AF. Structure and functions of aquaporin-4-based orthogonal arrays of particles. Int Rev Cell Mol Biol. 2011;287:1–41.

[207] Szentistvanyi I, Patlak CS, Ellis RA, Cserr HF. Drainage of interstitial fluid from different regions of rat brain. American Journal of Physiology-Renal Physiology. 1984;246(6):F835–F844.

[208] Carare R, Bernardes-Silva M, Newman T, Page A, Nicoll J, Perry V, et al. Solutes, but not cells, drain from the brain parenchyma along basement membranes of capillaries and arteries: significance for cerebral amyloid angiopathy and neuroimmunology. Neuropathology and applied neurobiology. 2008;34(2):131–144.

[209] Hadaczek P, Yamashita Y, Mirek H, Tamas L, Bohn MC, Noble C, et al. The "perivascular pump" driven by arterial pulsation is a powerful mechanism for the distribution of therapeutic molecules within the brain. Molecular Therapy. 2006;14(1):69–78.

[210] Rennels M, Blaumanis O, Grady P, et al. Rapid solute transport throughout the brain via paravascular fluid pathways. Advances in neurology. 1990;52:431.

[211] Ichimura T, Fraser P, Cserr HF. Distribution of extracellular tracers in perivascular spaces of the rat brain. Brain research. 1991;545(1):103–113.

[212] Pullen R, DePasquale M, Cserr HF. Bulk flow of cerebrospinal fluid into brain in response to acute hyperosmolality. American Journal of Physiology-Renal Physiology. 1987;253(3):F538–F545.

[213] Abbott NJ. Evidence for bulk flow of brain interstitial fluid: significance for physiology and pathology. Neurochemistry international. 2004;45(4):545–552.

[214] Proescholdt M, Hutto B, Brady L, Herkenham M. Studies of cerebrospinal fluid flow and penetration into brain following lateral ventricle and cisterna magna injections of the tracer [< sup> 14</sup> C] inulin in rat. Neuroscience. 1999;95(2):577–592.

[215] Dorr A, Sled J, Kabani N. Three-dimensional cerebral vasculature of the CBA mouse brain: a magnetic resonance imaging and micro computed tomography study. Neuroimage. 2007;35(4):1409–1423.

[216] Bradbury M, Westrop R. Factors influencing exit of substances from cerebrospinal fluid into deep cervical lymph of the rabbit. The Journal of physiology. 1983;339(1):519–534.

[217] Boulton M, Yonung A, Hay J, Armstrong D, Flessner M, Schwartz M, et al. Drainage of CSF through lymphatic pathways and arachnoid villi in sheep: measurement of 125l-albumin clearance. Neuropathology and applied neurobiology. 2008;22(4):325–333.

[218] Johnston M, Zakharov A, Papaiconomou C, Salmasi G, Armstrong D, et al. Evidence of connections between cerebrospinal fluid and nasal lymphatic vessels in humans, non-human primates and other mammalian species. Cerebrospinal Fluid Res. 2004;1(2):1–13.

[219] Ball KK, Cruz NF, Mrak RE, Dienel GA. Trafficking of glucose, lactate, and amyloid-β from the inferior colliculus through perivascular routes. Journal of Cerebral Blood Flow & Metabolism. 2009;30(1):162–176.

[220] Ross G, O'Callaghan J, Sharp D, Petrovitch H, Miller D, Abbott R, et al. Quantification of regional glial fibrillary acidic protein levels in Alzheimer's disease. Acta neurologica scandinavica. 2003;107(5):318–323.

[221] O'Callaghan JP, Miller DB. The concentration of glial fibrillary acidic protein increases with age in the mouse and rat brain. Neurobiology of aging. 1991;12(2):171–174.

[222] Verkhratsky A, Parpura V. Recent advances in (patho) physiology of astroglia. Acta Pharmacologica Sinica. 2010;31(9):1044–1054.

[223] Hamby ME, Sofroniew MV. Reactive astrocytes as therapeutic targets for CNS disorders. Neurotherapeutics. 2010;7(4):494–506.

[224] Cserr H, Cooper D, Suri P, Patlak C. Efflux of radiolabeled polyethylene glycols and albumin from rat brain. American Journal of Physiology-Renal Physiology. 1981;240(4):F319–F328.

[225] Groothuis DR, Vavra MW, Schlageter KE, Kang EWY, Itskovich AC, Hertzler S, et al. Efflux of drugs and solutes from brain: the interactive roles of diffusional transcapillary transport, bulk flow and capillary transporters. Journal of Cerebral Blood Flow & Metabolism. 2006;27(1):43–56.

[226] Li L, Zhang H, Varrin-Doyer M, Zamvil SS, Verkman A. Proinflammatory role of aquaporin-4 in autoimmune neuroinflammation. The FASEB Journal. 2011;25(5):1556–1566.

[227] Verkman A. Aquaporins: translating bench research to human disease. Journal of Experimental Biology. 2009;212(11):1707–1715.

Paper I

Molecular scaffolds underpinning macroglial polarization: an analysis of retinal Müller cells and brain astrocytes in mouse.

Rune Enger, **Georg Andreas Gundersen**, Nadia Nabil Haj-Yasein, Martine Eilert-Olsen, Anna Elisabeth Thoren, Gry Fluge Vindedal, Finn-Mogens S. Haug, Petur Henry Petersen, Maiken Nedergaard and Erlend A. Nagelhus
Glia. 2012 Dec;60(12):2018-26. doi: 10.1002/glia.22416. Epub 2012 Sep 17

Enger and Gundersen contributed equally to this study.

Paper II

Evidence that pericytes regulate aquaporin-4 polarization in mouse cortical astrocytes

Georg Andreas Gundersen, Gry Fluge Vindedal, Øivind Skare, Erlend A. Nagelhus
Submitted manuscript. 2013

Evidence that pericytes regulate aquaporin-4 polarization in mouse cortical astrocytes

Georg A. Gundersen[1,2]*, Gry Fluge Vindedal[1,2], Øivind Skare[3], and Erlend A. Nagelhus[1,2, 4]*

[1]Centre for Molecular Medicine Norway, Nordic EMBL Partnership, University of Oslo, 0318 Oslo, Norway.

[2]Letten Centre and Department of Physiology, Institute of Basic Medical Sciences, University of Oslo, 0317 Oslo, Norway.

[3]National Institute of Occupational Health, 0033 Oslo, Norway.

[4]Department of Neurology, Oslo University Hospital, Rikshospitalet, 0027 Oslo

*To whom correspondence should be addressed:

Professor Erlend A. Nagelhus, Centre for Molecular Medicine Norway, Nordic EMBL Partnership, University of Oslo, P.O. Box 1137 Blindern, N-0318 Oslo, Norway. E-mail: e.a.nagelhus@medisin.uio.no

Phone: +47 91736316

This work was supported by the Research Council of Norway (NevroNor grant #199453 and FRIMEDBIO grant #213964), Civitan Norway's Research Fund for Alzheimer's disease, and by the Letten Foundation.

Abstract

Aquaporin-4 (AQP4) water channels are concentrated in astrocytic endfoot membranes at the brain-blood and brain-cerebrospinal fluid interfaces. The mechanisms underpinning the polarized distribution of AQP4 are poorly understood. Here we tested the hypothesis that pericytes regulate AQP4 anchoring to perivascular membranes. Quantitative immunogold analysis revealed that AQP4 expression was higher in endfoot membranes abutting pericytes than in those facing endothelial cells. Similar findings were made for α-syntrophin, a member of the dystrophin associated protein complex (DAPC). The enrichment of α-syntrophin in membranes ensheathing pericytes persisted after *Aqp4* deletion. Our data support the concept that pericytes regulate AQP4 polarization.

Key words

Astrocytes; cerebrospinal fluid; glial cells; neurovascular unit; pericytes

Introduction

AQP4 regulates water transport across the blood-brain barrier (BBB) and along paravascular pathways.[1, 2] Early immunogold studies revealed that AQP4 has a polarized distribution, with tenfold higher density in glial endfoot membranes than in other membrane domains.[3] Later it was shown that the DAPC is essential for AQP4 polarization in glia. Notably, mice deficient in dystrophin,[4, 5] α-syntrophin,[6, 7] dystroglycan,[8] or α-dystrobrevin[9] show reduced perivascular AQP4 expression. The DAPC is attached to the perivascular basal lamina through binding between the α-subunit of dystroglycan and the extracellular matrix components laminin and agrin.[10] Hence, loss of agrin reduces AQP4 expression in glial endfeet surrounding blood vessels.[11]

The concept that vascular cells regulate AQP4 anchoring was bolstered by the discovery that pericyte-deficient mice showed abnormal AQP4 expression around blood vessels.[12] However, the mutant mice used in this study had abnormal vessel diameter, disrupted BBB, and increased brain water content, which could have indirect effects on the subcellular AQP4 distribution. In the present study we used mice with intact BBB and investigated whether AQP4 anchoring in astrocytic endfeet depends on their intimate relationship to pericytes.

Materials and Methods

Animals. Male wild-type (C57BL/6, Jackson Laboratories, Boulder, CO), *Aqp4*$^{-/-}$, α-*syntrophin*$^{-/-}$,[7] and *GLT1*-eGFP/*NG2*-DsRed double-transgenic[2] mice at 8-18 weeks of age were used in this study. The animals were allowed ad libitum access to food and

drinking water. All experiments comply with Norwegian laws and were approved by the Animal Care and Use Committee of Institute of Basic Medical Sciences, University of Oslo.

Fixation. The animals were deeply anesthetized with a mixture of chloral hydrate, magnesium sulphate and pentobarbital (142, 70 and 32 mg/kg body weight i.p., respectively) before transcardiac perfusion (flow rate ~8ml/min) with 2% dextran in 0.1 M phosphate buffer (PB; pH 7.4) for 15-20 sec and either 4% formaldehyde in PB for 15 minutes (for immunofluorescence experiments; 3 *GLT1*-eGFP/*NG2*-DsRed double-transgenic mice were used), 4% formaldehyde and 0.1% glutaraldehyde in PB for 20 minutes (for AQP4 immunogold cytochemistry; 5 wild-type and 5 *Aqp4*$^{-/-}$ mice were used), or bicarbonate-buffered 4% formaldehyde containing 0.2% picric acid at pH 6.0, followed by a similar fixative at pH 10.0 ("pH-shift" protocol)[3] (for α-syntrophin immunogold cytochemistry; 5 wild-type, 5 *Aqp4*$^{-/-}$, and 3 α-*syntrophin*$^{-/-}$ mice were used) .

Light microscopic immunocytochemistry. The perfused animals were stored at 4^{o} C overnight. The brain was removed and cryoprotected in sucrose (10%, 20% and 30% in PB), and sections were cut at 15 μm on a cryostat. Light microscopic immunocytochemistry was carried out using an indirect fluorescence method.[3] The primary anti-AQP4 antibody (Sigma, 2μg/ml) was revealed by donkey secondary antibodies with indodicarbocyanine (Cy5, Jackson ImmunoResearch Laboratories, Inc., West Grove, PA; 1:1,000). Cortical sections were viewed and photographed with a Zeiss LSM 5 PASCAL microscope equipped with epifluorescence optics, using filter BP 505-530, LP 560 and LP 650, and objective 20X/0.75 Plan-Apochromat,

40X/1.3 Oil Plan-Neofluar, or 63X/1.40 Oil Plan-Apochromat.

Embedding and electron microscopic cytochemistry. Small blocks of fixed cortex were subjected to freeze substitution as described previously.[3] In brief, the specimens were cryoprotected by immersion in graded concentrations of glycerol (10, 20, and 30%) in PB and plunged into liquid propane (-170°C) in a cryofixation unit (KF 80; Reichert, Wien, Austria). The samples were then immersed in 0.5% uranyl acetate dissolved in anhydrous methanol (-90°C) in a cryosubstitution unit (AFS; Reichert). The temperature was raised in steps of 4°C /h to -45°C. Samples were washed with anhydrous methanol and infiltrated with Lowicryl HM20 resin at -45°C with a progressive increase in the ratio of resin to methanol. Polymerization was carried out with UV light (360 nm) for 48 h. Ultrathin sections were cut with a Reichert ultramicrotome, mounted on nickel grids, and processed for immunogold cytochemistry as described previously.[3] Briefly, sections were incubated sequentially in the following solutions (at room temperature): (1) 50 mM glycine in Tris buffer (5 mM) containing 0.01% Triton X-100 and 50mM NaCl (TBST; 10 min); (2) 0.2% milk powder in TBST (10 min); (3) primary antibodies (AQP4, amino acid residues 249-323, Milipore, 1.5 µg/ml; α-syntrophin (Ab Syn259)[13], 1.2 µg/ml) diluted in the solution used in the preceding step (overnight); (4) same solution as in step 1 (10 min x 2); (5) same solution as in step 2 (10 min); (6) gold-conjugated IgG (GAR10 nm; Abcam), diluted 1:20 in TBST containing 2% human serum albumin or 0.2% milk powder and polyethylene glycol (0.5 mg/ml, 1 h). Finally, the sections were counterstained and examined in a Fei Tecnai 12 transmission electron microscope.

Detection and quantification of gold particles. The analyzer was blind to

genotypes. Digital images were acquired with a commercially available image analysis program ("analySIS" Soft Imaging Systems GmbH, Münster). The program had been modified for acquisition of high-resolution digital images and semiautomatic evaluation of immunogold-labeled cellular volumes and surfaces (membranes). For the present purpose, images of membrane segments were recorded at a nominal magnification of x43.000, in 2.048 x 2.048 (8-bit) images. All membrane segments that could be identified as belonging to perivascular endfeet of astrocyte cells were imaged. Membrane segments of interest were drawn in the overlay and assigned a type label. Gold particles in the neighborhood of each membrane-curve were detected semiautomatically, and the distance between each particle's centre of gravity and its membrane curve was calculated by the program. All images, with associated curves, particles, and measurements, were saved to allow later verification and correction. Further analyses were done in analySIS. Particles localized within 23.5 nm from their membrane curve were included in the automated calculation of the number of particles per unit length of membrane (linear particle density). The measurements were exported to the SPSS 18.0 for Mac software package (SPSS, Chicago, IL) for survey and quality control.

Statistical analysis of immunogold data. We used Poisson mixed models for the analyses of the gold particle counts in the AQP4 and α-syntrophin data. These models take into account the dependency between observations by including nested variance terms. Three variance terms were included, one for between animal variation, one for between membrane domain variation, and one for within membrane domain variation. These models were analysed by the R function glmer in the lme4 package, which gave us estimated differences in linear particle density between membrane domains

(endfoot membranes facing endothelial cells and pericytes, respectively) with corresponding *P* values. In the AQP4 analysis we allowed the within membrane variation to differ between membranes. The chosen model structures were based on likelihood ratio tests.[5]

Results

AQP4 immufluorescence labeling of *GLT1*-eGFP/*NG2*-DsRed double-transgenic mice, which express fluorescent reporters in astrocytes (Figure 1A) and pericytes (Figure 1B), revealed strong AQP4 signal in perivascular astrocytic processes adjacent to pericytes (Figure 1C,D).

Immunogold cytochemistry of wild-type mice confirmed AQP4's polarized distribution, with AQP4 signaling gold particles clustered over astrocytic endfoot membranes, in particular where in contact with pericytes (Figure 2A). Quantitative analysis revealed that the density of gold particles was 40% higher over membrane domains next to pericytes than over those facing endothelial cells (Figure 2B; values were 14.20 ± 0.81, n=38, and 10.15 ± 0.67, n=72, respectively). The amount of unspecific labeling was revealed in corresponding membranes of *Aqp4*$^{-/-}$ mice and was only 1-2% (values were 0.15 ± 0.04, n= 91, and 0.14 ± 0.11, n=18).

We next investigated whether the enrichment of AQP4 in specific endfoot membrane domains was paralleled with increased expression of the AQP4-anchoring molecule α-syntrophin. Indeed, α-syntrophin immunogold reactivity was 33% higher in membrane domains adjacent to pericytes versus endothelial cells (Figure 2C,D; values were 3.22 ± 0.39, n=61, and 2.43 ± 0.16, n= 215, respectively). Deletion of

Aqp4 reduced perivascular α-syntrophin labeling, as reported previously,[7] but did not affect the pattern of α-syntrophin distribution in endfoot domains. Thus, in *Aqp4*$^{-/-}$ mice the α-syntrophin immunogold signal was still 32% higher in endfoot membranes next to pericytes than over those next to endothelial cells (Figure 2E,F; values were 1.49 ± 0.19, n=53, and 1.13 ± 0.09, n=198). The density of gold particles over endfoot membranes adjacent to pericytes and endothelial cells in α-*syntrophin*$^{-/-}$ mice was 0.25 ± 0.12, n=30, and 0.17 ± 0.04, n=146, respectively. Thus, unspecific labeling in the α-syntrophin experiments amounted to less than 8% of the wild-type signal.

Discussion

Polarized distribution of membrane proteins is essential for normal function of cells and tissues. A hallmark of glia is their polarization,[14, 15] with AQP4 being concentrated in glial endfoot membranes bordering liquor and paravascular compartments.[3] Loss of AQP4 from perivascular membranes occurs in epilepsy, stroke, brain injury and Alzheimer's disease, but the mechanisms are poorly understood.[15]

We now demonstrate that perivascular astrocytic endfoot membranes differ in their AQP4 expression. Specifically, the density of water channels is higher in membrane domains abutting pericytes than in those facing endothelial cells. Thus, the expression of AQP4 not only depends on which compartment the membrane faces, but also on the adjacent cell type.

The enrichment of AQP4 in membrane domains next to pericytes suggests that pericytes regulate AQP4 anchoring. Indeed, the AQP4-anchoring molecule α-

syntrophin was also concentrated in membrane domains adjacent to pericytes. The clustering of α-syntrophin in these domains persisted after *Aqp4* deletion, indicating that pericytes can influence the DAPC independent of AQP4. How pericytes control the expression of endfoot scaffolding proteins is unknown, but one possibility is by secretion of agrin, which binds α-dystroglycan.[15] Altered agrin secretion from vascular cells may underlie loss of glial AQP4 polarization in disease.

The functional consequences of heterogeneous AQP4 expression along the vascular glial sheath are elusive. Brain-blood water diffusion distance is usually longer at sites where pericytes are interposed between the glial sheath and endothelial cells. It is conceivable that the higher water permeability of glial membranes at such sites can partly compensate for the longer diffusion distance. Moreover, the enrichment of AQP4 in glial membranes adjacent to pericytes may serve to facilitate fluid transport between the paravascular space and the brain parenchyma. Notably, CSF recycles into the brain along penetrating arterioles and enters the neuropil by AQP4 dependent mechanisms.[2] Finally, an intriguing possibility could be that the AQP4 supramolecular complex serves important signaling functions and thus are targeted to glial membranes adjacent to contractile vascular cells.

Platelet-derived growth factor B (PDGF-B) retention motif knockout mice lack pericytes and show reduced expression of perivascular AQP4 and α-syntrophin.[12] However, the mutant mice have vascular abnormalities that indirectly could affect AQP4 distribution, cf. Introduction. In the present study we have provided evidence that pericytes regulate AQP4 anchoring and polarization in normal mice. Our discovery that astrocytic processes contacting pericytes are equipped with specialized membrane domains adds complexity to the concept of astrocyte polarization and may pave the way for new understanding of mechanisms underlying loss of polarization in

disease.

Disclosure/Conflict of Interest

The authors declare no conflict of interest.

Acknowledgements

We thank Mrs. Bjørg Riber, Mrs. Karen Marie Gujord, Mrs. Jorunn Knutsen, Dr. Martine Eilert-Olsen, Dr. Nadia Nabil Haj-Yasein, and Dr. Johannes Helm, Institute of Basic Medical Sciences, University of Oslo, for expert technical assistance. Professor Stan C. Froehner, University of Washington, Seattle, kindly provided the α-syntrophin antibody Syn259 and *α-syntrophin*$^{-/-}$ mice, and Professor Ole P. Ottersen, University of Oslo, shared the *Aqp4*$^{-/-}$ mice.

References

(1) Haj-Yasein NN, Vindedal GF, Eilert-Olsen M, Gundersen GA, Skare O, Laake P, et al. Glial-conditional deletion of aquaporin-4 (Aqp4) reduces blood-brain water uptake and confers barrier function on perivascular astrocyte endfeet. *Proc Natl Acad Sci U S A* 2011 Oct 25;**108**(43):17815-17820.

(2) Iliff JJ, Wang M, Liao Y, Plogg BA, Peng W, Gundersen GA, et al. A paravascular pathway facilitates CSF flow through the brain parenchyma and

the clearance of interstitial solutes, including amyloid beta. *Sci Transl Med* 2012 Aug 15;**4**(147):147ra111.

(3) Nagelhus EA, Veruki ML, Torp R, Haug FM, Laake JH, Nielsen S, et al. Aquaporin-4 water channel protein in the rat retina and optic nerve: polarized expression in Muller cells and fibrous astrocytes. *J Neurosci* 1998 Apr 1;**18**(7):2506-2519.

(4) Frigeri A, Nicchia GP, Nico B, Quondamatteo F, Herken R, Roncali L, et al. Aquaporin-4 deficiency in skeletal muscle and brain of dystrophic mdx mice. *FASEB J* 2001 Jan;**15**(1):90-98.

(5) Enger R, Gundersen GA, Haj-Yasein NN, Eilert-Olsen M, Thoren AE, Vindedal GF, et al. Molecular scaffolds underpinning macroglial polarization: an analysis of retinal Muller cells and brain astrocytes in mouse. *Glia* 2012 Dec;**60**(12):2018-2026.

(6) Neely JD, Amiry-Moghaddam M, Ottersen OP, Froehner SC, Agre P, Adams ME. Syntrophin-dependent expression and localization of Aquaporin-4 water channel protein. *Proc Natl Acad Sci U S A* 2001 Nov 20;**98**(24):14108-14113.

(7) Eilert-Olsen M, Haj-Yasein NN, Vindedal GF, Enger R, Gundersen GA, Hoddevik EH, et al. Deletion of aquaporin-4 changes the perivascular glial protein scaffold without disrupting the brain endothelial barrier. *Glia* 2012 Mar;**60**(3):432-440.

(8) Noell S, Wolburg-Buchholz K, Mack AF, Beedle AM, Satz JS, Campbell KP, et al. Evidence for a role of dystroglycan regulating the membrane architecture of astroglial endfeet. *Eur J Neurosci* 2011 Jun;**33**(12):2179-2186.

(9) Lien CF, Mohanta SK, Frontczak-Baniewicz M, Swinny JD, Zablocka B, Gorecki DC. Absence of glial alpha-dystrobrevin causes abnormalities of the blood-brain barrier and progressive brain edema. *J Biol Chem* 2012 Nov 30;**287**(49):41374-41385.

(10) Satz JS, Ostendorf AP, Hou S, Turner A, Kusano H, Lee JC, et al. Distinct functions of glial and neuronal dystroglycan in the developing and adult mouse brain. *J Neurosci* 2010 Oct 27;**30**(43):14560-14572.

(11) Rauch SM, Huen K, Miller MC, Chaudry H, Lau M, Sanes JR, et al. Changes in brain beta-amyloid deposition and aquaporin 4 levels in response to altered agrin expression in mice. *J Neuropathol Exp Neurol* 2011 Dec;**70**(12):1124-1137.

(12) Armulik A, Genove G, Mae M, Nisancioglu MH, Wallgard E, Niaudet C, et al. Pericytes regulate the blood-brain barrier. *Nature* 2010 Nov 25;**468**(7323):557-561.

(13) Peters MF, Adams ME, Froehner SC. Differential association of syntrophin pairs with the dystrophin complex. *J Cell Biol* 1997 Jul 14;**138**(1):81-93.

(14) Derouiche A, Pannicke T, Haseleu J, Blaess S, Grosche J, Reichenbach A. Beyond polarity: functional membrane domains in astrocytes and Muller cells. *Neurochem Res* 2012 Nov;**37**(11):2513-2523.

(15) Wolburg H, Wolburg-Buchholz K, Fallier-Becker P, Noell S, Mack AF. Structure and functions of aquaporin-4-based orthogonal arrays of particles. *Int Rev Cell Mol Biol* 2011;**287**:1-41.

Figure 1

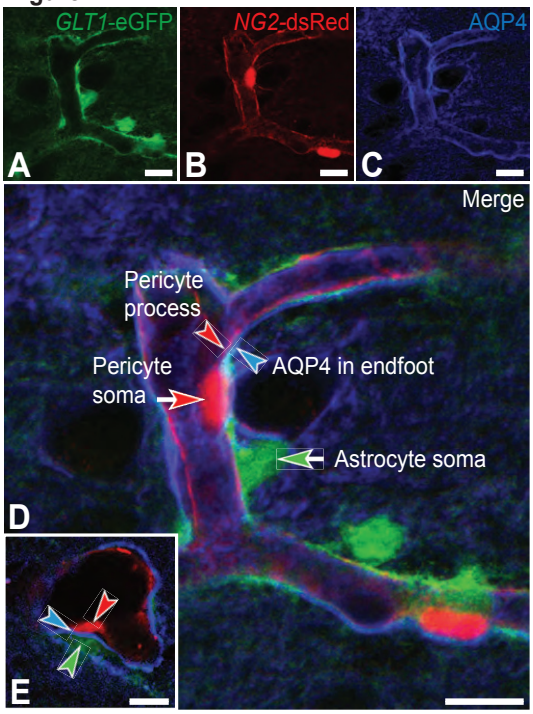
GLT1-eGFP
NG2-dsRed
AQP4
A
B
C
Merge
Pericyte process
Pericyte soma
AQP4 in endfoot
Astrocyte soma
D
E

Figure 2

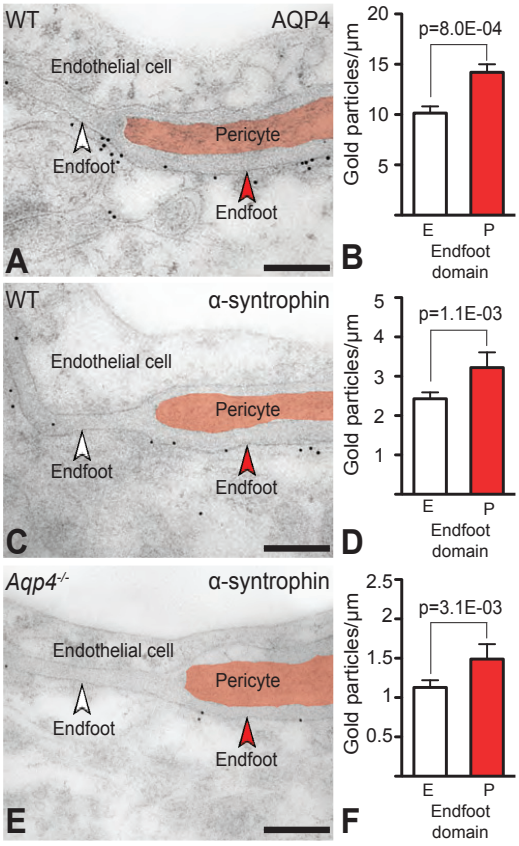
WT
AQP4
Endothelial cell
Pericyte
Endfoot
Endfoot
A
Gold particles/µm
20
15
10
5
p=8.0E-04
E
P
Endfoot domain
B
WT
α-syntrophin
Endothelial cell
Pericyte
Endfoot
Endfoot
C
5
4
3
2
1
p=1.1E-03
D
Aqp4-/-
α-syntrophin
Endothelial cell
Pericyte
Endfoot
Endfoot
E
2.5
2
1.5
1
0.5
p=3.1E-03
F

Figure legends

Figure 1. AQP4 immunofluorescence labeling is concentrated in astrocytic endfeet abutting pericytes. Micrographs from parietal cortex of *GLT1*-eGFP/*NG2*-DsRed double-transgenic mice showing the spatial relationship between astrocytes **(A)**, pericytes **(B)**, and AQP4 immunofluorescence labeling **(C)**. **(D)** Astrocytic cell bodies (green arrow) and their perivascular endfeet (green arrowhead) ensheathe pericyte cell bodies (red arrow) and processes (red arrowhead). The AQP4 immunofluorescence signal appears particularly strong in astrocytic endfeet adjacent to pericyte cell bodies and processes. **(E)** Transverse section of a capillary branch showing distinct AQP4 immunofluorescence (blue arrowhead) between a pericyte (red arrowhead) and the eGFP-filled cytoplasm of an astrocytic endfoot process (green arrowhead), corresponding to the endfoot membrane. Scale bars, A-E, 10 μm.

Figure 2. Immunogold labeling of AQP4 and α-syntrophin is concentrated in astrocytic endfoot membrane domains abutting pericytes. **(A)** Electron micrograph showing distribution of AQP4 immunogold labeling in parietal cortex of a wild-type (WT) mouse. Gold particles signaling AQP4 are clustered over astrocytic endfoot membranes, including membrane domains facing endothelial cells (E) and pericytes (P, marked red; white and red arrowheads, respectively). **(B)** Quantitative analysis of AQP4 immunogold labeling over astrocytic endfoot membrane domains. The density of gold particles over endfoot membranes abutting pericytes (P) is 40% higher than over those facing endothelial cells (E). P value is indicated (Poisson mixed models, cf. Materials and Methods; see Results for number of observations). **(C)** Electron

micrograph showing immunogold staining of α-syntrophin of a WT mouse. Labels as in (**A**). **(D)** Quantitative analysis reveals 33% higher density of α–syntrophin signaling gold particles over endfoot domains facing pericytes (P) compared to those facing endothelial cells (E). **(E)** α–Syntrophin immunogold labeling of an *Aqp4*$^{-/-}$ mouse. Labels as in (A). **(F)** The relative differences in α–syntrophin labeling density between endfoot membrane domains is preserved after deletion of *Aqp4*, being 32% higher over membranes facing pericytes than over those facing endothelial cells. Scale bars, A, C and E, 200 nm.

Paper III

Glial-conditional deletion of aquaporin-4 (Aqp4) reduces blood-brain water uptake and confers barrier function on perivascular astrocyte endfeet.

Nadia Nabil Haj-Yasein, Gry Fluge Vindedal, Martine Eilert-Olsen, **Georg Andreas Gundersen**, Øivind Skare, Petter Laake, Arne Klungland, Anna E. Thoren, John M. Burkhardt, Ole Petter Ottersen and Erlend A. Nagelhus
Proceedings of the National Academy of Sciences U S A. 2011 Oct 25;108(43):17815-20. doi: 10.1073/pnas.1110655108. Epub 2011 Oct 11.

Paper IV

A paravascular pathway facilitates CSF flow through the brain parenchyma and the clearance of interstitial solutes, including amyloid β.

Jeffrey J. Iliff, Minghuan Wang, Yonghong Liao, Benjamin A. Plogg, Weiguo Peng, **Georg Andreas Gundersen**, Helene Benveniste, G. Edward Vates, Rashid Deane, Steven A. Goldman, Erlend A. Nagelhus, Maiken Nedergaard
Science Translational Medicine. 2012 Aug 15;4(147):147ra111. doi: 10.1126/scitranslmed.3003748.

Our figures are included in the supplementary data.
